This is to certify that the

dissertation entitled

Design, Characterization, and Applications of
a Miniature Continuous Flow Analysis System

presented by

Charles J. Patton

has been accepted towards fulfillment
of the requirements for

Ph.D. degree in Chemistry

Stanley R. Crouch
Major professor

Date December 1, 1982

DESIGN, CHARACTERIZATION, AND APPLICATIONS OF A MINIATURE CONTINUOUS FLOW ANALYSIS SYSTEM

by

Chas. J. Patton

A DISSERTATION

Submitted to
Michigan State University
in partial fulfillment of the requirements
for the degree of

DOCTOR OF PHILOSOPHY

Department of Chemistry

1982

ABSTRACT

DESIGN, CHARACTERIZATION, AND APPLICATIONS OF A MINIATURE CONTINUOUS FLOW ANALYSIS SYSTEM

by

Chas. J. Patton

A modular, single channel, continuous flow analysis instrument that can be configured for either air-segmented continuous flow analysis (CFA) or flow injection analysis (FIA) has been developed. System components include a modified, commercially available, peristaltic pump, a dual-beam, fiber optic, filter photometer, and an electronic bubble gate that removes the air segment artifact from the detector signal when bubble-through flow cells are used for colorimetric CFA determinations. Instrumentation and hardware designed and built for use with this system are described in detail.

Performance of the miniature CFA system (0.1 cm ID manifold components and bubble-through flow cells) is characterized for a number of equilibrium based colorimetric determinations. Novel open tubular cadmium reactors (OTCRs) were developed and characterized that were used to reduce nitrate to nitrite in conjunction with automated colorimetric determinations of nitrate in water and seawater. Peaks with flats and less than 1% interaction were achieved in conjunction with OTCRs at a sampling rate of 120 hr^{-1}. Comparable performance in conjunction with packed bed cadmium reactors generally used for automated nitrate

determinations could only be achieved at half this sampling rate ($60\ hr^{-1}$).

Results from an experimental comparison of the performance (sampling rates, sample and reagent consumption, and precision of analytical results) of CFA and FIA are presented. Reagent consumption and sample dispersion in the miniature CFA system were less than in FIA systems equipped with either coiled open tubular reactors (0.05 cm ID) or single bead string reactors. The advantages of using single bead string reactors for merging zones FIA determinations are demonstrated. CFA and FIA are shown to be complementary techniques, and the relative merits of each for various applications are discussed.

Fedor Mikhailovich Dostoevski, the Russian novelist, said one time that, 'One sacred memory from childhood is perhaps the best education.' I can think of another quickie education for a child, which, in its way, is almost as salutary: Meeting a human being who is tremendously respected by the adult world, and realizing that that person is actually a malicious lunatic.

Slapstick -- Kurt Vonnegut

ACKNOWLEDGMENTS

I am extremely indebted to Professor Stanley Crouch for his guidance, enthusiasm, and friendship throughout the course of my research effort. Many thanks also to Professor Chris Enke who served as my second reader. His advice was consistently helpful and incisive. Who else would have known that B.V.D. stands for Bradlee, Vorhees, and Day? This information is now pinned discretely to my B.V.D.'s. The efforts of the other members of my Guidance Committee, Professors Tom Pinnavaia and George Leroi, are also appreciated. It was also a pleasure to teach for Professor Andrew Timnick, who allowed me to incorporate a continuous flow analysis experiment into his Chemistry 333 course.

A great deal of assistance (not necessarily constructive) was provided by my buddy and fellow sufferer, Eugene Ratzlaff — AKA: AZURE FLEETFANG. Together we managed to advance the 'Boy's Shop' approach to analytical instrumentation to new levels of perversity. Thanks, too, to Robert Thompson who shock-tested early versions of my instrument. You will be happy to know, Rob, that the leering grin of 'Bow tie Man' still haunts my troubled dreams. Sincere thanks are also extended to Keith Trischan who wrote several computer programs that were extremely useful in my work. The friendship and help of other Crouch Group members will not be forgotten.

The help, good humor (ice cream?), programming expertise, and down home philosophy of Dr. Tom Atkinson were invaluable. Thanks, too, to Marty Rabb for help with the design of electronic components of the miniature continuous flow analysis system. This work would have been impossible without the craftmanship of Russ Geyer, Ben Stutsman, Dick Menke, and Deak Watters in the Chemistry Department Machine Shop, Andy Seer and Manfred Langer in the Chemistry Department Glass Shop, and Ron Haas and Scott Sanderson in the Chemistry Department Electronics Shop.

Special thanks to Jo Kotarski who prepared the figures and drawings in this dissertation and to Margy Lynch for technical typing.

FOREWORD

This dissertation is more like a collection of short stories with a common theme, than a fully developed novel. With the exception of Chapter 1 where the origins and principles of air-segmented continuous flow analysis (CFA) and flow injection analysis (FIA) are discussed, the chapters are arranged in the approximate order that research reported was performed. As work progressed new lines of research began to suggest themselves. I have thus included more FIA experiments than I had planned at the onset of this project.

In Chapter 2 the miniature continuous flow analyzer that evolved during the course of this research is described in detail. Here I have attempted to provide sufficient information to allow others to use the system as it now exists and to modify it for new applications. Also included are procedures for data reduction and analysis.

A description of the electronic bubble gate that removes the air segment artifact from the detector signal when bubble-through flow cells are used with air segmented continuous flow analyzers can be found in Chapter 3. Details of individual circuit elements in the bubble gate are included. The results of experiments in which this bubble gate was used in conjunction with a commercial CFA system and the miniature CFA system described in Chapter 2 are also presented, and the performance of the latter is compared with performance reported for flow injection analysis.

The developmental work on open tubular cadmium reactors for routine nitrate determinations in water and seawater reported in Chapter 4 is the culmination of an idea that occurred to me in 1976 after I had returned from an ACS summer symposium on immobilized enzymes. The major obstacle to beginning this work was locating a source of small diameter cadmium tubing. Apparently it is used in the nuclear reactor industry. I had worked on this project sporadically for several years, but until about six months ago, the successful outcome of this project was still very much in doubt.

The experimental comparison of FIA and CFA presented in Chapter 5 resulted from some lively, late-night discussions with several FIA enthusiasts in attendance at the ACS summer symposium on flow injection analysis held in New York in 1981. Upon returning from this symposium, I realized that the miniature continuous flow analysis system which can be easily configured for either FIA or CFA determintions was ideally suited for an unbiased comparison of these two techniques. Please note that the results of this comparison pertain only to equilibrium based colorimetric determinations, and they should not be extrapolated to include determinations in which the formation of concentration gradients can be exploited (titrations, viscosity measurements, refractive index measurements), for which I believe FIA has some clear advantages over CFA.

Finally, in Chapter 6, some future applications for the miniature continuous flow analysis system are discussed.

TABLE OF CONTENTS

CHAPTER PAGE

TABLE OF FIGURES

FIGURE PAGE

FIGURE PAGE

LIST OF TABLES

TABLE PAGE

CHAPTER 1

HISTORICAL AND THEORETICAL INTRODUCTION TO CONTINUOUS FLOW ANALYSIS

A. Overview

Until about 1975 the term continuous flow analysis was used almost exclusively to describe a technique now known as air-segmented continuous flow analysis (CFA) that was invented by Leonard Skeggs [1] and developed commercially by the Technicon Corporation under the trade name, AutoAnalyzer. For a number of years an air segmented analytical stream was considered a prerequisite for continuous flow analysis, but in the mid-1970's two promising experimental approaches toward practical nonsegmented continuous flow analysis were reported almost simultaneously by Kent Stewart and coworkers in the United States [2] and Elo Hansen and Jaromir Ruzicka in Denmark [3]. Despite pronounced differences in hardware, the basic concept for nonsegmented continuous flow analysis was essentially the same for both groups. Ruzicka and Hansen named this technique flow injection analysis (FIA) by which it is commonly known today.

There have been a number of fairly thorough reviews of CFA [4-6] and FIA [7-10] which I shall not attempt to duplicate here. Instead I shall focus on the strengths and weaknesses of the two techniques in relation to each other. To do this, it is necessary to place the development and theoretical foundations of CFA and FIA into historical

perspective, since there is little question that both these elements have had a profound effect on the manner in which these two techniques are currently perceived.

B. Historical

1. CFA

Details concerning Skeggs invention of CFA and its ensuing early history are somewhat aprocryphal and inexorably linked to the Technicon Corporation. It appears that both the increased demand for clinical laboratory services and the technological boom that followed World War II provided Skeggs with both motivation and inspiration to automate routine colorimetric determinations. He dismissed the possibility of building a machine to manipulate the test tubes and pipets used for conventional batch analysis as being overly complex and impractical [1]. Instead, he began to explore the feasibility of performing assays sequentially in a continuously flowing stream contained within a network of small diameter open tubes (now called a manifold). At some point in the late 1940s or early 1950s, Skeggs began to build prototype CFA systems and devised novel solutions to problems posed by the CFA approach. He found, for example, that dialysis was particularly adaptable to CFA, and he used it to separate low molecular weight analytes from blood and serum proteins that interfere in many assays. His most significant innovation, however, was unquestionably 'the bubble'. Intermixing of samples as they passed through the manifold in boxcar fashion severely limited the performance of Skeggs' early systems. He soon discovered, however, that insertion of air bubbles into the

analytical stream at regular intervals reduced this mixing dramatically. Thus the bubble became and remains the sine qua non of CFA.

In the mid 1950s, the Technicon Corporation bought and patented Skeggs' CFA concept and prototype instrumentation, and in 1957 they marketed a single channel CFA system, the AutoAnalyzer, which was the first in a series of highly successful and profitable CFA instruments. It must be appreciated that virtually none of the hardware that CFA practicioners presently take for granted was available when Skeggs began his developmental work. Reliable multichannel peristaltic pumps, and more importantly, durable and inert pump tubes that could deliver relatively small volumes with good precision had to be developed and manufactured in quantity. The same is true for the multitude of specialized manifold components such as dialysis blocks, mixing coils, and fittings that now can be obtained from a number of suppliers. Technicon must be credited with developing and constantly improving the hardware and technology that transformed CFA from a laboratory curiosity into a highly practical and sophisticated technique.

While a typical present-day CFA instrument is much the same as the first AutoAnalyzer with respect to the basic components and their general arrangement in the system, the hardware itself and the way in which data are acquired and processed has now evolved through three major design changes as summarized in Table 1-1. Several comments are in order here. First, CFA was developed by Technicon primarily for clinical determinations and in general, new technology has been aimed at this market. While first generation CFA instruments were general purpose systems that were readily adapted for non-clinical

Table 1-1. Evolution of Technicon's air-segmented continuous flow analyzers.

First Generation Systems	Number of Channels	Determinations per hour	Comments
1957 – AutoAnalyzer I	1	20	Designed for determination of glucose or blood urea nitrogen in clinical samples.
1963 – Tandem AutoAnalzyer	2	20	Simultaneous determinations of glucose and blood urea nitrogen.
1964 – Electrolyte Analyzer	4	20	Simultaneous determinations of potassium and sodium by flame photometry; carbon dioxide and chloride by colorimetry.
1964 – Prototype Multi-channel Analyzer [a]	8	20	Single detector and movable cuvets. Results for all determinations recorded on a single chart.
1966 – SMA 12/30	12	30	Production model of Skeggs and Hochstrasser's prototype instrument.
Second Generation Systems			
1967 – SMA 12/60	12	60	Major redesign of pumps, manifold components, flow cells.
1970 – AutoAnalyzer II	1	20-60	SMA technology in single channel form. Primarily for non-clinical applications.
Third Generation System			
1972 – SMAC	>20	150	Major redesign of sampler, pump, and manifold components. Computer data acquisition and processing.

[a] Skeggs, L.T.; Hochstrasser, H. Clin. Chem. (Winston-Salem, NC) 1964, 10, 918-936.

applications, a trend toward specialized multichannel systems that perform standard determinations at a single work station is apparent in the second generation SMA 12/60 (sequential, multichannel analyzer, 12 channels, 60 samples per hr) and in the third generation SMAC (sequential multichannel analyzer with computer) system. Second, Technicon has tended to reserve its best technology for its large, clinically-oriented customers. Although SMA technology was made available to non-clinical customers in the form of the AAII single channel instrument, state-of-the-art SMAC technology in single channel form is still unavailable.

2. FIA

The origins and early history of FIA have recently been reviewed by Kent Stewart [12] and Horacio Mottola [13]. Stewart traces the FIA concept—sample injection into a continuously flowing stream with continuous downstream detection--back to James and Martin's original work on gas chromatography in 1952 [14]. Mottola sets the clock somewhat later, at Blaedel and Hicks' [15] development of a continuous flow kinetics instrument in 1962. FIA in its present form, however, did not appear until the mid 1970s and evolved through two distinct pathways which have now merged for the most part into a single technique containing elements of both original approaches. FIA as developed by Stewart, Beecher, and Hare [2] has very obvious connections to the non-segmented, continuous flow, post column LC reaction colorimeter designed by Spackman, Stein, and Moore [16] for amino acid analysis. The carrier (reagent) stream was propelled through 0.025 cm ID teflon tubing at relatively high pressure, and samples were introduced through

a multiport sampling valve. It is unfortunate that much of this group's early work is buried in rather obscure literature sources. Ruzicka and Hansen's first apparatus on the other hand seems much more related to CFA systems. A peristaltic pump was used to propel the carrier stream through much larger (0.15 cm ID) polyethylene tubing. Samples were literally injected, at first directly through the walls of the tubing and later through a septum, with a hypodermic needle and syringe. Clearly FIA, was not invented by a single group, but Ruzicka and Hansen deserve a tremendous amount of credit for their developmental efforts. They coined the generic term for nonsegmented continouous flow analysis, recognized the great potential of the technique, developed many novel applications for its use, and continue to promote it with unflagging enthusiasm.

At the time FIA was being developed, the hardware required was readily available from a number of suppliers. By the early 1970s, peristaltic and reciprocating LC pumps were for the most part perfected and a wide variety of small diameter polymeric tubings from which FIA reactors are usually fabricated were readily available. So too were low dead volume connectors and fittings designed primarily for use with LC systems. In addition, the absence of air segments simplified interfacing the flow stream to a variety of detectors. Part of the great appeal of FIA, especially in small industrial and academic laboratories, is the ready availability of hardware and the ease with which the FIA technique can be adaptd to existing equipment. In addition, FIA's lack of association with commercial concerns (until quite recently) has led to freer and faster dissemination of information and technological advances.

The sampling rates achieved with relatively simple single channel FIA systems often surpass those of third generation CFA systems. In general, high (>200 hr^{-1}) sampling rates are possible only when the flow rate is high and the residence time of samples in the reactor is short. This was particularly true for early systems that were often wasteful of reagents and limited to very fast chemical reactions. As sample dispersion in FIA systems became better understood, however, these shortcomings have been minimized. The trend in FIA has been toward lower flow rates, smaller diameter reactors, and smaller sample volumes. Multiport valves have gained almost universal acceptance as the sample introduction method. Innovations in FIA hardware and methodology continue to be reported at a rapid pace.

C. Principles

1. CFA

The spatial arrangement of interconnectd modules for a generalized CFA instrument is shown in Fig. 1-1A. It is common practice to aspirate samples sequentially from containers positioned on the sampler into the manifold where chemical separations and reactions are effected. Usually an analyte-free wash solution contained in a reservoir on the sampler is aspirated between each sample. The sampler probe's residence time in a sample or the wash solution, t_s or t_w, respectively, and the flow rate of the pump tube to which it is connected determine the volume of sample drawn into the manifold. Failure to control these variables rigidly, therefore, can adversely affect the precision of analytical results. Sample and wash slugs are uniformly segmented with air bubbles as they enter the manifold and are thus divided into a

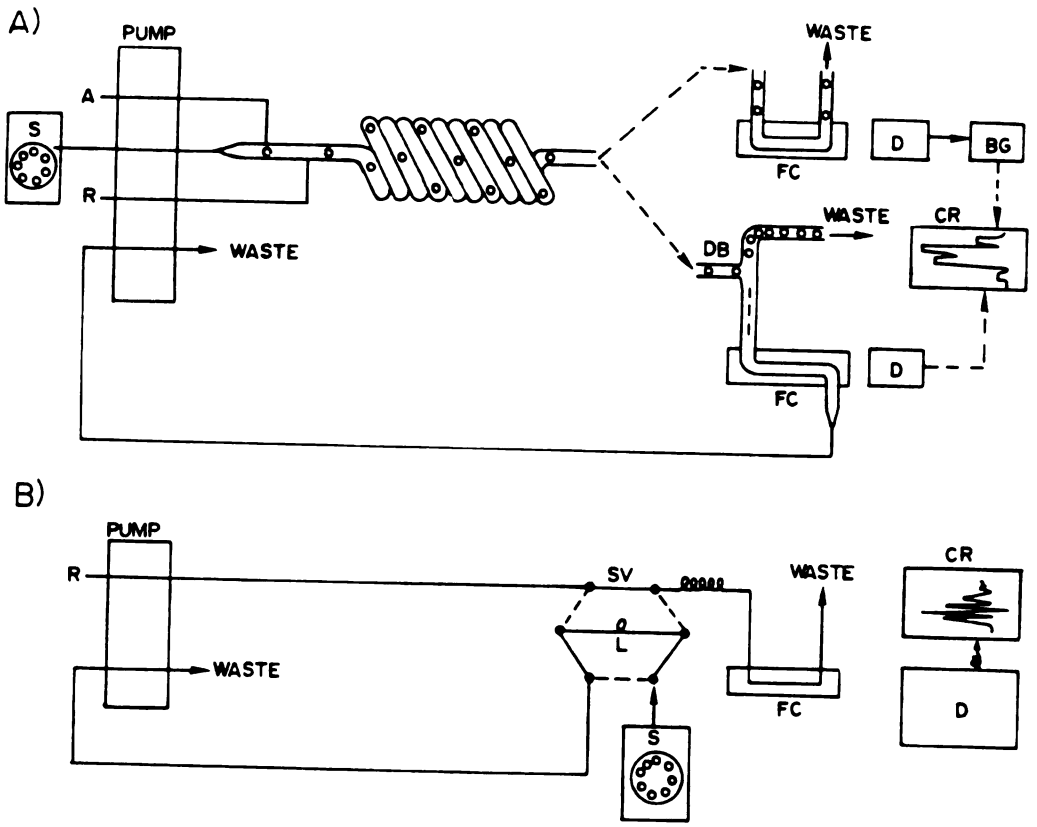

Figure 1-1. Diagrams of generalized CFA and FIA instruments. S = sampler, SV = sampling valve, L = sample loop, DB = debubbler, D = detector, FC = flow cell, BG = bubble gate, CR = chart recorder, A = air, R = reagent. A) CFA. B) FIA.

number of nominally identical subunits. The segmented stream is proportioned with reagents at various points along the manifold as it is propelled toward the flow- through cuvet of a recording photometer. The highly reflective air segments pose special problems for photometric detection in CFA. In first and second generation systems air segments are removed from the analytical stream just prior to detection; in third generation systems the air bubble artifact is removed electronically, a technique known as bubble gating.

In the absence of dispersion, the trace observed at the recording photometer of a CFA instrument would resemble a train of square waves. Transitions to or from some time invariant signal level proportional to the analyte concentration in the wash solution or a sample (base line or sample steady states) would be instantaneous. In the trace actually observed, however, these transitions are more gradual and steady states are approached along skewed rise and fall curves shown in Fig. 1-2. Data for this figure were obtained experimentally with the miniature CF system that was developed during the course of this research and they will be discussed in more detail in paragraphs that follow, and in Chapter 2. Deviation of these recorded signals from the idealized square wave output function is quite obvious. Data sets plotted to the right and left of the dashed vertical line in this figure were obtained with bubble gated and debubbled flow cells, respectively. Note that steady state was fully attained in the broad center peak (t_s=30 s), but that steady states were not achieved at shorter sample and wash intervals (t_s=8s, t_w=2s) which were used to generate the peaks on either side of the center peak. The sequence of peaks to the right of the center peak is known as an interaction test pattern. Here samples were

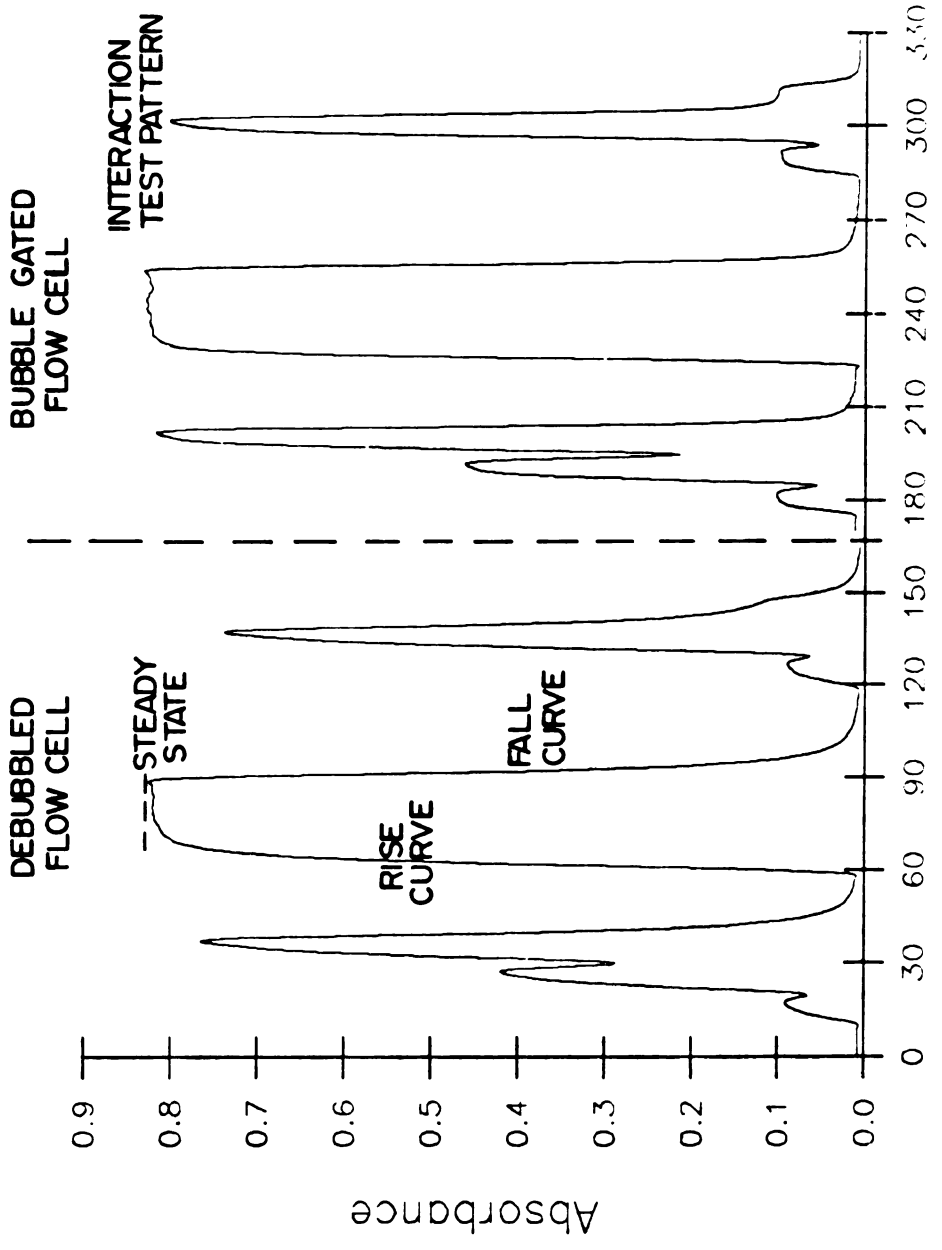

Figure 1-2. Signals recorded for the same flow stream with bubble gated and debubbled flow cells.

determined in the concentration sequence of low, high, low and it is apparent that the tail of the high-concentration peak contributes significantly to the height of the second low-concentration peak. Percent interaction (%I) is defined as the difference in absorbance between the second and first low-concentration peaks divided by the absorbance of the high-concentration peak. This quantity multiplied by 100 is the percent interaction. The extent of sample interaction depends on the magnitude and nature of dispersion experienced by samples as they pass through the flow system.

Dispersion in CFA arises from two distinct processes. The first is large scale convective mixing (longitudinal dispersion) that occurs in unsegmented zones of the system--e.g., sample lines, flow cell debubblers, flow cells. Here flow is essentially laminar and, as a result, recorded signals are deformed exponentially [17] relative to the idealized square wave output function. An empirical linear relationship between concentration and time for longitudinal dispersion is given by Equation 1-1.

$$\ln(A_{ss}-A_t) = \ln A_{ss}-t/b \qquad (1-1)$$

where A_{ss} is the steady state absorbance, A_t is the absorbance of the peak profile at any time t, and b, the exponential factor, is the slope constant. Equation 1-1, due to Walker, *et al.* [18] is a formalized version of an equation first reported by Thiers, *et al.* [19]. It is customary to express the magnitude of longitudinal dispersion in terms of b. Walker [17] showed that because of the exponential relationship between absorbance and time, peak heights within 90, 95, and 99% of steady state result when t_s = 2.3b, 3.0b, and 4.6b, respectively, and

that percent interaction of 7, 1, or 0.5 % will occur when the time between samples (t_s+t_w) is 2.65b, 4.6b, or 5.3b, respectively. This of course assumes that longitudinal dispersion is much greater than axial dispersion as is the case for first and second generation CFA systems.

The second effect, axial dispersion, occurs in the air segmented analytical stream. Here large scale mixing between liquid segments is prevented by air bubbles, while mixing within segments is greatly enhanced by so-called bolus flow [20]. The only medium for intersegment mass transfer in the segmented stream is the stagnant liquid film that wets the walls of the flow system. By this mechanism, analyte molecules initially contained in a single segment are incorporated into succeeding liquid segments that were initially analyte free. After an arbitrary period of flow, the concentration of analyte molecules in any segment is approximated by Equation 1-2,

$$C_k/C = e^{-q}q^k/k! \qquad (1\text{-}2)$$

where C is the analyte concentration in the initial undispersed segment, C_k is the analyte concentration in segment k (k=0,1,2...), and q is a dimensionless parameter which in simplest terms is the ratio of the liquid volume that wets the walls of the entire flow system (V_f) and the volume of a single liquid segment (V_s). Note that the expression on the right hand side of Equation 1-2 is the Poisson distribution. When the sample is a series of analyte containing segments, as is the usual case in CFA, the concentration distribution is given by the summation of Equation 1-2 and for a large number of segments the cumulative Poisson distribution is approximated by the cumulative

Gaussian distribution. Therefore axial dispersion is generally expressed in terms of the standard deviation, σ, of the cumulative Gaussian distribution. In this case q is equal to the displacement of the 50% maximum concentration point in the dispersed sample profile from the leading edge of the undispersed sample slug (k=0), and $\sigma \simeq (q)^{1/2}$. Note that both σ and q are dimensionless in the sense that they are measured in terms of segment number. Equation 1-2 was the first model of axial dispersion in CFA and is due to Hrdina [21]. The trouble with this and several other models that followed it, most notably those of Begg [22], Thiers [23], and Walker [24], is that they did not relate axial dispersion to relevant experimental variables--e.g., residence time, flow rate, segmentation frequency, tube diameter. For a more detailed discussion of axial dispersion in CFA see reference 25 and the figures therein.

Longitudinal dispersion can be minimized by improved design of system components--e.g., 'pecking' samplers [26], bubble gated flow cells [27-29] — or its effects can be removed after the fact by means of a data processing technique known as curve regeneration that was first reported by Walker [30]. Here the final steady state absorbance is calculated before it is physically attained by means of Equation 1-3.

$$A_{ss} = A_t + b \frac{dA_t}{dt} \qquad (1\text{-}3)$$

Details of curve regeneration are discussed in Chapter 2. The effectiveness of bubble gating and curve regeneration is illustrated in Figures 1-2 and 1-3, respectively. In both figures curve tracings to

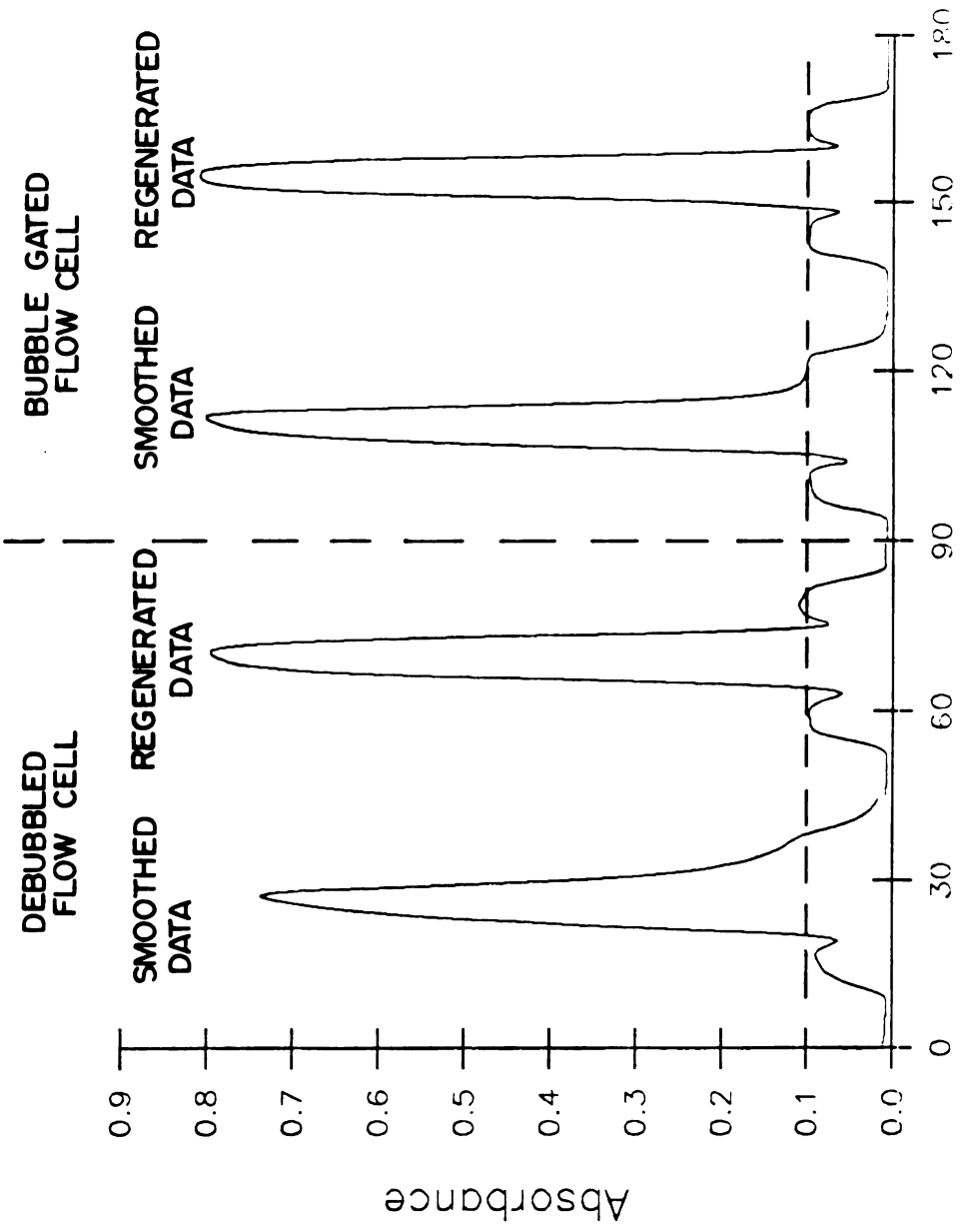

Figure 1-3. Expanded scale plot of smoothed and regenerated interaction test patterns shown in Figure 1-2.

the right of the dashed lines pertain to the bubble gated flow cell. Dispersion is very obviously less in the bubble gated flow cell. Peak heights more nearly approach steady state and interaction is reduced. The value of b estimated for the bubble gated and debubbled system were 1.0 s and 2.3 s, respectively. This information was used to regenerate the bubble gated and debubbled data sets and the curves that resulted are shown in Figure 1-3. Smoothed and regenerated data are plotted side by side for each data set to facilitate comparison. Note that the effects of longitudinal dispersion are greatly reduced for data sets obtained with either flow cell and that the peak profiles closely resemble the integrated Gaussians predicted by Hrdina's model.

Axial dispersion is fundamental to CFA as it is currently practiced because flow systems fabricated from wettable materials are required for hydraulic stability in segmented streams. In 1976 Snyder and Adler [25] experimentally verified Hrdina's model and presented a semiempirical derivation of it. The unique feature of their derivation was that V_f was expressed in terms of the length and diameter of the flow system. This allowed q (and therefore σ) to be related to experimental variables. They then extended the model to account for slow mixing between segments and the liquid film [20]. Previous models had assumed instantaneous mixing. Later Snyder [31] recast the extended model into a form that made the effects of major experimental variables on axial dispersion more obvious as shown in Equation 1-4.

$$\sigma_t^2 = \left[\frac{538 d_t^{2/3}(F + 0.92 d_t^3 n)^{5/3} \eta^{7/3}}{\gamma^{2/3} F D_{w,25}} + 1/n\right]\left[\frac{2.35(F + d_t^3 n)^{5/3} \eta^{2/3} t}{\gamma^{2/3} F d_t^{4/3}}\right] \quad (1\text{-}4)$$

Here σ_t is the standard deviation of the peak expressed in seconds, d_t is the internal diameter of the flow system in cm, F is the liquid flow rate in mL s^{-1}, n is the segmentation frequency in Hz, t is the residence time of the sample in the flow system in s, η is the viscosity of the liquid in poise, γ is the surface tension of the liquid in dyne cm^{-1}, and $D_{w,25}$ is an empirical diffusion coefficient (cm^2 s^{-1}) that pertains only to diffusion in coiled tubes [31]. The basic assumptions of the model follow: 1) air segment volumes are the minimum required to totally occlude a tube of a given diameter ($7\pi/24\ d_t^3 \simeq 0.92\ d_t^3$); 2) the flow system is perfectly wetted; 3) longitudinal mixing in the film is negligible; and 4) the flow system is free of mixing effects (longitudinal dispersion). Generally the experimenter has control over only d_t, n, F, and t, although it should be noted that a surfactant is generally added to reagents to avoid changes in γ that would otherwise occur as the concentration of the analyte varied [24].

It is clear from Equation 1-4 that σ_t is proportional to the square root of t. The effect of the other major variables (F, d_t, n) is not so apparent, but they can be readily visualized with the aid of Figure 1-4A and 1-4B. Part A of this figure shows the relationship between σ_t and n for several values of d_t when F and t are fixed at 0.5 mL min^{-1} and 300 s, respectively, and values for minor variables are in keeping with a similar set of calculations by Snyder [32]. Here we see that for each value of d_t, σ_t passes through a minimum. As d_t decreases, σ_t decreases while the value for n where σ_t is minimum increases. Part B of this figure shows the relationship between σ_t and n for several values of F when d_t is fixed at 0.1 cm and all the other variables are the same as for Figure 1-4A. Note that the minimum value

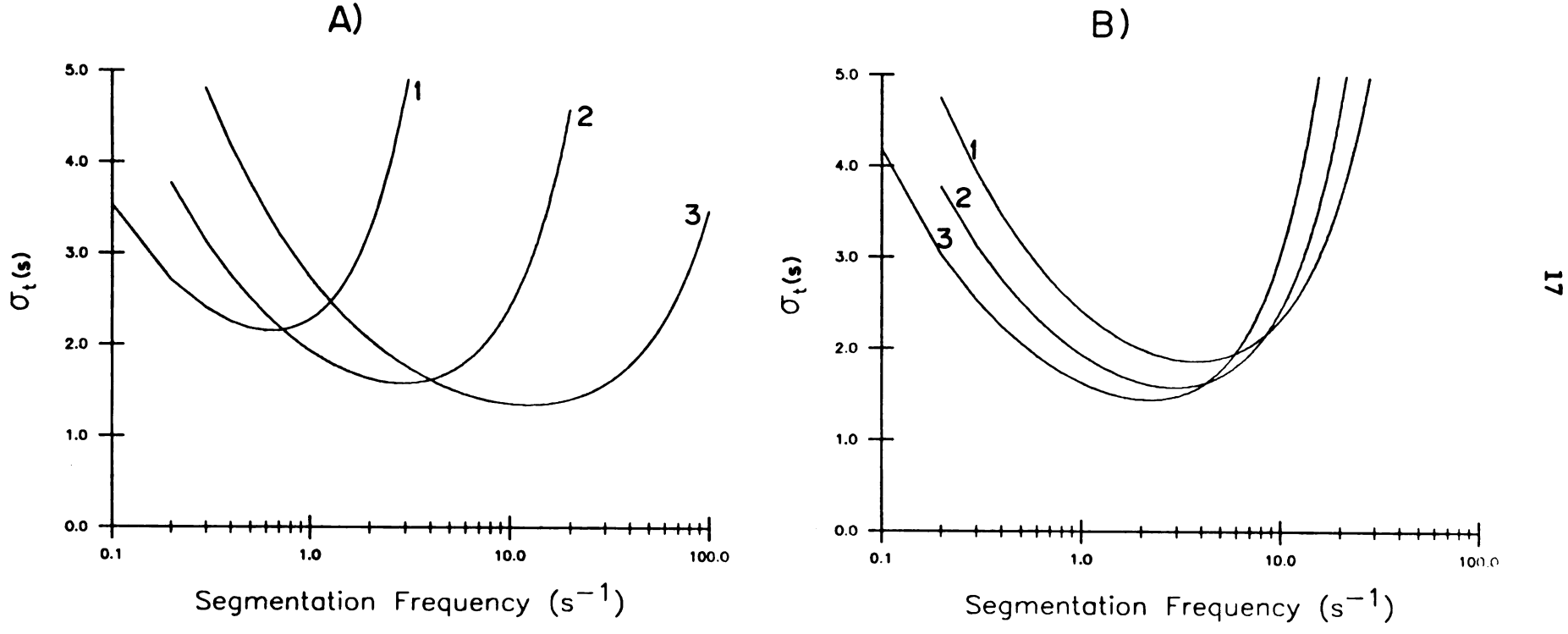

Figure 1-4. Variation of σ_t as a function of n, d_t, and F for t = 300 s. A) F = 0.0083 mL s^{-1}. 1: d_t = 0.2 cm. 2: d_t = 0.1 cm. 3: d_t = 0.05 cm. B) d_t = 0.1 cm. 1: F = 0.0167 mL s^{-1}. 2: F = 0.0083 mL s^{-1}. 3: F = 0.0042 mL s^{-1}. Minor variables: $\eta = 8.9 \times 10^{-3}$ poise, γ = 32 dyne cm^{-1}, $D_{w,25} = 5 \times 10^{-5}$ cm^2 s^{-1}.

for σ_t decreases as F decreases and also that these minima occur at lower values of n.

These trends explain, in part, the relative performance of Technicon's second and third generation CFA systems. The values of F, n, and d_t for second generation systems are about 1.5 mL min^{-1}, 0.5 s^{-1}, and 0.2 cm, while for third generation systems they are about 0.6 mL min^{-1}, 1.5 s^{-1}, and 0.1 cm. If we assume t = 600 s and retain the same values for minor variables as before, values of σ_t calculated for second and third generation systems are 3.82 s, and 2.57 s, respectively. Snyder [32] has suggested that for peaks with appreciable steady state intervals (flat tops) the time between samples should be about 8 σ_t. Therefore the predicted sampling frequencies for second and third generation systems are about 120 hr^{-1} and 175 hr^{-1} respectively. Second generation systems generally are limited to a maximum sampling frequency of about half the theoretical limit because of longitudinal dispersion in the sample line and in flow cell debubblers. In third generation systems the sampling frequency (150 hr^{-1}) approaches the theoretical limit more closely because longitudinal dispersion is minimized with pecked sampling and bubble-through flow cells. Although there is no theoretical limit to the extent that axial dispersion can be decreased by reduction of d_t and F, there are several practical constraints imposed by flow cell volumes, precision and delivery rates of pumps, and other factors. Snyder takes these into account in references 31 and 32, and I shall discuss them in more detail in Chapter 2.

2. FIA

The arrangement of components for a generalized FIA instrument is shown schematically in Fig. 1-1B. A nonsegmented carrier stream (the reagent for the simplest case) is pumped continuously through a polymeric tube that terminates at a detector which for the sake of simplicity we shall assume to be a recording photometer. Samples are abruptly introduced into the carrier stream either by means of a syringe or (usually) a multiport valve. The sample mixes with the carrier stream enroute to the detector. For systems with a sampling valve the amount of sample introduced into the reaction network is determined solely by the sample loop volume. Provided that the loop is completely filled prior to injection, the residence time of the sample line in a sample does not affect the precision of analytical results. Furthermore, the low dead volume of the sample line, valve, and sample loop, and the nonwettable materials from which they are made generally preclude the need for a wash solution. A slug of air aspirated between successive samples is usually sufficient to purge remnants of the previous sample and the carrier stream from the sample line and sample loop, respectively.

At the moment of injection, a sample with initial concentration C_o is entrained by the carrier stream which propels it through the reactor toward the detector. To a first approximation, sample molecules in the center of the reactor flow toward the detector with twice the mean velocity of the carrier while those at the wall are stationary (i.e., laminar flow). Convective mixing of the sample with the carrier occurs along the stream lines and dilutes the sample so that the maximum sample concentration, C_{max}, sensed at the detector is some fraction of

C_o. The ratio of C_o to C_{max} provides a useful empirical measure of dispersion, D [33] in FIA systems. Ruzicka and Hansen classify dispersion in FIA as limited (D = 1 to 3), medium (D = 3 to 10), or large (D $\geq$ 10). If the flow rate and reactor diameter are held constant, the injected sample volume, S_v, and the reactor length, L, have a major influence on D, which approaches unity either as S_v increases or L decreases, as illustrated in Figure 1-5A and 1-5 B. Further details can be found in the figure captions. So far in our discussion we have only considered dispersion of the sample by convection in a straight tube. Under these conditions, skewed peaks with infinitely long tails would be predicted. Tailing of FIA peaks is much less severe than this, however, due to radial diffusion and secondary flow that we shall now briefly discuss.

Sample molecules in stagnant zones near the reactor wall are transported into more rapidly flowing stream lines by radial diffusion, and thus tailing is reduced. At very low flow rates, in fact, radial diffusion becomes the dominant contributor to dispersion, and under these conditions a Gaussian peak profile results. Peak shapes actually observed in the normal range of operating conditions for FIA, however, generally reflect the combined effects of convection, radial diffusion and, if the reactor is coiled (the usual case for FIA), secondary flow. Vanderslice *et al.* [34] presented numerical solutions to convection-diffusion equations that allow calculations of dispersion in straight open tubes under a variety of experimental conditions. The problem with such models, however, is that they fail to account for secondary flow--flow perpendicular to the axis of the reactor resulting from centrifugal forces—that develops in a coiled tubes. All other factors

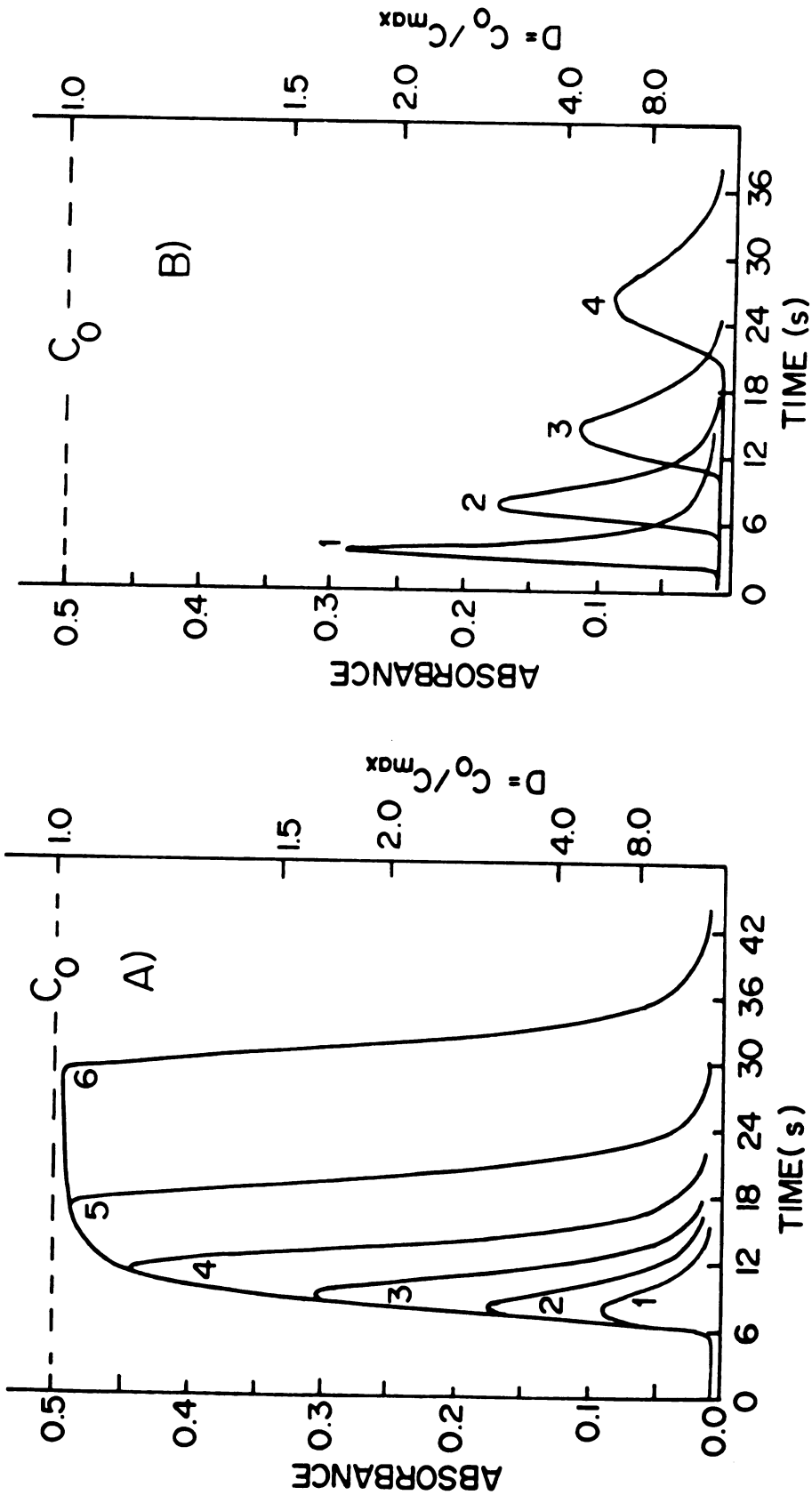

Figure 1-5. Dispersion in FIA as a function of injected sample volume (S_V) and reactor length (L). Carrier stream = pH 9.5 borate buffer, sample = 10 μM phenol red in pH 9.5 borate buffer, flow rate = 2.0 mL min^{-1}, coiled Teflon reactor diameter = .05 cm. A) L = 50 cm. S_V: 1 = 25 μL, 2 = 50 μL, 3 = 100 μL, 4 = 200 μL, 5 = 400 μL, 6 = 800 μL. B) S_V = 50 μL. L: 1 = 10 cm, 2 = 50 cm, 3 = 100 cm, 4 = 200 cm.

being equal, dispersion in a tightly coiled tube is about 2 to 3 times less than in a straight tube [5,35]. The extent of secondary flow increases as the coil diameter approaches the inside diameter of the tube and as the mean velocity of the carrier system increases. Note that secondary flow actually stabilizes the laminar flow regime [36] so that there is no physical basis for the notion of 'incipient turbulance' in coiled open tubes.

It is also possible to minimize dispersion in FIA systems by using packed rather than open tubular reactors. More care must be taken in the preparation of packed reactors, especially if small diameter particles are used, and the pressure drop may be too great to allow a peristaltic pumping system to be used. Recently, however, FIA reactors have been reported in which a small diameter tube is packed with solid glass spheres with diameters only slightly less than that of the tube [37]. The pressure drop across these so-called single bead string reactors (SBSR) or pearl string reactors are only slightly greater than that of an open coiled tube of comparable diameter, and dispersion in an SBSR is 2 to 3 times less than that of tightly coiled open tube. Also the extent of dispersion in SBSRs is less affected by changes in the flow rate then are coiled open tubular reactors [38]. This is an obvious advantage for FIA because reagent consumption decreases with decreasing flow rates. Furthermore, the lower dispersion obtained with SBSRs should allow longer reaction times with less dispersion.

So far we have only considered dispersive effects in the reactor. The total dispersion of the system, however, is also dependent on dispersion that occurs in the injector and detector, which is seldom negligible. Chemical kinetics, too, greatly influence FIA peak heights

and widths. If the FIA system is used only to transport the sample to a detector, limited dispersion is desirable so that even though the two ends of the sample plug experience mixing with the carrier, there remains a central undispersed zone. This is clearly not acceptable when it is desired to measure the end product of some reaction between the sample and the carrier stream. Here the entire sample volume must mix with the reagent and remain in the reactor for a sufficient period of time for the reaction to proceed to an appreciable extent prior to detection. Medium dispersion systems are generally used in these cases and a compromise must be reached between adequate mixing and reaction time on one hand and excessive dispersion of the sample zone on the other. If the sampling rates generally associated with FIA (90-150 hr^{-1}) are to be maintained, maximum residence times are on the order of 30 s. With the advent of SBSRs, however, the maximum residence time might be extended to 60-90 s, if several samples can reside in the reactor at a given time with minimal interaction.

At present there is no general model for FIA that allows dispersion to be calculated <u>a priori</u> from experimental variables such as tube ID, flow rate, and residence time. Betteridge provides a good summary of dispersion in FIA based on the tanks in series model [39] in Table II of reference 7. It must be noted, however, that at present only trends can be predicted. This is because subtle differences in the geometries of sample injectors and flow cells, as well as differences in wall roughness in reactors and connectors can profoundly influence the total observed dispersion [40]. Also, because there is a gradient both axially and radially within the dispersed sample zone, measurement of some property within this zone will always result in a composite

average of concentration distributed across or along the reactor. This is entirely different from CFA where each segment is essentially homogeneous. Nonetheless, for a given FIA system, dispersion generally is highly reproducible and therefore the precision of analytical results is good. Furthermore for a number of applications such as kinetic assays, titrations, viscosity measurements, and other techniques where a gradient can be exploited, FIA offers possibilities that are not easily achieved by CFA.

CHAPTER 2

INSTRUMENTATION, DATA ACQUISITION AND PROCESSING, AND OPERATIONAL PROCEDURES

A. General Considerations - CFA

In Chapter 1 the origins of dispersion in CFA systems were discussed largely from a theoretical point of view. It is now worthwhile to examine limitations to this theoretical treatment that are imposed by hardware used to implement real CFA systems. Returning to Snyder's model and assuming that the dwell time, t, is fixed at 300 s and that the values of minor variables [32] are assigned as follows: γ = 32 dynes cm^{-1}; $\eta = 8.9 \times 10^{-3}$ poise; $D_{w,25} = 5 \times 10^{-5}$ cm^2 s^{-1}, it is a simple matter to calculate the magnitude of axial despersion, σ_t, as a function of liquid flow rate, F, segmentation frequency, n, and manifold inside diameter, d_t. Results of such calculations, shown in Table 2-1, reveal that for each value of d_t and F, there exists a value of n (n_{opt}) where σ_t is minimum. Two trends are observed in this table. First, n_{opt} increases as d_t decreases, and second for any fixed value of d_t, as F decreases, n_{opt} decreases continuously. Note, however, that σ_t at first decreases as F decreases, but at some point further reduction in F causes σ_t to increase. The minimum σ_t value ($\sigma_t$min) and the associated value of n_{opt} for each value of d_t are underlined in Table 2-1. Note the steady decrease in σ_t that occurs as d_t and F decrease. This trend is without theoretical limit. In

Table 2-1. Theoretical values of σ_t as a function of F and d_t calculated with Snyder's model[a] for t = 300 s.

	d_t = 0.2 cm		d_t = 0.1 cm		d_t = 0.05 cm		d_t = 0.025 cm	
F_1 ($\mu L\ s^{-1}$)	n_{opt}	σ_t	n_{opt}	σ_t	n_{opt}	σ_t	n_{opt}	σ_t
50.0	1.31	2.94	5.0	2.84	19.0	3.08	70	3.60
25.0	1.00	2.46	4.2	2.13	16.4	2.14	61	2.38
16.7	0.90	2.29	3.7	1.87	14.9	1.77	56	1.90
8.3	0.60	2.16	2.9	1.58	12.4	1.35	48	1.33
4.2	0.45	2.15	2.2	1.44	9.80	1.10	40	0.98
1.7	0.25	2.31	1.4	1.42	6.8	0.96	30	0.74
0.8	0.15	2.53	0.9	1.48	5.0	0.93	24	0.65
0.4	0.08	2.80	0.6	1.60	3.3	0.96	17	0.62

[a] Values for minor variables: Y = 32 dyne cm^{-1}; $\eta = 8.9 \times 10^{-3}$ poise; $D_{w,25} = 5 \times 10^{-5}\ cm^2\ s^{-1}$. Underlined values indicate minimum n and σ_t values at each value for d_t.

practice, however, the range over which n, d_t, and F can be varied is quite limited due to restrictions imposed by the pumping system and flow cell volumes.

In CFA the multichannel peristaltic pumps used to aspirate samples into the manifold, and to proportion samples with air and reagents, are far from pulseless. Pump pulsations can cause nonuniform proportioning that is manifested as noise on the steady state portions of recorded signals. This problem is minimized if air segments are added in phase with pump pulsations, that is, at the time each roller leaves the platten surface. Under these conditions, however, n is restricted to a fairly narrow range of values that is determined by the pump speed and the number of pump rollers. The range of allowed segmentation frequencies is further restricted if bubble-through flow cells are used, because in order to measure the absorbance of individual liquid segments, the flow cell volume (V_c) must be considerably less than the liquid segment volume (V_s). Flowcells with volumes of about 2 μL (path length = 1.0 cm, ID = 0.05 cm) are commercially available and so the minimum value of V_s can be conservatively set at about 4 μL (twice V_c). At any flow rate, the maximum segmentation frequency (n_{max}) can be determined by dividing F by V_s. If the values for σ_t are now calculated assuming these restrictions, results shown in Table 2-2 are obtained. In this table values in parentheses are for n when $n_{opt} < n_{max}$. The minimum axial dispersion is achieved when d_t = 0.1 cm, with values for F in the range of 8.33 to 4.17 μL s^{-1} (0.50 to 0.25 mL min^{-1}). Choice of the higher flow rate is advantageous because, as shown in Chapter 1, dispersion due to mixing effects decreases as the flow rate increases, other things being equal. The experimental CFA system that

Table 2-2. Minimum values for σ_t as a function of F and d_t when limitations in n imposed by flow cell volume are taken into account.

		d_t = 0.2 cm	d_t = 0.1 cm	d_t = 0.05 cm
F (μL s^{-1})	n_{max} (s^{-1})[b]	σ_t (s)	σ_t (s)	σ_t (s)
50.0 (3.33)[a]	12.5	2.94 (1.3)[c]	2.84 (5.0)	3.12
25.0 (1.67)	6.2	2.46 (1.0)	2.13 (4.2)	2.34
16.7 (1.11)	4.2	2.29 (0.9)	1.82 (3.7)	2.12
8.3 (0.55)	2.1	2.16 (0.6)	1.62	2.02
4.2 (0.28)	1.0	2.15 (0.45)	1.61	2.13
1.7 (0.11)	0.4	2.31 (0.25)	1.78	2.41
0.8 (0.05)	0.2	2.53 (0.15)	1.98	2.69

[a] Values in parentheses indicate F in units of mL min^{-1}.

[b] Minimum segment volume = 4 μL = 2 V_c.

[c] Values in parentheses are for n_{opt} when $n_{opt} < n_{max}$.

I shall now describe was designed to operate within this optimum range of experimental variables.

B. Pump

The Model IP-12 variable speed, 12 channel peristaltic pump (Brinkmann Instruments, Westbury, NY) used for all work reported here was modified locally by replacing the standard roller assembly (8 rollers) with one containing 16 rollers. This pump is equipped with a two decade (00-99) digital control that allows linear adjustment of the motor speed in the range of 0 to 13.2 RPM in 0.13 RPM increments. At a speed control setting of 42, nominal and experimentally determined flow rates for Technicon SMA Flow-Rated pump tubes agreed to within about 10%. Table 2-3 lists segmentation frequencies and delivery factors associated with commonly used speed control settings.

The pump was further modified as follows. An optical chopper with 16 blades (one in line with each roller) was attached to one end of the roller assembly and an opto-interrupter (positioned so that the emitter and detector were on opposite sides of the chopper) was mounted on the pump frame. The signal from the opto-interrupter provided timing pulses that were used to synchronize injection of air segments with roller lift-off. Also, notched metal end blocks were attached to the pump housing on opposite sides of the roller assembly. These allowed pump tubes to be stretched (slightly) across the roller assembly. When pump tubes were held under constant tension in this way, flow rate stability was improved.

Technicon SMA Flow-Rated pump tubes were used in all experiments. A light spray of silicone lubricant was applied to the tubes on a

Table 2-3. Segmentation frequencies and delivery factors as a function of speed control settings on the modified Brinkmann IP-12 peristaltic pump.

Speed Control Setting	Segmentation Frequency (s^{-1})	Delivery Factor[a]
14	0.5	0.33
28	1.0	0.67
42	1.5	1.00
56	2.0	1.33
70	2.5	1.67
84	3.0	2.00
98	3.5	2.33

[a]Factor by which nominal pump tube flow rate must be multiplied to estimate actual flow rate.

weekly basis. Previous experience has shown that this practice approximately doubled tube life. A list of nominal flow rates for pump tubes at several different pump speeds can be found in Table 2-4. The 'COLOR CODE' heading in this table refers to the color of two plastic shoulders bonded to each pump tube that identify the nominal flow rate.

C. Air Segment Phasing

Two methods were used to add air segments in phase with pump pulsations. In the first method that was originally reported by Habig, et al. [27], two pump tubes (A and B) are connected as shown in Fig. 2-1A. Tube A acts as a compressor for tube B which is connected to the air inlet port of the manifold. Inside tube B, uniform segments of compressed air are trapped between rollers and when the forward roller leaves the platten, this compressed air rapidly expands into the manifold. For 0.1 cm ID manifolds, best results were obtained when the nominal flow rates of tubes A and B were 0.05 and 0.10 mL min^{-1}, respectively. I developed an alternate method for air phasing that used information from the optical chopper (described in the previous section) to actuate a normally closed miniature solenoid valve (LIF valve, Lee Company, Westbrook, CN). The inlet of the valve was connected to a source of low pressure gas (a pump tube or a cylinder of compressed gas); the outlet was connected to the air inlet port on the manifold, as shown in Figure 2-1B. The TTL pulse train from the opto-interrupter triggered a monostable-multivibrator which generated a delay pulse that was adjusted to terminate at the moment of roller lift-off. The falling edge of the delay pulse triggered a second monostable that generated the pulse used to actuate the valve. The

Table 2-4. Flow rates for standard pump tubes at various speed control settings of the IP-12 pump.

Technicon Number	Color Code	Nominal Flow Rate (mL min^{-1}) Pump Speed Control Settings 14	28	42[a]	56	70	84
116-0549P01	orn-blk	.005	.010	.015	.020	.025	.030
02	orn-red	.010	.020	.030	.040	.050	.060
03	orn-blu	.017	.033	.050	.070	.083	.100
04	orn-grn	.033	.067	.100	.130	.167	.200
05	orn-yel	.053	.107	.160	.210	.267	.320
06	orn-wht	.077	.153	.230	.310	.383	.460
07	blk-blk	.107	.213	.320	.430	.533	.640
08	orn-orn	.140	.280	.420	.560	.700	.840
09	wht-wht	.200	.400	.600	.800	1.00	1.20
10	red-red	.267	.533	.800	1.07	1.33	1.60
11	gry-gry	.333	.667	1.00	1.33	1.67	2.00
12	yel-yel	.400	0.80	1.20	1.60	2.00	2.40
13	blu-blu	.533	1.07	1.60	2.13	2.67	3.20
14	grn-grn	.667	1.33	2.00	2.67	3.33	4.00

[a]Standard speed.

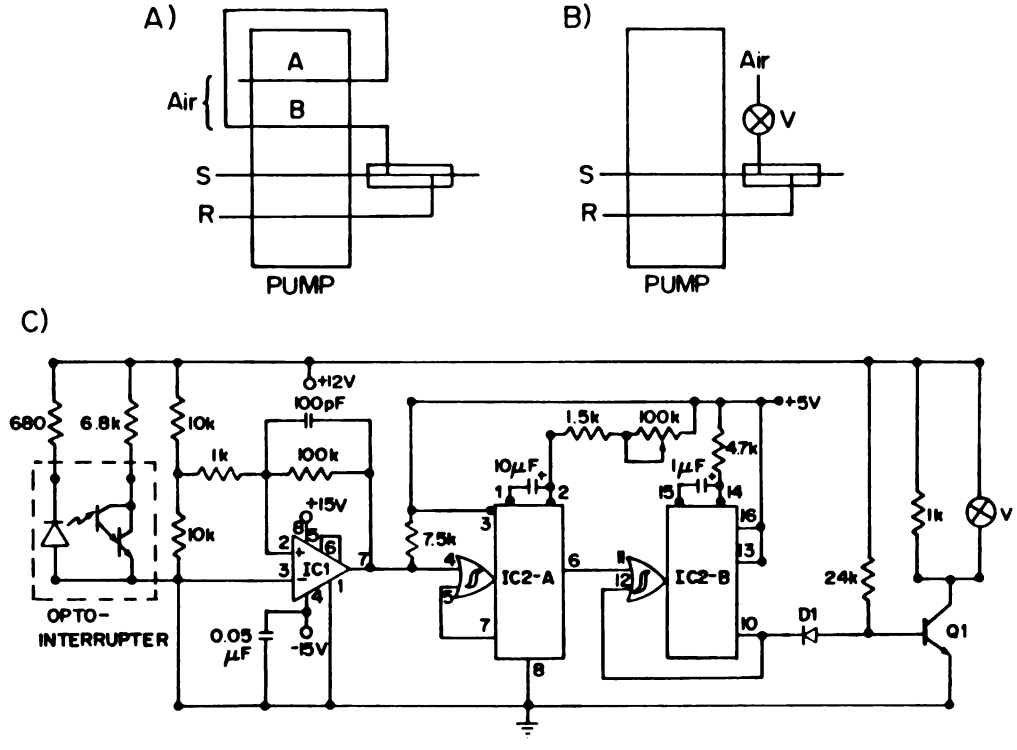

Figure 2-1. Methods for phasing air injection with pump pulsations. A) Dual pump tube method. B) Solinoid valve method. C) Schematic diagram of solinoid valve controller. IC1 = LM311 comparator, IC2 = 96LS02 dual monostable multivibrator, D1 = germanium diode, Q1 = 2N3904 NPN transistor. All resistances in ohms.

circuit diagram for the valve controller is shown in Fig. 2-1C. This method of air injection has two advantages. First, a source of compressed gas external to the pump can be used to segment the analytical stream. Thus the number of pump channels required for a given manifold can be reduced. Second, if a variable-modulus counter is added to the circuit, air segments can be added in phase with with every second, third, etc., roller lift-off. The latter feature would be particularly useful for teaching excercises. For routine work, however, I used the dual pump tube method of air segment phasing because it was simple and reliable.

D. Detector

A schematic diagram of the dual beam, fiber optic photometer designed for the miniature continuous flow analysis system is shown in Figure 2-2. Models 03000 and 03100 miniature tungsten-halogen lamps (Welch-Allyn, Skanetelles Falls, NY) were used interchangably as the light source. Both lamps have identical voltage and current requirements (3.5 V at 0.75 Amp), but the model 03100 has a flame formed lens that approximately doubles the radiant energy impinged on the fiber optic bundle. These lamps are rated for only 20 hours of operation at 3.5 Volts, but lifetimes in excess of 150 hours were obtained when the lamps were operated at about 3.3 volts, as was customary.

An EK-15 randomized, bifurcated fiber optic bundle (Dolan-Jenner, Woburn, MA) made from either glass or quartz fibers was used to transmit light from the source to the front windows of the flowcells. The fiber optic-flowcell interfaces are rectangular, black delrin blocks that slide along dovetail grooves machined in the base plate of

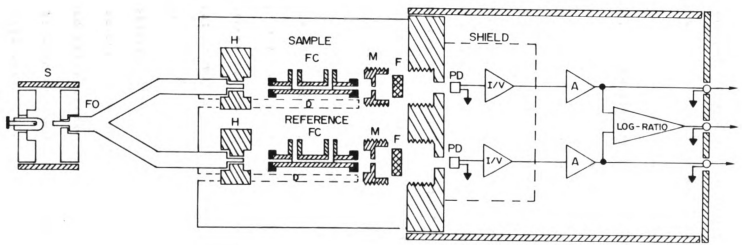

Figure 2-2. Schematic representation of the dual-beam, fiber optic, filter photometer designed for the mCFA system. S = source, FO = randomized, bifurcated fiber optic bundle, H = fiber optic/flow cell holder, D = dovetailed slide, FC = flow cell, M = flow cell/interference filter mount, F = interference filter, PD = photodiode, I/V = operational amplifier current-to-voltage converter, A = second stage amplifier.

the photometer. Flowcells with saphire windows, a 1.0 cm pathlength, and an internal diameter of 0.05 cm were obtained commercially (PN 178-B724-02, Technicon Instruments, Tarrytown, NY). Generally the reference channel was used only to compensate for source drift and in these cases a 1.5 cm x 0.2 cm diameter delrin rod, center bored with a 0.05 cm hole, replaced the reference flowcell. Wavelength discrimination was accomplished with 1.27 cm diameter, narrow bandwidth ($\sim$8 nm), 3-cavity interference filters (Ditric Optics, Hudson, MA). Threaded, circular mounts machined from black delrin hold the interference filters in place centered directly in front of the photodiodes. The front faces of these mounts were center drilled to allow insertion of the rear flowcell end cap to a depth of about 0.2 cm. This arrangement allows for easy installment and removal of flowcells and interference filters, and insures proper optical alignment.

Silicon photodiodes with an operational range of 200-1200 nm (HUV-040B, E.G. & G., Electro-optics Division, Princeton, NJ) were used as detectors. These were operated without external bias to minimize dark current. Photocurrent was converted to voltage with simple operational amplifier current-to-voltage converters that had fixed transfer functions of about 2×10^8 V/A. The photodiodes and current-to-voltage converters were shielded from other circuit elements by a metal cover. It should be noted that these photodiodes have a maximum response at about 900 nm, and interference filters with good near IR blocking properties must be used to avoid stray light problems. Variable gain (2-100) second stage amplifiers invert and amplify signals from the current-to-voltage converters. The gain of each amplifier is adjusted with a 10-turn potentiometer. These were mounted on top of the photo-

meter housing and permitted the sample and reference signals to be balanced, usually at a level of about 5 volts. This type of electronic balancing provided an effective and much simpler alternative to mechanical slits. Sample and reference signals are connected to the inputs of a log-ratio amplifier (AD755, Analog Devices, Norwood, MA). This device provides an output of 1.0 volt per absorbance unit. Base line drift of the sample and reference channels are approximately 10% per hour for the first hour and about 1-2% per hour thereafter, but as expected, drift of the ratioed signal is negligible over the same time intervals. Sample, reference, and log-ratio outputs are made accessible through BNC connectors mounted on the rear panel of the photometer housing. Refer to Figure 2-2 for further details. Schematic diagrams for the photometer's first and second stage amplifiers are shown in Figure 2-3.

E. Bubble Gate

The electronic bubble gate that removes the air segment artifact from the detector signal when bubble-through flow cells are used with the photometer has been described previously [29]. A detailed schematic diagram of this bubble gate is shown in Figure 2-4. Note that a second sample-and-hold amplifier was added to this circuit so that both transmittance and absorbance (log-ratio) signals could be acquired simultaneously. A full description of this device operating over a wide range of experimental conditions can be found in Chapter 3. A different circuit that can be used to trigger and clear the buble gate's monostable multivibrator is shown in Figure 2-5. This circuit appears to eliminate the need to autorange the comparator threshold level (see Chapter 3, B.3, and Figure 3-2), but is has not been

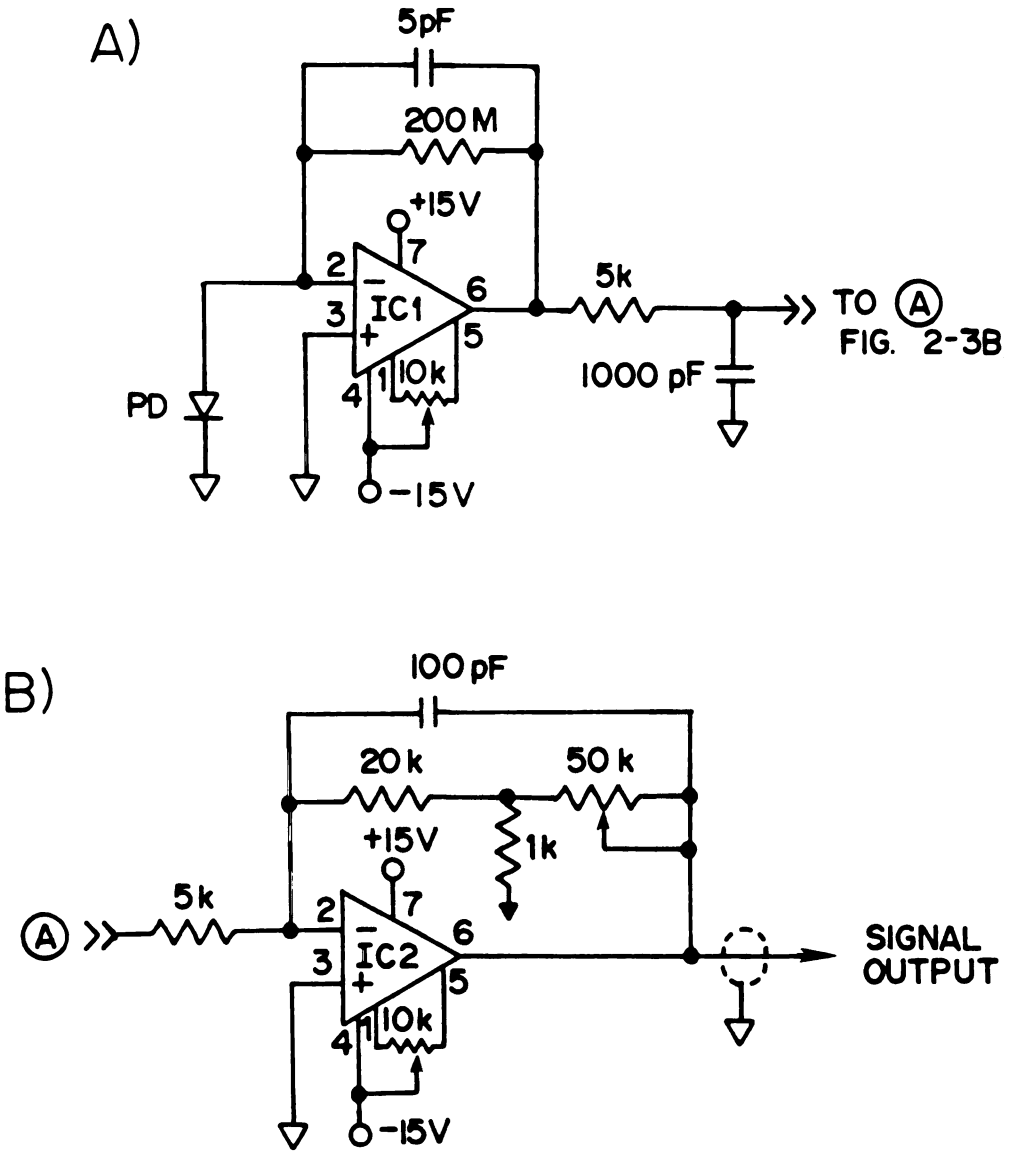

Figure 2-3. Schematic diagrams of detector circuits. A) Photodiode (PD) and current-to-voltage converter. B) Second stage variable-gain inverting amplifier. IC1 and IC2 = LF351 FET input operational amplifiers. All resistances in ohms. Power supply bypass capacitors omitted for clarity.

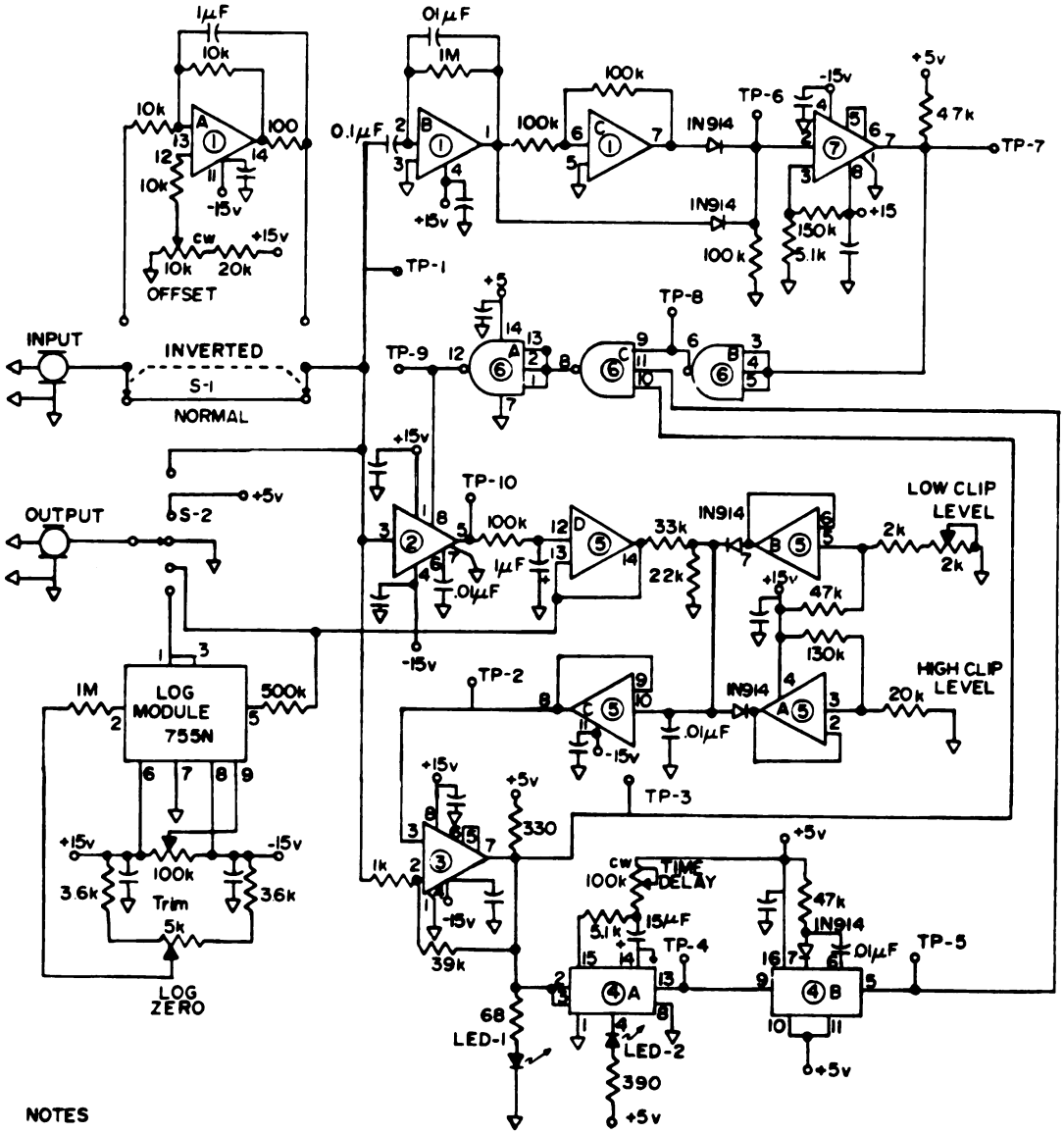

NOTES

1. ○ = Chip #
2. Circuits are as indicated:
   - ①⑤ TL084
   - ② LF398N
   - ③⑦ LF311N
   - ④ SN74LS123N
   - ⑥ SN7410N
3. All P.S. Bypass Caps are .047μF

Figure 2-4. Detailed schematic diagram of the bubble gate designed for the mCFA system.

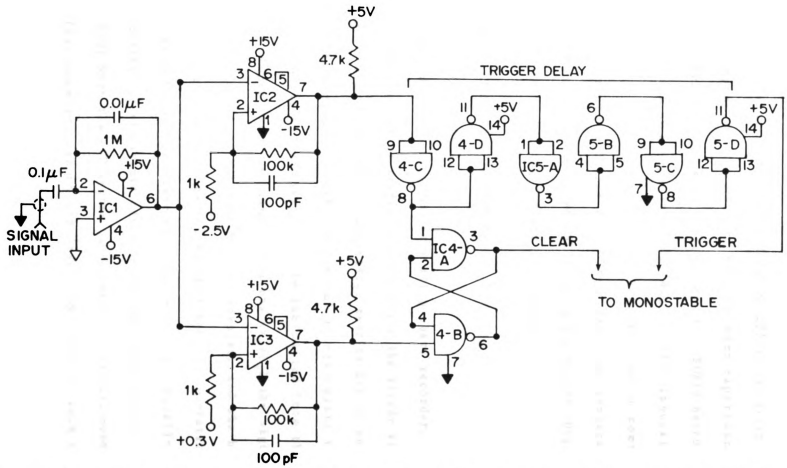

Figure 2-5. Schematic diagram of a modified circuit to trigger and clear the monostable multivibrator of the bubble gate. IC1 = LF351 operational amplifier. IC2,IC3 = LM311 voltage comparators. IC4,IC5 = SN7400 quad 2-input NAND gates. All resistances in ohms.

characterized fully at present.

F. Data Acquisition

Data were recorded with a Model SR-255 10 in. strip chart recorder (Heath Company, Benton Harbor, MI). In many experiments, data were logged simultaneously with a microcomputer. FORTH based software routines written by Eugene Ratzlaff [41], in this laboratory, acquired data points (voltage and time of acquisition) on command from the update pulse of the bubble gate. These data were temporarily stored in RAM and later shipped to an LSI 11/23 minicomputer (Digital Equipment Corp., Maynard, MA) for further processing.

G. Data Processing Techniques

1. Data Reduction

When data are recorded on a strip chart recorder, data reduction is a simple matter of reading and recording the steady state absorbance value of each peak. Before analytical results can be calculated, however, the baseline absorbance , which is equivalent to the reagent blank in batch colorimetry, must be subtracted from the peak absorbance. Under usual sampling conditions ($t_s > t_w$) the signal level does not return fully to baseline between samples, and the baseline absorbance for each peak is estimated by linear interpolation between the initial and final baseline absorbance values. Baseline drift due to instability of electronic circuits and the light source is less than 1% per hour when the mCF system is operated in the dual beam mode. Larger drifts, however, can result from other factors such as build up of particulate matter on flow cell windows, instability of reagents, or partial blockage of pump tubes. If the refractive index of samples is

significantly different from that of the wash solution, a small fraction of the total absorbance measured for a sample is due to refractive index effects. The contribution of refractive index to the absorbance measured for a sample can be quantitated if the normal reagent solution is substituted with one from which the reagent necessary for chromophore formation has been omitted. When samples are redetermined under these conditions, the baseline corrected absorbance of the resulting peaks is due only to refractive index changes. Corrections are made by subtracting these values from the peak heights measured under standard conditions.

2. Graphical Procedures for Estimation of b and σ_t

As discussed in Chapter 1, two constants, b and σ_t, provide measures of longitudinal and axial dispersion, respectively, and therefore describe for the performance of a given CFA system. Both these constants can be extracted from rise or fall curves by simple, graphical procedures. The data plotted in Figure 1-2 will be used to provide working examples of these procedures. Data for this figure were obtained experimentally with a manifold similar to the one shown schematically in Figure 1-1A. In this system values for n, d_t, F, and t were 2 s^{-1}, 0.1 cm, .014 mL s^{-1}, and 85 s, respectively. Samples were aqueous phenol red solutions and the reagent was borate buffer (pH=10) containing Brij-35 surfactant. The analytical stream flowed sequentially through two identical flow cells (1.0 cm x 0.05 cm ID). The first flow cell was bubble gated while the second was debubbled, and data (time and voltage) from both flow cells were acquired simultaneously with a microprocessor. Data were then shipped to the LSI 11/23 minicomputer where they were converted to absorbance and then

smoothed and derivatized by means of a moving, 7-point polynomial Savitzky-Golay algorithm [42]. The smoothed data points were also regenerated according to Equation 1-3. Processed data acquired for the rise curve of the high concentration sample (the broad center peaks in Figure 1-2) with the bubble gated and debubbled flow cells are listed in Tables 2-5 and 2-6, respectively. Values of b used to regenerate these data sets were determined as described below.

Inspection of Equation 1-1 reveals that b is simply the inverse negative slope of the linear portion of a plot of $\ln(A_{ss}-A_t)$ versus time. In Figure 2-6 smoothed absorbance values and smoothed values for the difference between A_{ss} and A_t are plotted as a function of time for both data sets. The right y-axis in this figure is logarithmic and pertains to the $(A_{ss}-A_t)$ values, while the left y-axis is linear and relates to the A_t values. See the figure caption for further details. The slopes of the linear portions of the logarithmic plots for data obtained with the bubble gated and debubbled flow cells were -0.736 and -0.371, respectively, which correspond to b values of 1.36 s and 2.70 s. Note that the flow cell debubbler approximately doubled the magnitude of longitudinal dispersion for this CF system.

It is also possible to determine b emperically by regenerating the data sets with different values for b and plotting the results on a graphics terminal. If the value chosen for b is too small, regenerated peaks will still appear to be exponentially deformed. Larger than optimum values for b on the other hand result in regenerated peaks that are excessively noisy and have large spikes at the leading edge of rise and fall curves that extend above and below the sample and base line steady state absorbance levels. Optimum b values determined in

Table 2-5. Data for the first 10 s of the rise curve for the steady state peak shown in Figure 1-2. This data set pertains to the bubble gated flow cell.

time (s)	A_t [a]	A_t^* [b]	dA_t^*/dt	$A_t^\dagger$ [c]	ln $(A_{ss}-A_t^*)$	$A_t^\dagger$ norm
63.49	.0096	.0043	.0429	.0472	-.2000	.9524
64.01	.0180	.0225	.0837	.1061	-.2225	.8801
64.54	.0590	.0732	.1312	.2044	-.2879	.7594
65.05	.1600	.1593	.1737	.3330	-.4099	.6015
65.53	.2771	.2726	.1999	.4725	-.5971	.4303
66.01	.3938	.3931	.2045	.5977	-.8442	.2766
66.52	.5031	.5013	.1888	.6902	-1.1341	.1630
*67.03 [d]	.5945	.5921	.1595	.7516	-1.4658	.0877
67.54	.6640	.6629	.1253	.7882	-1.8320	.0427
68.04	.7136	.7140	.0930	.8071	-2.2164	.0195
68.55	.7490	.7490	.0655	.8146	-2.6037	.0103
69.03	.7722	.7720	.0443	.8163	-2.9757	.0082
69.50	.7863	.7869	.0291	.8160	-3.3215	—
*70.00	.7955	.7960	.0190	.8150	-3.6119	—
70.50	.8021	.8022	.0126	.8149	-3.8728	—
70.98	.8062	.8066	.0088	.8154	-4.1105	—
71.46	.8103	.8097	.0067	.8164	-4.3200	—
71.99	.8116	.8123	.0054	.8176	-4.5375	—
72.51	.8144	.8147	.0043	.8190	-4.7915	—
73.01	.8172	.8169	.0033	.8202	-5.0995	—
73.50	.8186	.8186	.0022	.8208	-5.4262	—

[a] A_t = raw absorbance.

[b] A_t^* = smoothed absorbance.

[c] $A_t^\dagger$ = regenerated absorbance.

[d] *...* inclusive data points used to calculate regeneration factor. See text for details.

Table 2-6. Data for the first 10 s of the rise curve for the steady state peak shown in Figure 2-1. This data set pertains to the debubbled flow cell. All other notation is shown in Table 2-5.

time (s)	A_t	A_t^*	dA_t^*/dt	$A_t^\dagger$	$\ln (A_{ss}-A_t^*)$	$A_t^\dagger$ norm
68.55	.0118	.0100	.0248	.0670	-.2070	.9243
69.03	.0184	.0210	.0480	.1315	-.2206	.8392
69.50	.0449	.0492	.0765	.2250	-.2564	.7170
70.00	.0968	.0976	.1050	.3390	-.3210	.5695
70.50	.1643	.1629	.1280	.4574	-.4154	.4179
70.98	.2391	.2385	.1418	.5647	-.5370	.2824
71.46	.3157	.3169	.1451	.6506	-.6810	.1757
*71.99	.3944	.3931	.1391	.7129	-.8442	.1003
72.51	.4644	.4627	.1270	.7548	-1.0208	.0517
73.01	.5239	.5232	.1118	.7804	-1.2046	.0240
73.50	.5733	.5735	.0960	.7942	-1.3883	.0108
73.99	.6158	.6167	.0810	.8030	-1.5784	.0037
74.50	.6524	.6526	.0675	.8080	-1.7696	.0009
75.01	.6850	.6832	.0559	.8117	-1.9675	—
75.53	.7060	.7077	.0459	.8133	-2.1602	—
76.03	.7281	.7268	.0374	.8129	-2.3413	—
76.54	.7420	.7426	.0304	.8125	-2.5195	—
77.02	.7550	.7564	.0250	.8139	-2.7091	—
77.50	.7685	.7669	.0207	.8145	-2.8806	—
77.99	.7760	.7758	.0171	.8151	-3.0534	—
*78.47	.7824	.7836	.0140	.8159	-3.2340	—

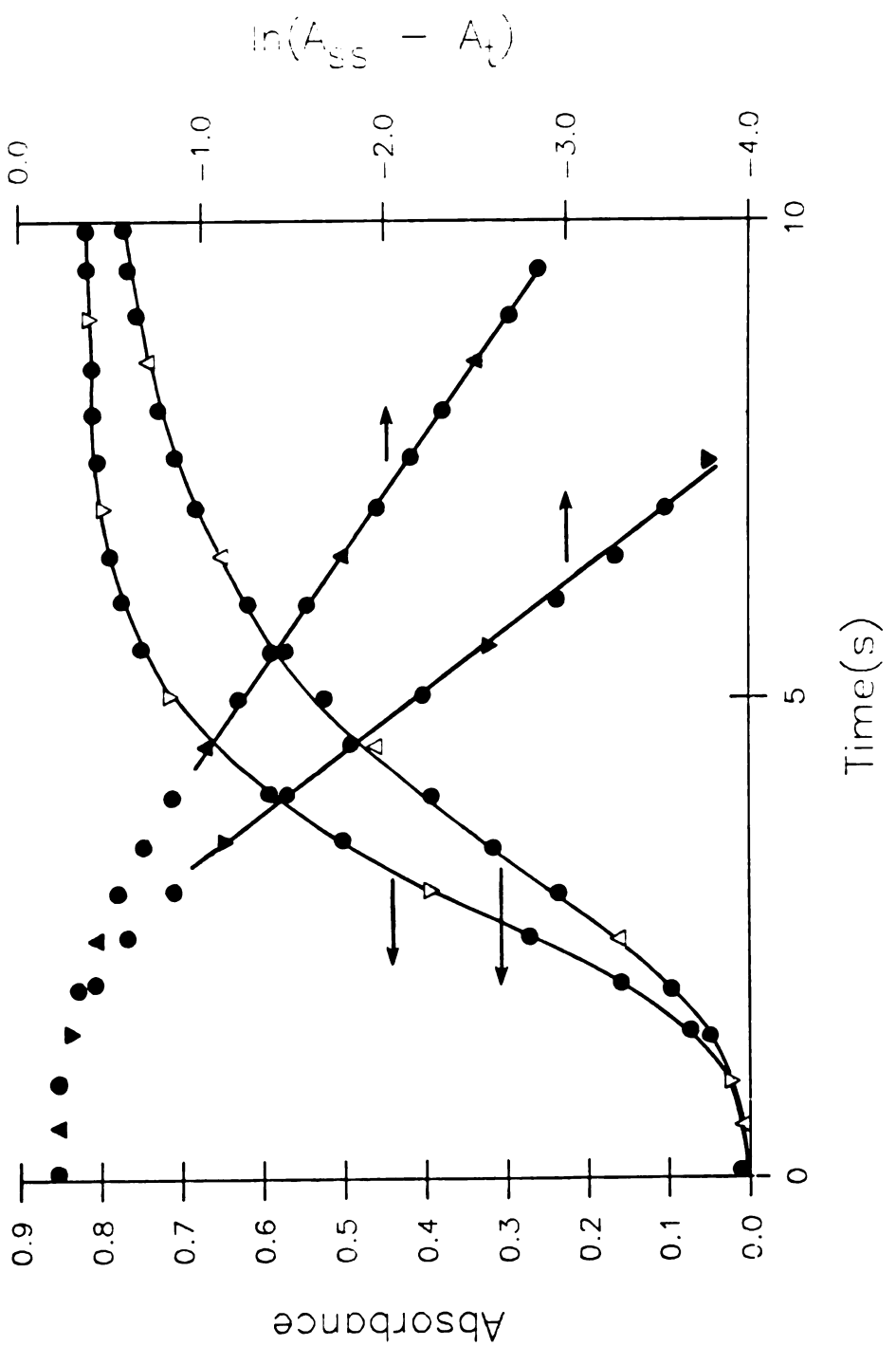

Figure 2-6. Extraction of b from rise curves of CFA peaks. Bubble gated flow cell: ∇ = smoothed A_t points, ▼ = smoothed (A_{ss}-A_t) points. Debubbled flow cell: Δ = smoothed A_t points, ▲ = smoothed (A_{ss}-A_t) points.

this way for the bubble gated and debubbled data sets were 1.0 s and 2.3 s, respectively. These values are somewhat smaller than those determined graphically. This is because the derivative of absorbance with respect to time that is required to regenerate the data amplifies both the hydraulic and electronic noise associated with the CF system. In this regard, the choice of smoothing parameters can have a pronounced effect on the quality of regenerated data. I found that 5 to 7-point Savitzky-Golay smooths and derivatives gave the best results with this CF system.

As shown in Figure 1-3, regeneration of both data sets resulted in peaks that closely resembled the integrated Gaussian curves predicted by Snyder's model. The value of σ_t can be estimated by plotting the values for regenerated data points on a cumulative probability scale as a function of time [17]. Because the limits of the probablity scale are 0 to 1, regenerated data must be normalized by dividing the difference between the sample steady state absorbance and the regenerated absorbance at each time, by the difference between the absorbance of the sample and baseline steady states [17]. Values for normalized, regenerated data can be found in the last column of Tables 2-5 and 2-6. As shown in Figure 2-7, normalized points of both data sets fall on the same straight line. Thus the assumption that regenerated peaks approximate cumulative Gaussian curves is good. On the cumulative probability scale, the interval between 0.16 and 0.50 corresponds to one standard deviation. This interval is indicated by dashed horizontal lines in Figure 2-7. Vertical lines dropped from the points where the horizontal lines intersect the plot cross the time axis at 2.4 s and 3.7 s (Δt=1.3 s). Thus σ_t measured for this CF system (n=2 s^{-1},

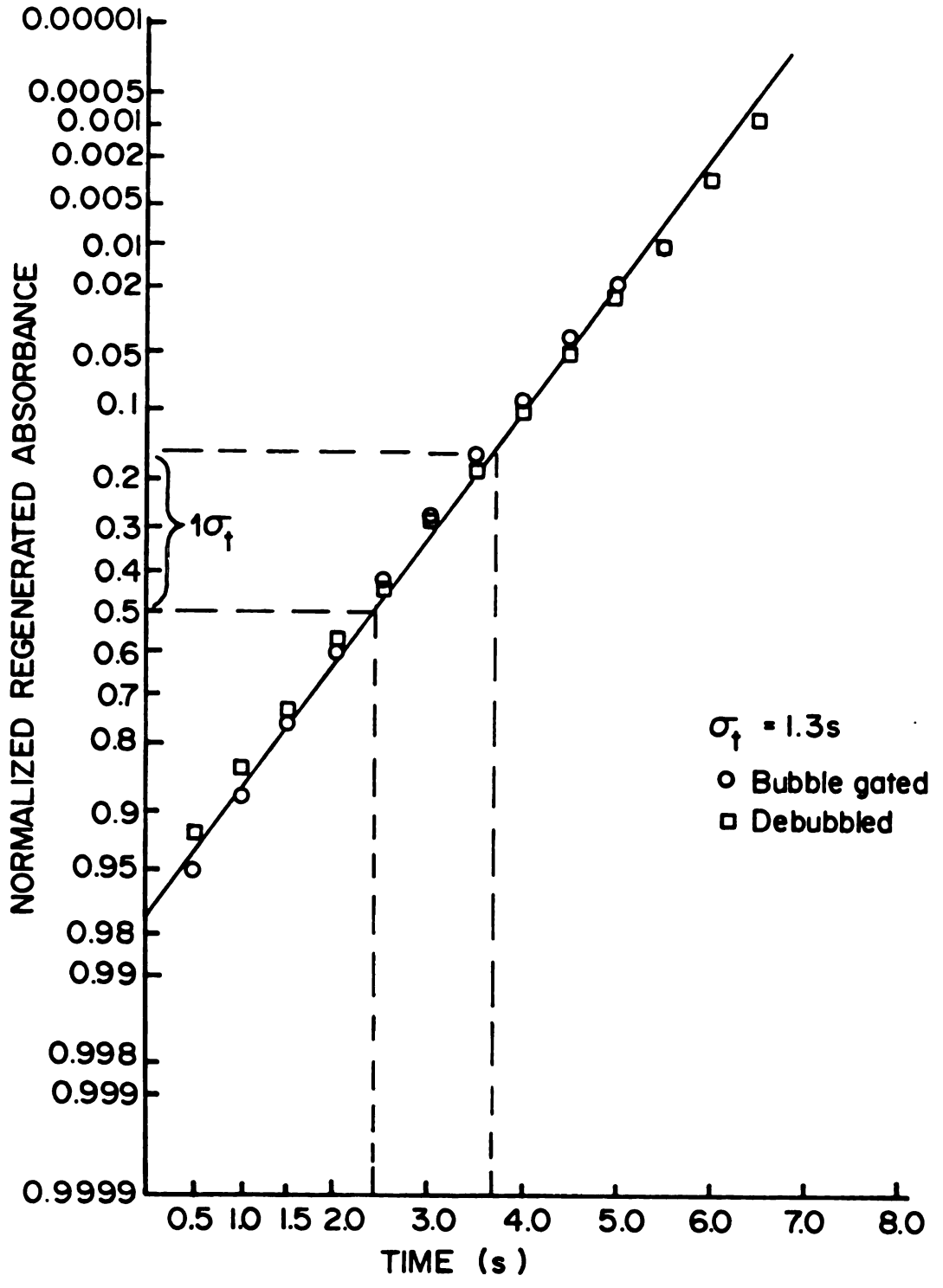

Figure 2-7. Graphical estimation of σ_t by means of a cumulative probability plot.

d_t=0.1 cm, F=.014 mL s^{-1}, t=85 s) is approximately 1.3 s. This compares favorably with the value calculated with Snyder's model (σ_t=1.0 s) assuming these values for major variables, and values for minor variables as in the first section of this chapter.

H. Manifold Components

1. CFA

For the most part, manifold components (mixing coils, connectors) were fabricated locally. Glass tubing (1.0 cm ID x 2.3 cm OD) in various lengths was wrapped around 0.8 cm or 3.0 cm mandrels in the Chemistry Department Glass Shop. The resulting coiled glass tubes served as mixing and time delay coils, respectively. The latter were mounted in water tight plexiglass jackets so that they could be thermostated by means of a circulating water bath. For many applications mixing coils fabricated from 0.10 cm ID x 0.18 cm OD Micro-line tubing (#18160, Thermoplastics Scientifics, Inc., Warren, NJ) were highly suitable. To form coils the tubing was wrapped around glass rods. Tube ends were secured to the rod with masking tape. The rod was immersed in boiling water for about one minute and then removed and placed in cold water for about five minutes. A similar method was used by Amador [43] to fabricate mixing coils from polyethylene tubing. These plastic coils have a number of advantages. They are easy to make, inexpensive, flexible, unbreakable, and compatible with Omnifit flangeless gripper fittings (Thermoplastics Scientifics, Inc., Warren, NJ) that allow zero dead volume connections to be made between coil ends and reagent addition tees. The major disadvantage of these plastic coils is that they are considerably less wettable than glass coils.

Therefore hydraulic instability (surging due to back pressure, and bubble break-up) is likely to occur. Usually these problems can be eliminated if the surfactant concentrations in reagents are approximately doubled relative to the concentrations that would be used for a glass manifold. For determinations that are adversely affected by surfactants or that require heating to acceleratre chemical reactions, glass mixing coils are best.

Specially designed fittings are required to connect sample, air, and reagent pump tubes to various points along the flow system of the CFA instrument. It is particularly important to minimize the dead volume of these fittings to prevent increased dispersion due to mixing effects. In general fittings should have central bores that match the inside diameters of mixing coils and side arm bores that are no larger than those of the pump tubes to which they are connected. A large assortment of manifold fittings are commercially available from a number of suppliers, but they are relatively expensive. For this reason I designed the fittings illustrated in Fig. 2-8 that were fabricated in the Chemistry Department Machine and Glass Shops. For most applications only two basic fitting types are required: 1) sample inlet blocks, and 2) reagent addition tees. These fittings were machined from plexiglass rods. The central and side arm bores were 0.10 and 0.05 cm, respectively. Pump tubes are connected to the fittings by means of stainless steel side arms (0.05 cm ID). These press-fit into holes drilled at right angles to the center bore of the fitting. Side arms were secured with epoxy cement. Further construction details for inlet blocks and reagent tees can be found in Figures 2-8A and 2-8B, respectively. Flow stream debubblers were constructed from

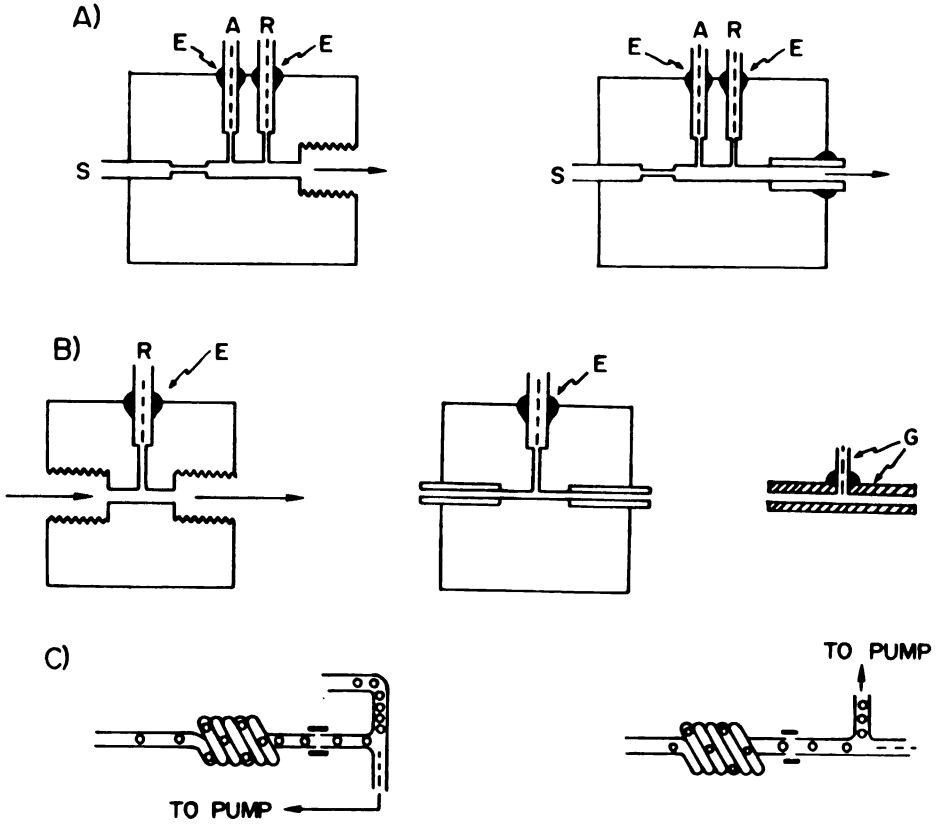

Figure 2-8. Manifold components designed for the mCFA system. A = air inlet, R = reagent inlet, S = sample inlet, E = epoxy cement, G = glass. A) sample inlet blocks: left, used for plastic coils. Right, used for glass coils. B) Reagent addition tees: left, used for plastic coils. Middle and right used for glass coils. C) Flow stream debubblers.

0.10 cm ID glass tubing. Debubblers can be used in two ways. Either the bubbles can be pumped away, usually at about twice the rate at which they were introduced, or the analytical stream can be pumped away at about 75% of the total (air + liquid) flow rate so that bubbles (and a small portion of each liquid segment) are forced to waste. Both configurations are illustrated in Figure 2-8C. The former is generally used to debubble flow streams prior to passage through packed bed reactors, while the latter is generally used to debubble flow cells. Readers with an interest in more exotic fitting types are refered to William Furman's, Continuous Flow Analysis: Theory and Practice [6].

2. FIA Manifold Components

Reaction coils for FIA manifolds are generally constructed from flexible, nonwettable, polymeric tubing. In this work open tubular reactors were made from lengths of 0.05 cm ID Teflon ^{TM} tubing. Tubes were terminated with Omnifit flangeless gripper fittings and then wrapped in tight overlapping coils around a 1.0 cm diameter glass rod. The coiled tubing was slipped off the rod and secured at two points with plastic cable ties. Packed single bead string reactors (SBSRs) were fabricated from 0.08 cm ID Teflon tubing and 0.05 cm diameter glass beads (Propper Manufactoring Company, Long Island City, NY). A gripper fitting was attached to one end of the tube which was then crimped (directly above the gripper fitting) with a pair of surgical forceps. A disposable pipet tip (the tip must be trimmed slightly to allow free passage of the beads) was attached to the other end of the tube by means of a plastic sleeve. This assembly was then mounted in a vertical position and the pipet tip was partially filled with the glass beads. When the pipet tip was tapped gently, the beads began to enter

and fill the tube. I found that the packing procedure worked best when the pipet tip and tube were completely filled with water before the beads were added. The packed tube was crimped just above the topmost bead and terminated with a gripper fitting. The SBSR was then coiled and secured with cable ties.

Three different modes of sample injection (A-C) were used for FIA experiments as illustrated in Figure 2-9. In mode A, a Type 50 six-port rotary valve (Rheodyne Inc., Cotati, CA) was used. A shaft attached to the valve core was turned manually to switch between the 'LOAD' and 'INJECT' positions. Dual and single four-port slider valves (Alltech Associates, Deerfield, IL) were used for modes B and C, respectively. The sliders on these valves were pneumatically actuated. External sample loops determined the injected sample volume in modes A and B. In mode C sample volume was determined by the time interval that the slider remained in the 'INJECT' position. Reproducible timing was achieved by means of a microprocessor controlled valve actuator [44]. The parts of both valve types in contact with solutions were made from Teflon and had 0.8 cm bores. The tee connectors used for reagent addition are illustrated in Figure 2-9D. Details of more specialized manifold components can be found in Ruzicka and Hansen's Flow Injection Analysis [10].

I. Plumbing

Short lengths of Teflon tubing (.04 cm ID, .05 cm OD) were used for sample and reagent withdrawal lines. These were attached to pump tubes either by direct insertion, or by means of plastic sleeves if there was a poor match between the ID of the pump tube and the OD of

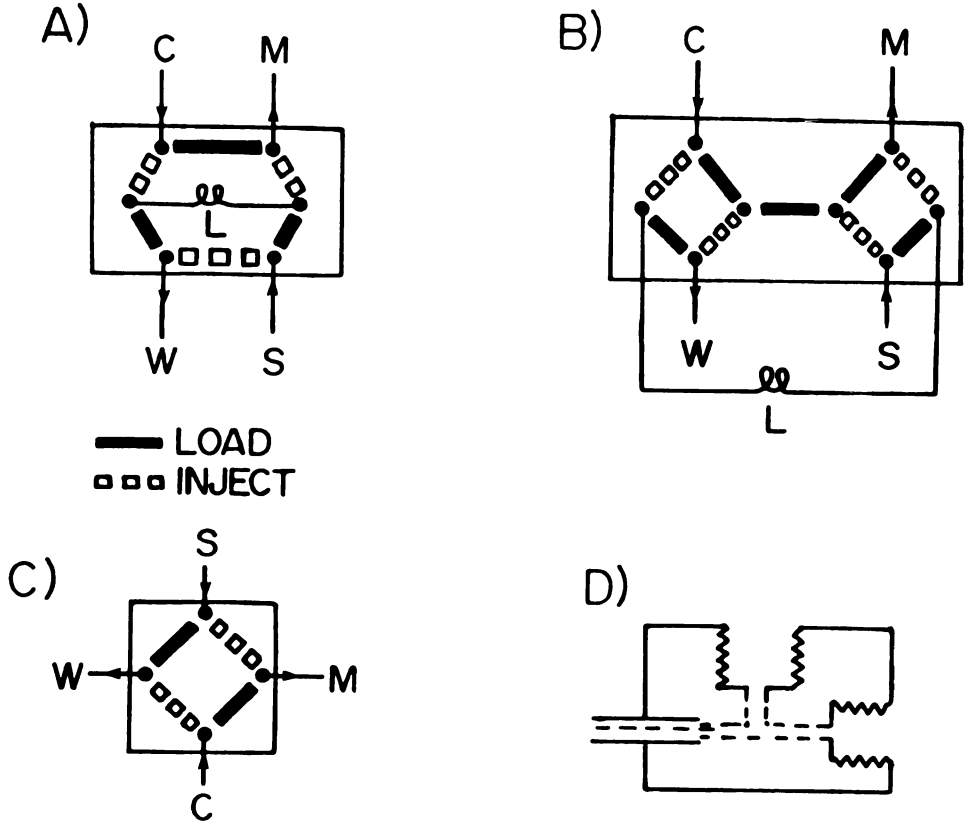

Figure 2-9. Manifold components for FIA. C = carrier stream inlet, M = to manifold, W = to waste, S = sample inlet, L = sample loop. A) Six-port rotary valve. B) Dual four-way slider valve. C) Single four-way slider valve. D) Reagent addition tee.

the Teflon tube. The same techniques were used to connect the delivery end of the pump tubes to manifold fittings (see Figures 2-10A and 2-10B). A stock of worn pump tubes were kept on hand from which sleeves were made. Plastic sleeves were also used to connect glass mixing coils to fittings on CFA manifolds. Note that the coil and fitting ends must be butted securely within the sleeve. Otherwise the integrity of the air segmented stream was degraded (e.g. -- air bubbles were trapped in the void volume between the coil and fitting ends) and increased dispersion due to mixing effects was noticeable. The LC fittings used in conjunction with plastic mixing coils (for both CFA and FIA) insured zero dead volume connections (see Figures 2-10C and2-10D).

A few words about sample introduction methods used for FIA and CFA are in order here. In FIA it is best to withdraw samples from their containers into the sample loop as shown in Figure 2-11A. Note that in this configuration, the sample does not pass through the pump before it reaches the sample loop. Therefore the time required to fill the sample loop is short and cross contamination of successive samples is minimized. In CFA on the other hand, samples generally pass through the pump before they enter the manifold a shown in Figure 2-11B. Because the sample moves through the pump tube under essentially laminar flow conditions, considerable mixing occurs either between successive samples, or between a sample and the wash solution. The intersample air segment (IAS) that enters the sample line when it is cycled between a sample and the wash solution (or the reverse) provides a partial barrier to intersample mixing. If additional IASs are introduced at the start of each sample and wash interval by rapid,

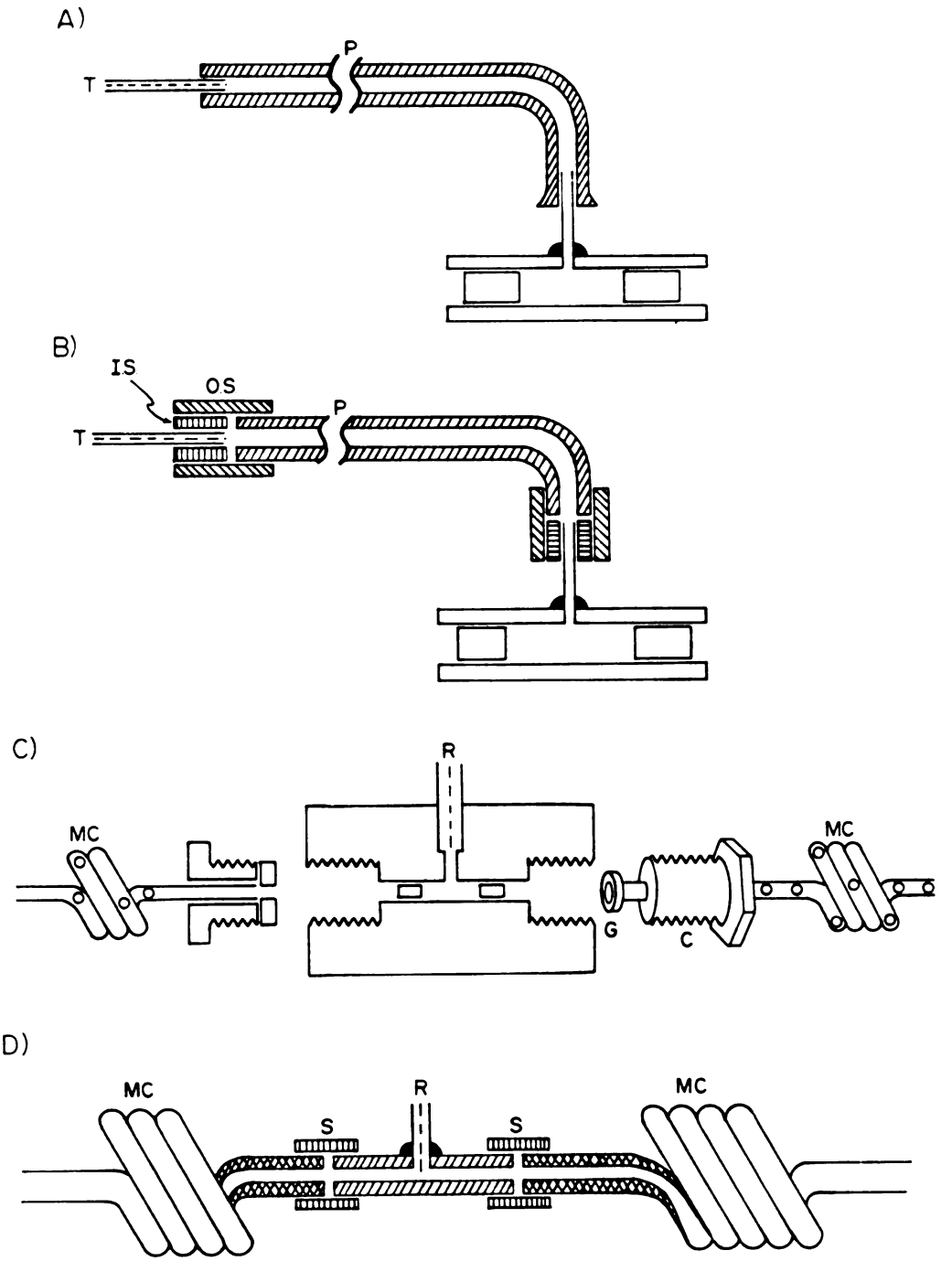

Figure 2-10. Methods for interconnecting various manifold components used for continuous flow analysis. T = teflon tubing, P = pump (not shown), I.S. = inner plastic sleeve, O.S. = outer plastic sleeve, MC = mixing coil, R = reagent inlet, G = gripper fitting, C = standard HPLC connector, S = plastic sleeve.

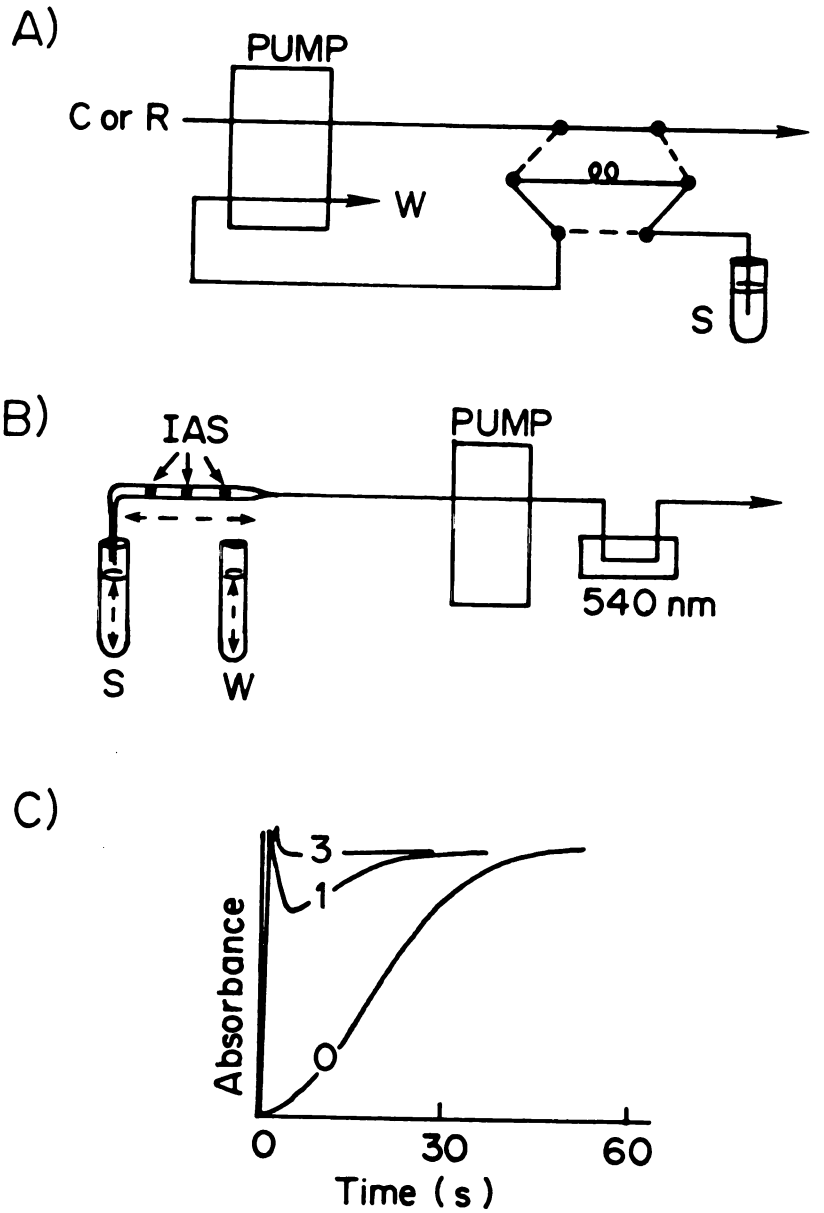

Figure 2-11. A) Preferred method of sample introduction for FIA systems. C = carrier stream, R = reagent, S = sample, W = to waste. B) Pecked sample introduction used for CFA systems. S = sample, W = wash solution, IAS = intersample air segment. C) Effect of IAS on dispersion that occurs in the sample lines of CFA systems.

repetitive withdrawal and insertion of the sample line ('pecking'), mixing within the pump tube can be greatly reduced as shown in Figure 2-11C.

This figure is a generalized composite of data collected from a number of individual experiments in which no manifold was used. Instead, one end of a pump tube was connected directly to the flow cell and the other end was fitted with a 20 cm length of Teflon tubing (.025 cm ID) that served as the sample withdrawal line as shown in Figure 2-11B. The sample and wash solutions used in these experiments were alkaline phenol red and distilled water, respectively. The absorbance at 540 nm (λ_{max} for alkaline phenol red) was recorded while the sample line was manually cycled between the two solutions at 60 s intervals. As previously mentioned, one IAS forms naturally when the sample line is transferred from one solution to the other. The IAS can be eliminated, however, if the pump is turned off during this operation. Additional IASs can be introduced by pecking. In this way the amount of dispersion that occurred in the sample line and pump tube was monitored as a function of the number of IASs introduced at the leading edge of each sample and wash slug at several different flow rates.

Results for one set of experiments where the flow rate was 0.32 mL min^{-1} are shown in Figure 2-11C. With no IAS, dispersion in the sample line and pump tube was large. With one IAS, dispersion was reduced, but still significant. With three IASs, however, dispersion was almost eliminated. As expected, in the absence of an IAS, dispersion decreased as the flow rate increased. When three IASs were introduced at the leading edge of each sample and wash slug, however, dependence of dispersion on flow rate was minor. These experiments underscore the

importance of pecked sampling for minimum dispersion in CFA experiments.

CHAPTER 3

DESIGN AND CHARACTERIZATION OF AN ELECTRONIC BUBBLE GATE FOR AIR-SEGMENTED CONTINUOUS FLOW ANALYSES

A. Overview

As already mentioned, photometric detection with CFA systems is complicated by the presence of air segments in the analytical stream. In commercially available first and second generation systems, the analytical stream is debubbled just prior to detection. Unfortunately, this expedient allows previously segregated liquid segments to mix in the debubbler and flow cell, and therefore the rate at which analyses can be performed is reduced. As shown in Chapter 2, mixing effects that occur in flow cell debubblers and flow cells can be removed (after the fact) by analog [45,46] or digital [47] curve regeneration techniques, or they can be eliminated by using bubble-through flow cells and a gated detector (bubble gating) as is done with the Technicon third generation SMAC clinical analyzer. This chapter deals exclusively with the latter approach.

Habig and co-workers [27] appear to have developed the first bubble gate, which was activated by conductance changes within a specially designed flow cell. They concluded, however, that their design was preliminary and was not suitable for routine use. Subsequently a more robust electronic bubble gate was described by Neeley,

et al. [28]. The same group later reported a slightly modified version of this circuit [48] which they incorporated into a high performance colorimeter for a miniaturized CF analyzer. This bubble gate repetitively sampled and stored the detector signal at a frequency determined by an adjustable internal time base. Then, for a fixed time interval, the stored signal level was compared with the real-time signal level by means of a window comparator circuit. When the stored and real-time signal levels were within the limits of the window comparator, the real-time signal level was stored in a second sample-and-hold circuit connected to the readout device.

The bubble gate reported here is much simpler. It uses the periodic fluctuations of the detector signal, caused by the successive passage of air and liquid segments through the flow cell, to synchronize the time of data acquisition and temporary storage with the brief interval during which each liquid segment completely fills the flow cell. Data are presented to demonstrate that improved performance of both commercially available and custom built CF analyzers can be achieved using the bubble gate described. The analytical performance of a miniature CF (mCF) system with 0.1 cm ID manifold components and a bubble gated detector used for the colorimetric determination of nitrite and silicate in water is presented. Results of nitrite determinations obtained with mCF system are compared with those reported for flow injection analysis.

B. Experimental

1. CF Systems

The filter photometer used with the mCF system is described fully in Chapter 2. The 0.2 cm ID manifold CF (AAII CF) system consisted of a Pump III (with air bar), and an Industrial S.C. colorimeter equipped with 1.5 cm x .15 cm ID debubbling flow cells and 540 nm interference filters (Technicon Instruments Inc., Tarrytown, NY). In bubble gating experiments with the AAII CF system, the Technicon colorimeter was modified by removing capacitors C-201, C-203, and C-204 from the 'control module' circuit board. This modification reduced the rise time of the detector signal from about 0.3 s to about 10 ms. Also, the sample side debubbling flow cell was removed and replaced with a 1.5 cm x .1 cm ID bubble-through flow cell (Gamma Enterprises, Inc., Mt. Vernon, NY). The cell was mounted directly onto the phototube housing with an adaptor to occlude the phototube entrance and exclude stray light. The colorimeter was then adjusted in the usual manner. The 'telemetry output' (0-5 V) of the colorimeter was connected to the bubble gate described below through a unity gain inverting amplifier with offset. This made the logarithmic output of the colorimeter compatible with the logic of the bubble gate which is described in detail below.

Manifold components for the AAII CF system were obtained commercially from standard sources, while those for the mCF system were for the most part custom made as described in Chapter 2. Technicon SMA Flow-Rated Pump tubes were used for both systems.

Data were recorded with a Model SR-255 10 inch strip chart recorder (Heath Co., Benton Harbor, MI). In some experiments data were simultaneously logged with a microcomputer (see Chapter 2).

2. Determination of Nitrite and Silicate

a. Nitrite Reagents

The sulfanilamide (SAN) reagent was prepared by dissolving 10 g SAN in 500 mL of deionized, distilled water (DDW) and 100 mL of concentrated HCl contained in a 1 L volumetric flask. This solution was diluted to the mark with DDW, mixed, and transferred to an amber bottle. Then 0.5 mL Brij-35 wetting agent was added.

The N-(1-Naphthyl) ethylenediamine dihydrochloride (NED) reagent was prepared by dissolving 1.0 g NED in 1 L of DDW. This solution was transferred to an amber bottle, and 0.5 ml Brij-35 was added.

b. Nitrite Standards

The primary nitrite standard was prepared by dissolving 0.345 g (5 mmol) of dried, analytical reagent grade sodium nitrite in 1 L DDW. Working standards in two ranges were prepared by dilution of the primary standard using digital microliter pipets and volumetric flasks.

c. Silicate Reagents

The molybdate reagent was prepared by dissolving 10.8 g of ammonium molybdate and 2.8 mL of concentrated sulfuric acid in about 500 mL of DDW contained in a 1 L volumetric flask. This solution was diluted to the mark with DDW, mixed, and transferred to a plastic bottle. Then 2 mL of an aqueous sodium lauryl sulfate solution was added.

The tartaric acid reagent was prepared by dissolving 100 g of tartaric acid in 950 mL of DDW contained in a 1 L plastic bottle.

The stock stannous chloride solution was prepared by dissolving 10 g of stannous chloride in 20 mL of 50% (V/V) hydrochloric acid.

Heating is sometimes required to effect complete dissolution. This solution was stored in a plastic bottle.

The working stannous chloride reagent was prepared by adding 0.5 mL of the stock reagent to 50 mL of 1.2 N HCl solution contained in a plastic bottle. This solution is not stable for more than about 8 hours.

The wetting agent was prepared by dissolving 10 g of sodium lauryl sulfate in 100 mL of DDW.

d. Silicate Standards

The primary silicate standard was prepared by fusing 0.3007 g (5 mmol) of dried silicon dioxide (Alfa-Ventron, 99.9%) with 0.7 g of sodium carbonate in a platinum crucible. Heating was effected with a compressed air-natural gas flame. After the melt formed a glass ($\simeq$5 min), heating was discontinued and the crucible was allowed to cool. When cooling was complete, DDW was added to the crucible which was then covered and allowed to stand overnight. The next day the contents of the crucible were transferred quantitatively to a 1 L volumetric flask. This solution was diluted to the mark with DDW and transferred to a plastic bottle.

Working standards in the range of 5 to 45 μM were prepared by dilution of the primary standard by means of digital microliter pipets and 100 mL volumetric flasks. Working standards were transferred to plastic bottles immediately following their preparation to avoid the possibility of silica in the glass volumetric flasks being leached into the standards.

3. Bubble Gate

When bubble-through flow cells are used with colorimetric, air-segmented CF analyzers, the detector signal closely resembles a square wave. With an air-segmented blank solution the detector output varies between the 100% T level (5.0 V in our case) and the 0% T level (0.0 V), as shown in Figure 3-1. As an air segment traverses the flow cell, it reflects most of the light away from the photodetector, and the signal approaches the 0% T level (0.1 to 0.4 V in our case). The actual magitude of the signal observed in the presence of an air segment is somewhat erratic, and it decreases as the transmittance of the two adjoining liquid segments decreases. When the air segment exits the flow cell, the detector rapidly rises to a level that corresponds to the transmittance of the liquid segment (see Figure 3-1). The bubble gate described here uses the information encoded in the periodic fluctuations of the detector signal to synchronize the time of data acquisition and temporary storage with the brief interval during which each liquid segment completely fills the flow cell.

The schematic diagrams presented in Figure 3-2 depict the functional units of the bubble gate circuit. In the basic bubble gate circuit (Figure 3-2A) comparator IC1 converts the detector signal to a TTL logic level signal that indicates the presence or absence of an air segment in the flow cell. This is accomplished by setting the threshold level of the comparator at about 0.5 V. A HI logic level at the output of the comparator indicates the absence of an air segment in the flow cell. Note, however, that the logic level transitions of the comparator lag the entrance and exit of air segments into and out of the flow cell by several ms because of the time required for the

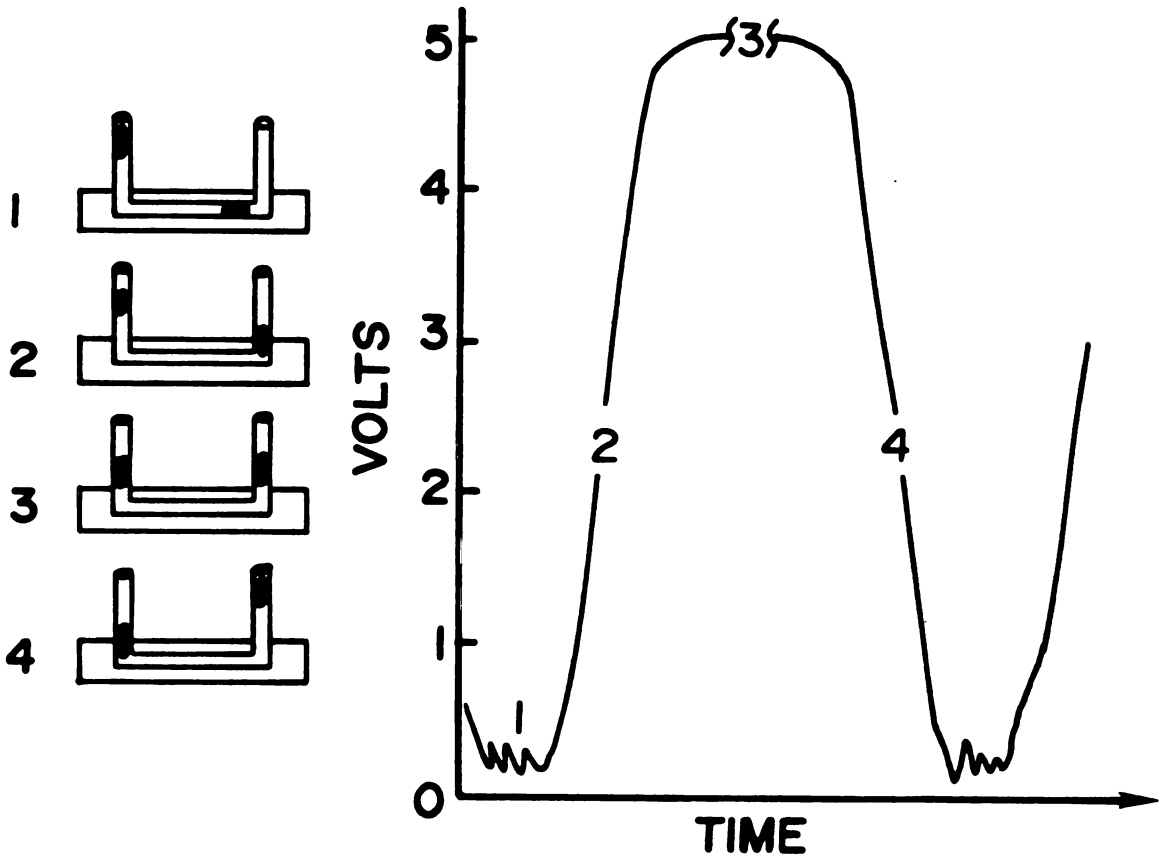

Figure 3-1. Fluctuations in the detector signal caused by the successive passage of liquid and air segments through the flow cell: Position 1, air segment completely within cell. Position 2, air segment exiting cell. Position 3, cell completely filled by liquid segment. Position 4, air segment entering cell.

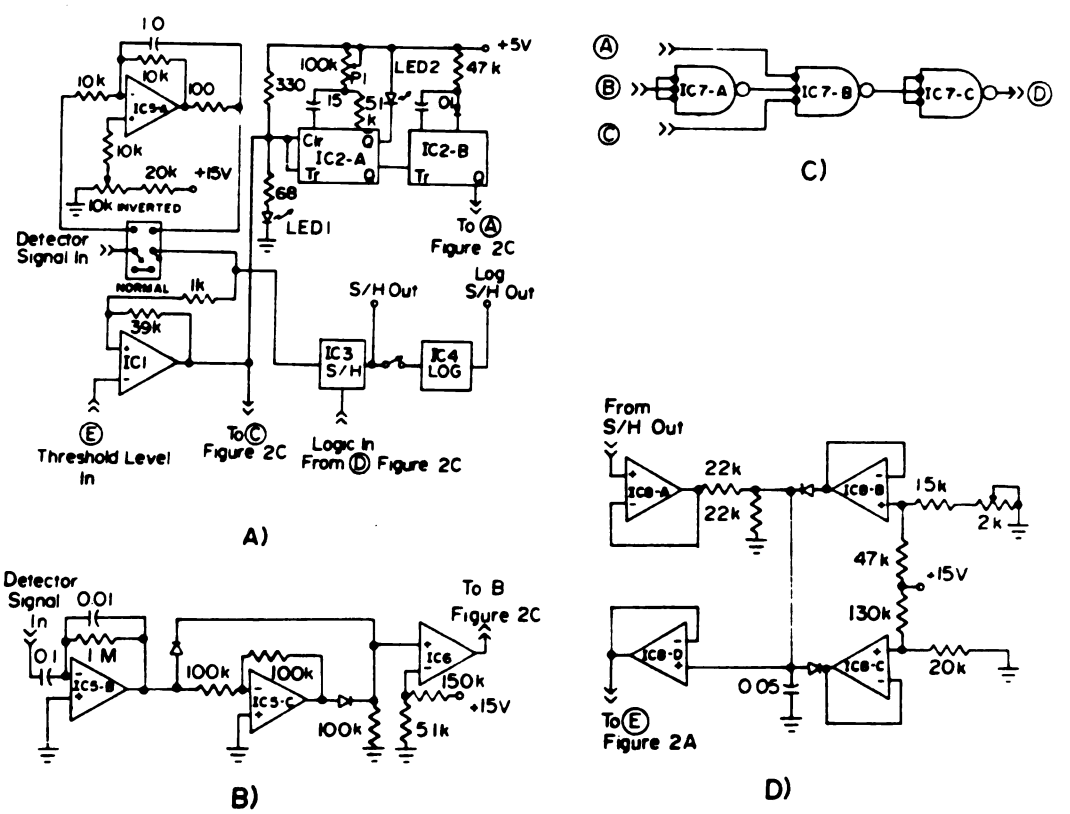

Figure 3-2. Generalized schematic diagrams of bubble gate circuitry. All resistances in ohms, all capacitances in microfarads. A) Basic bubble gate, IC1 = LF311 FET input comparator, IC2, 74LS123 dual monostable multivibrator, IC3 = LF398 sample-and-hold amplifier, IC4 = AD755 logarithmic amplifier, IC5 = TL084 quad FET input operational amplifier. B) Differential edge sensor, IC5 = TL084 quad FET input operational amplifier, IC6 = LF311 FET input comparator. C) Sample-and-hold amplifier update logic, IC7 = 7410 triple 3-input NAND gate. D) Automatic threshold adjustment for comparator, IC1. IC8 = TL084 quad FET input operational amplifier.

detector signal level to cross the threshold level of the comparator. The rising edge of the comparator output triggers monostable multivibrator IC2-A, which generates a time delay pulse. The duration of this pulse is adjusted with potentiometer P1 to terminate at the approximate midpoint of the interval during which a liquid segment completely fills the flow cell. Two light emitting diodes (LED1 and LED2) facilitate this adjustment by giving visual indication of the logic states of the comparator and monostable, respectively. The falling edge of the time delay pulse triggers monostable IC2-B which generates a pulse with a fixed width of approximately 100 μs. A gated version of this 100 μs pulse is used to update sample-and-hold amplifier IC3 which samples on a TTL HI and holds on a TTL LO.

Irregularities in the segmentation pattern of the analytical stream, generated when the sample probe is cycled between samples and the wash solution, can produce two conditions which cause the basic bubble gate to malfunction. First, irregular liquid segments that completely fill the flow cell for a time interval much shorter than the selected time delay interval cause the comparator and the monostable to get out of phase; several liquid segments of normal length must pass through the flow cell before these two circuit elements are again synchronous. Erroneous sample-and-hold amplifier updates could occur in the interim. This problem was corrected by clearing monostable IC2-A with the falling edge of the comparator output so that the time delay pulse is aborted in the event that it is still in progress when an air segment enters the flow cell. Second, irregular liquid segments that completely fill the flow cell for a time interval approximately equal to the duration of the delay pulse can cause incorrect sample-and-hold

amplifier updates because of the lag between the initial entry of an air segment into the flow cell and the logic level transition of the comparator output as discussed previously. This problem was eliminated with the differential edge sensor circuit shown in Figure 3-2B, which generates a TTL HI at its output whenever the detector signal has a non-zero derivative. Because the output of this circuit responds to changes in the detector signal level almost instantaneously, it can be used to eliminate the possibility of sample-and-hold amplifier updates at the time of initial entrance or exit of an air segment into or out of the flow cell. Three conditions must be sastisfied in order to update the sample-and-hold amplifier:

1) The output of the monostable IC2-B must be HI.

2) The output of the differential edge sensor must be LO.

3) The ouput of comparator IC1 must be HI.

Figure 3-2C shows the logic that prevents sample-and-hold amplifier updates when the above conditions are not satisfied.

This bubble-gate circuit will not operate when the signal level of a liquid segment is less than the threshold level of comparator IC1. If the threshold level of the comparator were to be fixed at 0.5 V, liquid segments with transmittance less than about 0.1 would be indistinguishable from air segments, and the bubble gate would be restricted to an operational range of 100% T to 10% T. However, because an air segment's effective transmittance is not constant but decreases as the transmittance of the two liquid segments adjoining it decreases, it is possible to extend the lower operational limit of the bubble gate considerably by using the detector signal level stored in the sample-and-hold amplifier for automatic adjustment of the

comparator threshold to an appropriate level. This function is performed by the circuit shown in Figure 3-2D. A buffered voltage divider applies one-half of the sample-and-hold amplifier output to the threshold level input of comparator IC1 through a unity gain buffer (IC8-D). Two active diode clippers limit the maximum and minimum threshold levels to about 2 V (fixed) and 0.1 V to 0.5 V (adjustable), respectively. This circuit extends the bubble gate's lower limit of operation to about 3% T (1.5 A), and in addition improves performance in the high transmittance range because it provides greater separation between the comparator threshold level and the somewhat erratic detector signal produced by the passage of air segments through the flow cell.

A logarithmic amplifier (Model AD755, Analog Devices, Norwood, MA) is also included in the bubble gate circuitry so that peak heights are linear functions of concentration.

A detailed schematic diagram of the bubble gate can be found in Chapter 2.

It should also be noted that bubble-gating can be accomplished with a microcomputer and appropriate software. Apparently this approach was used by the designers of the Technicon SMAC clinical CF system.

C. Results and Discussion

1. Introduction

The bubble gate was tested with the Technicon AutoAnalyzerII CF System (AAII CF System) and the mCF system described in Chapter 2. The colorimetric determinaion of nitrite via a modified Griess reaction

procedure [49] was chosen as the reference assay with which the performance of the two CF systems could be evaluated and compared. A composite manifold diagram for both CF systems is shown in Figure 3-3. Pecked sampling did not improve the performance of either the standard or the bubble-gated AAII CF system noticeably. As described in Chapter 2, however, it did improve the performance of the mCF system. Therefore, pecked sampling was used routinely with the mCF system. For both systems the time required to reach steady state and the percent interaction were determined as described below.

2. Steady State Experiments

A set of five aqueous nitrite standards with nominal concentrations of 5 μM, 15 μM, 25 μM, 35 μM, and 45 μM were prepared, and the detector gain was adjusted such that these standards produced a response of approximately 10%, 30%, 50%, 70%, and 90% full scale, respectively, on the strip-chart recorder. With the AAII system each standard was sampled in triplicate for 5 s, 10 s, 20 s, 30 s, 40 s, 50 s, and 60 s with a 60 s wash between each sample to minimize carryover. With the mCF system each standard was sampled in triplicate for 5 s, 10 s, 15 s, 20 s, 25 s, 30 s, and 60 s with a 30 s wash between each sample. The average peak height for each sampling interval was divided by the steady-state peak height (60 s sampling interval) and multiplied by one hundred to obtain the per cent of steady state (%SS) as a function of sample time. A grand average of %SS for all five standards at each sampling interval was then calculated. The results of this calculation showed that %SS was independent of concentration to within about 1% for the 5 s and 10 s sampling intervals and to within about 0.5% for sampling intevals greater than 10 s. The increased scatter in

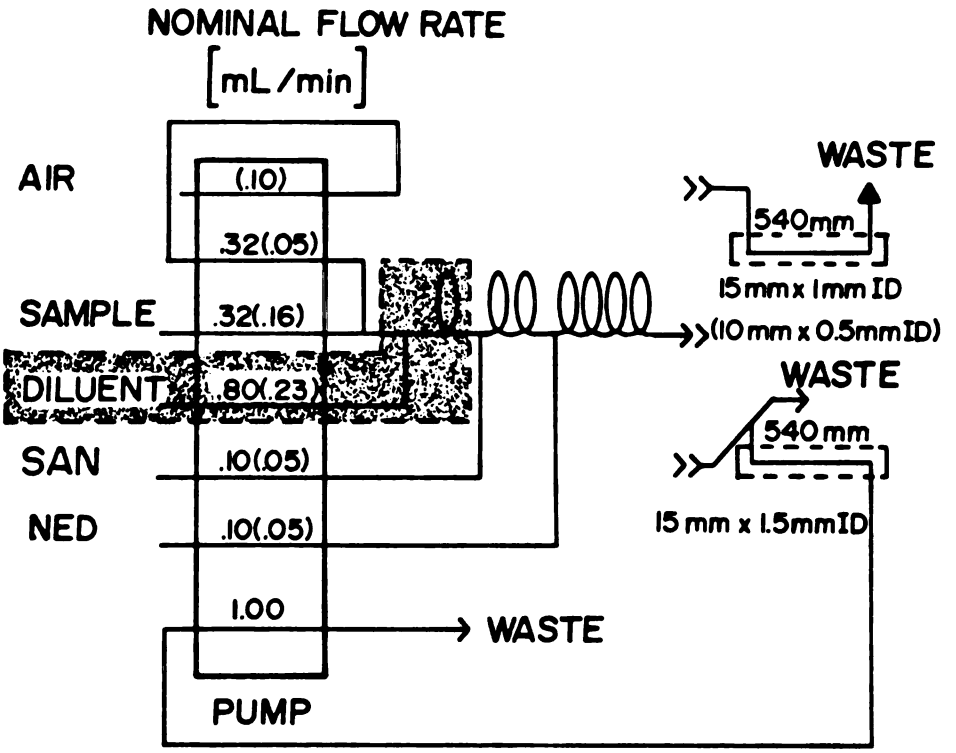

Figure 3-3. Composite diagram of various CF manifolds used for nitrite determinations. Values outside or within parentheses refer to AAII or mCF manifolds, respectively.

the peak heights at shorter sampling intervals is probably a result of the manual sampling employed.

Results of the %SS experiments are presented graphically in Figure 3-4. Values for major experimental variables can be found in Table 3-1 as well as the estimated dispersion, σ_t, of the air segmented sample slug during its passage through the CF system. The latter quantity was calculated according to the model of Snyder and Adler [25,20]. Values of minor variables shown in Table 3-1 were in keeping with a similar set of calculations by Snyder [32].

As shown in Fig. 3-4, bubble gating reduced the sampling time required for the AAII CF system to reach 98 %SS by about 8 s. A similar reduction in the sampling time required for the mCF system to reach 98 %SS was achieved by using the pecked sampling techique. An apparent trend for the mCF system also shown in this figure is a decrease in the sampling time required to attain a given %SS as the segmentation frequency, n, increases. Note, however, that with the mCF system, n was increased by increasing the pump speed (and therefore the liqiud flow rate, F) in order to keep air segmentation in phase with the roller lift off of the peristaltic pump, as discussed in Chapter 2. Thus the residence time, t, for the sample slug in the manifold decreased as n and F increased (see Table 3-1). To differentiate between the effects of n and F, the experiment was repeated for $n = 1.5\ s^{-1}$, $F = 0.0067\ mL\ s^{-1}$ and $n = 3.0\ s^{-1}$, $F = 0.014\ mL\ s^{-1}$ with t held constant at 110 s by altering the length and number of mixing coils in the manifold. As shown in Figure 3-5, the same trend was observed. These results were were contrary to the predictions of Snyder's model [10] (see Table 3-1). This was not surprising, because

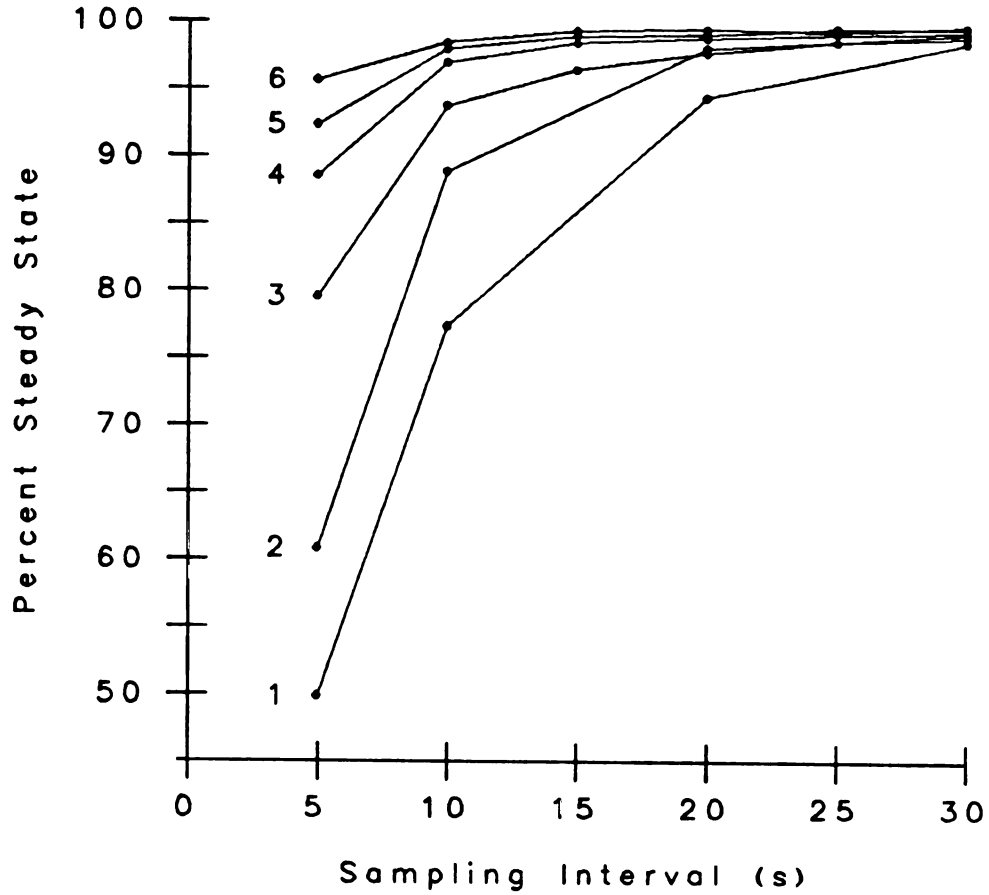

Figure 3-4. Results of percent steady state (%SS) experiments: 1, standard AAII CF system. 2, bubble gated AAII CF system. 3, bubble gated mCF system without pecked sampling. 4-6, bubble gated mCF system with pecked sampling and n equal to 1.5, 2.0, and 3.0 s^{-1}, respectively.

Table 3-1. Major variables[a] for %SS experiments.

Experimental Variable	AAII CF SYSTEM		mCF SYSTEM					
	Standard	Bubble Gated	Without Pecking	With Pecking				
Flow cell path length (cm)	1.5	1.5	1.0	1.0	1.0	1.0	1.0	1.0
Full scale absorbance[b]	≅0.5	≅0.6	0.5	0.5	0.5	0.5	0.5	0.5
Pump speed control setting	—	—	42	42	56	84	42	84
n (s^{-1})	0.5	0.5	1.5	1.5	2.0	3.0	1.5	3.0
d_t (cm)	0.2	0.2	0.1	0.1	0.1	0.1	0.1	0.1
F_ℓ (ml s^{-1})	0.022	0.022	0.0067	0.0067	0.0083	0.013	0.0067	0.013
t (s)	200	200	130	130	100	65	110	110
σ_t calc (s)	—	2.13	1.08	1.08	0.94	0.82	0.99	1.07

[a] minor variables: viscosity (η) = 8.9×10^{-3} poise, surface tension; (γ) = 3.2×10^{1} dyne cm^{-1}; effective diffusion coefficient ($D_{w,25}$) = 5×10^{-5} cm^2 s^{-1}.

[b] For the standard and bubble-gated AAII CF systems, Standard Calibration Control settings were 2.32 and 2.02, respectively.

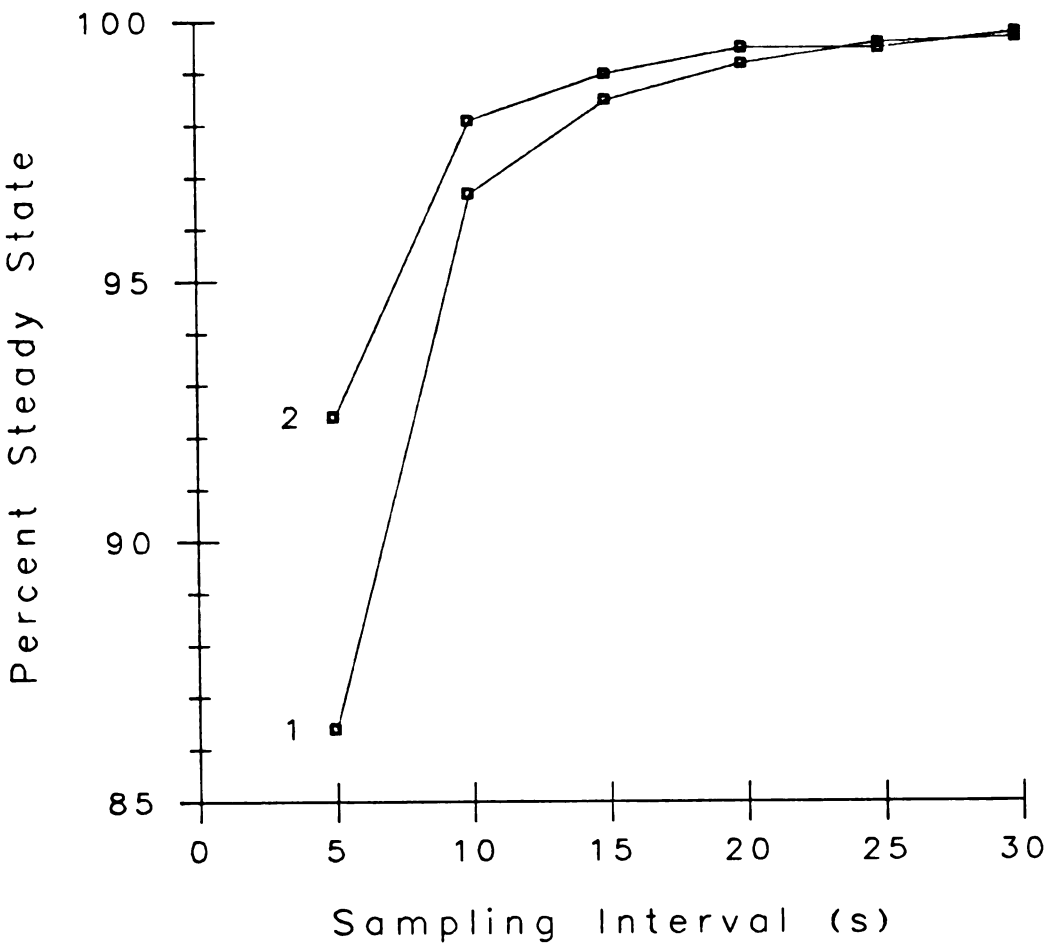

Figure 3-5. Effect of segmentation frequency and liquid flow rate on %SS with the residence time of the sample slug in the mCF system held constant at 110 s: 1, n = 1.5 s^{-1}, F = 0.0067 mL s^{-1}. 2, n = 3.0 s^{-1}, F = 0.013 mL s^{-1}.

Snyder's model assumes that mixing effects in unsegmented zones of the CF system are negligible. As discussed in Chapter 2, this assumption is weak even for CF systems with bubble-through flow cells. Other factors being equal, mixing effects decrease as the flow rate increases. At standard pump speed, approximately 20 seconds elapse between the time of sampling and the time at which the leading edge of the sample slug is segmented with air. Doubling the pump speed halves this interval. As demonstrated earlier, pecked sampling and bubble gating reduce mixing effects, but clearly do not eliminate them. This set of experiments suggests that the decreased dispersion of the sample slug observed when the pump speed was doubled resulted primarily from a decrease in mixing effects and that the concomitant doubling of the segmentation frequency had little effect.

3. Sample Interaction

Percent interaction (%I) was determined by the method of Thiers, et al. [50]. Nitrite standards in the concentration sequence of 5 μM, 45 μM, 5 μM were used throughout the experiments. Sampling intervals for the AAII and mCF systems were fixed at 30 s and 25 s, respectively, and %I was determined as a function of wash interval. When the second low standard produced a shoulder peak, the peak height just prior to the fall was recorded. Results of these experiments can be found in Table 3-2. On the AAII CF system with and without bubble gating, 1.0 %I was achieved using 10 s and 15 s wash times, respectively. On the mCF system a 5 s wash time resulted in 1.0 %I and 0.5 %I at standard and twice standard pump speeds, respectively. The decrease in %I at higher flow rates is again presumed to result primarily from decreased mixing effects as discussed previously.

Table 3-2. Percent interaction.

	AAII CF SYSTEM		mCF SYSTEM		
Wash Interval(s)	Standard	Bubble Gated	$n=1.5\ s^{-1}$	$n=2.0\ s^{-1}$	$n=3.0\ s^{-1}$
5	1.7	1.0	1.0	0.7	0.4
10	1.4	0.8	0.5	0.4	0.2
15	0.8	0.5	0.2	0.2	<0.1
20	0.5	0.3	0.1	<0.1	<0.1
30	0.2	0.1	—	—	—

4. Mixing Effects

It is apparent from the foregoing experiments that mixing effects contribute significantly to the observed loss of wash in both of the CF systems used for this study. I was able to minimize mixing effects in the mCF system by using standard pump tubes with nominal flow rates approximately half that of the desired flow rate, and then operating the pump at about twice standard speed. Under these conditions analysis rates which approximate theoretical limits assuming Snyder's 8 σ_t criteria [10], were achieved as is demonstrated in the final section of this chapter. A better approach would be to use a miniaturized pump fitted with shorter pump tubes. It is also possible to remove the effects of longitudinal dispersion by means of curve regeneration as described in Chapter 2.

D. Analytical Results

1. Nitrite Determinations

Aqueous nitrite standards were determined with the mCF analyzer with the manifold shown in Figure 3-3. Note that the dilution pump tube and first mixing coil (shaded area of Figure 3-3) were omitted to increase sensitivity. A nitrite concentration range of 2 μM to 18 μM was chosen to allow direct comparison of the mCF procedure with a recent flow injection analysis (FIA) procedure for the determination of nitrite [51]. The FIA procedure used the merging zones technique to minimize reagent consumption and a novel 'intermittant flow' technique to increase the sampling rate. Performance of the mCF system at several sampling rates in terms of linearity of standard curves, %I, and the precision of five replicate determinations of the 6 μM standard can be

found in Table 3-3. Recordings of data obtained at analysis rates of 360 hr^{-1} and 120 hr^{-1} are shown in Figure 3-6. Also listed in Table 3-3 are experimental conditions and performance criteria reported for the FIA procedure.

Inspection of Table 3-3 reveals that even at a sampling rate of 360 hr^{-1}, where precision was limited because of manual sampling, the performance of the mCF system is comparable to that of the FIA system which had a maximum sampling rate of about 70 hr^{-1}. Note also that on a per assay basis, the sample and reagent requirements of the mCF system were less than those of the FIA system. These results conflict with the usual claims made about the performance of FIA relative to CFA. The sampling rate of about 70 hr^{-1} reported by Zagatto, et al. [12] is somewhat superior to sampling rates generally achieved with second generation CFA systems, but is decidedly inferior to sampling rates achieved with the mCFA system. Furthermore, the FIA system required an elaborate system of valves to inject both samples and the reagent into the carrier stream, and to vary the flow rate of the carrier stream during the course of each determination. In this respect the mCFA system is much simpler than the FIA system with the exception of the gated detector.

2. Silicate Determinations

Aqueous silicate standards were determined with the manifold shown schematically in Figure 3-7. All mixing coils were made from 0.1 cm ID Micro-line tubing. The lengths of tubing used to make the first, second, and third mixing coils were approximately 250 cm, 100 cm, and 50 cm, respectively. These provided about 230 s, 70 s, and 30 s reaction times after the addition of the molybdate, tartaric acid, and

Table 3-3. Comparison between mCFA and FIA for colorimetric nitrite determinations.

	mCFA[a]						FIA
Sample Time(s)	5	10	10	15	15	20	—
Wash Time(s)	5	5	10	5	15	10	—
Analysis Rate (hr^{-1})	360	240	180	180	120	120	70
Sample Volume (µl)	32	64	64	96	96	128	500
Reagent Volume[b] (µl)	28	42	56	56	83	83	150
Precision (%RSD)	0.74	0.38	0.13	0.11	0.24	0.28	0.5
%I	0.98	0.56	0.20	0.57	0.14	0.25	1
Slope	0.032	0.033	0.033	0.033	0.033	0.033	No Data
Y Intercept	0.0054	0.0055	0.0058	0.0061	0.0050	0.0068	No Data
r_{xy} (correl. coeff.)	1.00	1.00	1.00	1.00	1.00	1.00	No Data

[a] Pump speed = 70 ($n = 2.5\ s^{-1}$) and $t = 100$ s for all experiments.

[b] Combined volume of SAN and NED reagents delivered during the time required for one sample and wash interval.

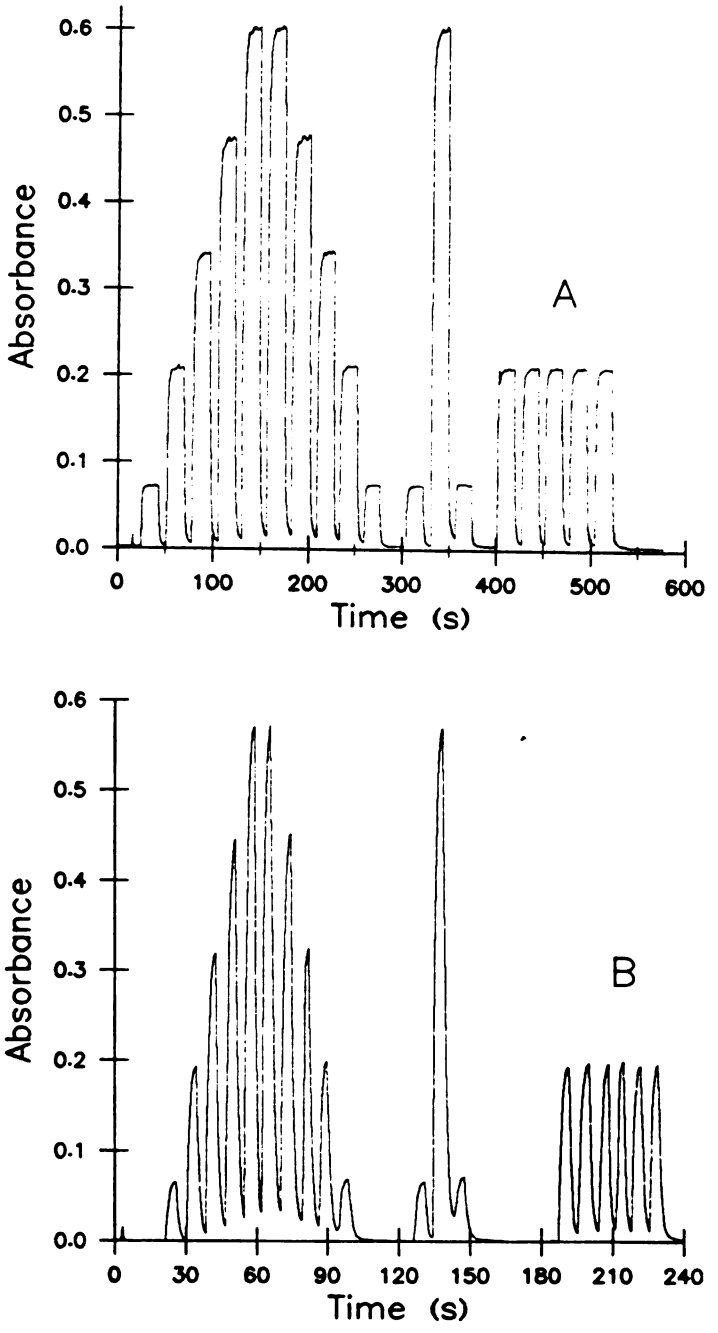

Figure 3-6. Recording of 2, 6, 10, 14 and 18 μM nitrate standards run in ascending and descending order, followed by an interaction test pattern and replicate determinations of the 6 μM standard. A) 120 samples hr^{-1}. B) 360 samples hr^{-1}.

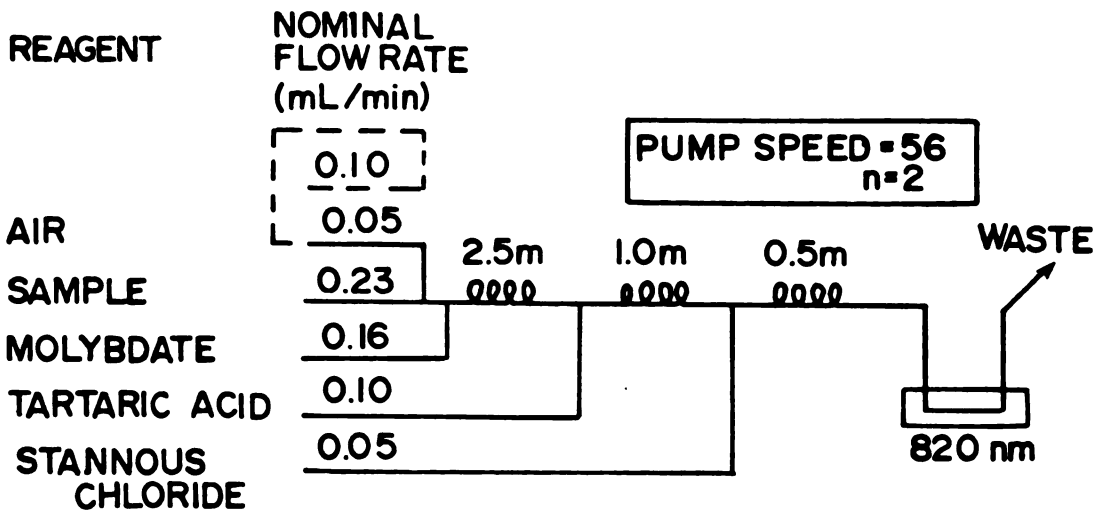

Figure 3-7. Diagram of the manifold used for silicate determinations with the mCF system.

stannous chloride reagents. Silicate was determined by a reduced, β-12-silicomolybdic acid procedure [52,53] that has an absorption maxima at about 820 nm. This procedure was adapted from an AAII CFA procedure used to determine silicate in seawater [7].

Aqueous silicate standards with nominal concentrations of 5, 15, 25, 35, and 45 μM were determined at several values of t_s and t_w. Data from these experiments are summarized in Table 3-4. Precision was estimated from five replicate determinations of the 15 μM standard at each sampling rate. Recordings of data obtained at analysis rates of 180 and 120 samples h^{-1} are shown in Figure 3-8. Inspection of Table 3-4 reveals that precision and interaction were both about 1% or less at all sampling rates. Linearity of standard curves were also very good. The maximum sampling rates that were achieved with acceptable precision and interaction were less than for nitrite detrerminations, but this was expected because the dwell time of samples in the silicate manifold was three times longer than in the nitrite manifold.

E. Conclusions

At present, third generation CFA systems with bubble gated detectors are not commercially available in single channel form, and the high cost, complexity, and specializd nature of the Technicon SMAC CFA system restricts its use to major clinical laboratories. This explains in part why many academic and small industrial laboratories have embraced FIA which is currently perceived in these circles as a versatile, less costly, and more efficient alternative to CFA. The data presented here, however, demonstrate that in conjunction with the bubble gate circuit, high performance, miniature CFA systems can be

Table 3-4. Performance of mCFA[a] system for colorimetric silicate determinations

Sample Time(s)	10	15	20	23
Wash Time(s)	10	5	5	7
Analysis Rate (hr^{-1})	180	180	144	120
Sample Volume (μL)	51	76	102	117
Reagent Volume (μL)[b]	137	137	172	206
Precision (%RSD)	1.1	0.8	0.4	0.4
Percent Interaction	0.07	0.90	0.97	0.16
Slope	.010	.0105	.011	.011
Y Intercept	0.000	0.000	0.000	0.000
r_{xy} (correl. coeff.)	1.00	1.00	1.00	1.00

[a] Pump speed = 56 (n = 2.0 s^{-1}) and t = 300 s for all experiments.

[b] Combined volume of molybdate, tartaric acid, and stannous chloride reagents delivered during the time required for one sample and wash interval.

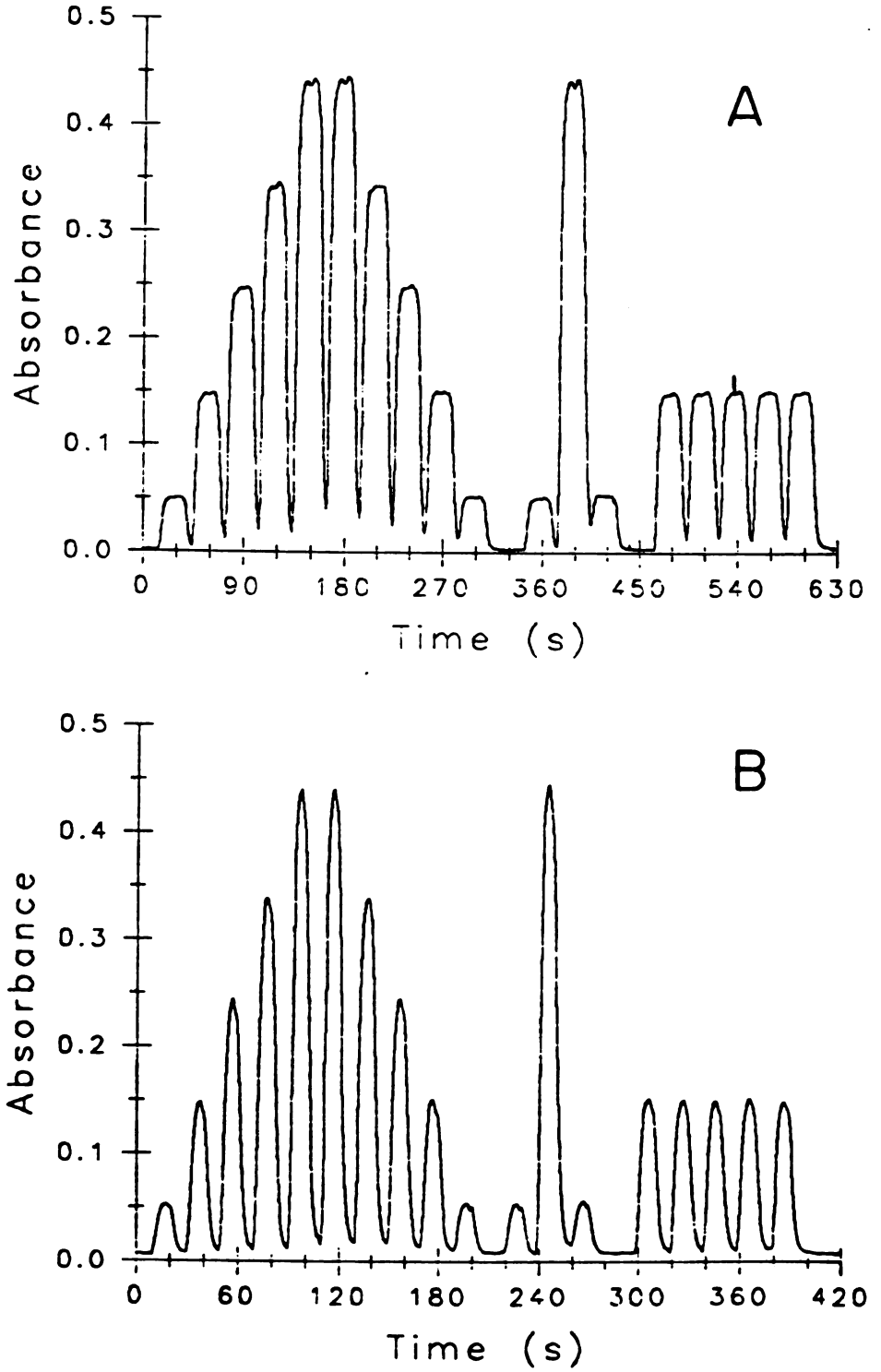

Figure 3-8. Recording of 5, 15, 25, 35 and 45 µM silicate standards run in ascending and descending order followed by an interaction test pattern and replicate determinations of the 15 µM standard. A) 120 samples hr^{-1}. B) 180 samples hr^{-1}.

assembled and operated with moderate ease, and that such CFA systems need not be more elaborate or expensive than comparable FIA systems. In fact, the combined cost of electronic components for the bubble gate and a 2 μL bubble-through flow cell (≃$500) required for the mCFA system is comparable to the cost of sampling valves and valve controllers required for FIA systems, while the cost of other major system components (samplers, pumps, detectors) is about the same for either technique. Hopefully the results reported here will encourage researchers in academic and small industrial laboratories to think seriously about custom designed mCFA systems. Such systems should be particularly advantageous for the automation of routine colorimetric determinations in which the analytical reaction requires more than about 30 s to reach an appreciable degree of completion, especially when low dispersion of samples is required to achieve maximum sensitivity. For an experimental comparison of FIA and mCFA, see Chapter 5.

CHAPTER 4

NOVEL CADMIUM REACTORS FOR DETERMINATION OF NITRATE IN WATER AND SEAWATER BY SEGMENTED, CONTINUOUS FLOW COLORIMETRY

A. Overview

Nitrite in water and seawater is routinely determined colorimetrically with high specificity, sensitivity, and precision by diazotization with sulfanilamide and coupling with N-(1-Napthhyl)-ethylenediamine as described in Chapter 3. An equally simple and sensitive colorimetric assay for nitrate has yet to be devised, and for this reason nitrate is generally determined as nitrite after it is reduced to that species with a suitable reagent. Although procedures for reduction of nitrate to nitrite with zinc [54], hydrazine/Cu^{2+} [55], and immobilized nitrate reductase [56] have been reported, they have not been widely applied. This is because the reduction with zinc is too vigorous at ambient temperatures, reduction with hydrazine/Cu^{2+} is sluggish and difficult to control, and enzymatic reduction, although highly specific, requires reagents that are relatively expensive and difficult to prepare. Cadmium metal has proved to be a much more suitable reagent for reducing nitrate to nitrite, and is generally used in the form of packed bed reactors, although reactors fabricated from cadmium wire inserted into narrow plastic tubes [57,58] have also been reported.

Unfortunately, packed bed and tubular wire cadmium reactors are incompatible with segmented, continuous flow analyzers because the analytical stream must be debubbled prior to entry into these types of reactors. Air segments cause channeling in the packed bed reactors and as a result, reduction efficiency decreases and sample dispersion increases. Tubular wire reactors will not support a stable segmentation pattern and so generally the analytical stream is segmented on the downstream side of such reactors. By now it should be obvious that other factors being equal, dispersion will be greater for a system in which air segments must be removed and reintroduced downstream, than for a system where segmentation is uniform and continuous. This means that in determinations incorporating packed bed or wire reactors, the sample and wash intervals required to achieve acceptable levels of precision and interaction will increase, which of course decreases the rate at which determinations can be performed. Furthermore, the flow characteristics of packed bed reactors can change during the course of a run due to accumulation of particulate matter, which will change the back pressure, and therefore the flow rate through the reactor.

Reactors fabricated from cadmium tubing should eliminate these problems. They would support a stable segmentation pattern in a similar fashion to other mixing coils that make up the manifold, the difference of course being that the inner walls of the cadmium tube are active rather than passive.

B. General Considerations

Reduction of nitrate to nitrite is generally 90 to 98% complete in packed bed cadmium reactors (PBCRs) under neutral to mildly alkaline

conditions. The dimensions of the reactor, as well as the size distribution of the cadmium particles with which it is packed, will have a major influence on reduction efficiency. Larger reactors and smaller cadmium particles lead to higher reducing power. It must be stressed, however, that the active surface area of cadmium particles with similar size distributions can be quite variable and may change during the course of the reduction. For example Davidson and Woof [59] reported that different forms of cadmium -- e.g., spongy, electrolytically precipitated, filings, powder -- had different reducing powers on a weight-to-weight basis. These conclusions are somewhat suspect because they did not consider differences in the surface areas of the different forms of cadmium, nor did they account for changes in pH that are likely to occur during the course of the reduction due to reaction of dissolved oxygen with cadmium. Certainly one of the major difficulties in achieving good precision with cadmium reactors is the maintenance of a reproducibly active surface during the course of experiments.

There are several ways to increase the active surface area of cadmium particles. For example, if cadmium filings are reacted with nitric acid prior to packing, their reducing power is increased [60]. This is because nitric acid pits the cadmium and thus the surface area is increased. It is also well established [59,61] that amalgamated, silverized, or copperized cadmium is more reactive than pure cadmium. Amalgamated cadmium tends to form lumps [61,62] and is therefore not well suited for the preparation of PBCRs. Copperized cadmium on the other hand, does not lump and is highly reactive. For this reason it has been widely used for the preparation of PBCRs. Several workers [62,63] have suggested that Cu^{2+} is a product of nitrate reduction in

such reactors. Recently, however, Sherwood and Johnson [64] presented convincing evidence that copper is not directly involved in the reduction process; instead it functions primarily as a surface activator.

Other variables such as pH and the amount of dissolved oxygen and chloride in samples and reagents also affect the reduction efficiency of a given cadmium reactor. These effects may go unnoticed in relatively large (25 cm x 0.8 cm ID) PBCRs used for batch reduction of nitrate to nitrite in natural water samples [62], because of the great excess of cadmium relative to the amount of nitrate present in samples. As PBCRs are miniaturized to make them compatible with continuous flow analyzers [65,49], however, control of reaction parameters becomes much more critical, and changes in the active surface of the cadmium that can occur during the course of the reduction become more apparent. Nydahl [61] reported a detailed study on the optimum conditions for the reduction of nitrate to nitrite with PBCRs. This study was highly useful in my work with open tubular cadmium reactors (OTCRs). I will therefore summarize his results in the paragraphs that follow to provide some background information necessary to understand the results with OTCRs presented later.

C. Summary of Nydahl's Work

1. pH Effects

Equations 4-1, 4-2, and 4-3 [61] suggest that

$$NO_3^- + 2H^+ + 2e^- \longrightarrow NO_2^- + H_2O \qquad (4\text{-}1)$$

$$NO_2^- + 6H^+ + 4e^- \longrightarrow H_3NOH^+ + H_2O \qquad (4\text{-}2)$$

$$NO_2^- + 8H^+ + 6e^- \longrightarrow NH_4^+ + 2H_2O \qquad (4\text{-}3)$$

the pH at which the reduction occurs has a major influence on reduction products. Nydahl [61] found that in the pH range of 1 to 3, hydroxylamine is the major product. Small amounts of ammonia are also formed. Reduction rates decrease sharply in the pH range of 3 to 5, and nitrite is the major reduction product. The rate of nitrate reduction continues to decrease in the pH range of 7 to 9, and 95 to 99+% of nitrate originally present in samples is recovered as nitrite. The fraction depends on the flow rate through the PBCR and its size. As the pH increases in this range, either the size of the PBCR must be increased, or the flow rate of sample through it must be decreased to achieve the same degree of reduction. The rate of reduction of nitrite to hydroxylamine also decreases as the pH increases, but even at pH 9.5, slight reduction of nitrite still occurs. Nydahl reported the same trends for copperized cadmium but found that the rate of reduction observed for both nitrate and nitrite was a factor of 10 to 20 times greater for copperized cadmium than for pure cadmium. These results emphasize the importance of pH control during the reduction process for all types of cadmium reactors. The presence of dissolved oxygen in

samples and reagents makes pH control more difficult than might be expected.

2. Dissolved Oxygen Effects

Cadmium(II) ions are a product of the reduction of nitrate to nitrite as shown in Equation 4-4.

$$Cd + NO_3^- + 2H^+ \rightarrow Cd^{2+} + NO_2^- + H_2O \qquad (4\text{-}4)$$

Because hydrogen ions are consumed in this reaction, the pH of unbuffered samples increases slightly during reduction. For samples containing micromolar concentrations of nitrate, however, this increase is negligibly small. Nydahl [66] pointed out, however, that a much more significant increase in pH occurred within reactors because dissolved oxygen in samples and reagents reacts quantitatively with cadmium as shown in Equation 4-5.

$$Cd + 1/2O_2 + 2H^+ \rightarrow Cd^{2+} + H_2O \qquad (4\text{-}5)$$

Under mildly alkaline conditions this reaction proceeds at a rate about 30 times faster than the rate at which nitrate is reduced to nitrite. The concentration of oxygen in dilute aqueous solutions in equilibrium with air is on the order of 0.5 mg-At L^{-1} [67] which, in accordance with the reaction stoichiometry, is equivalent to 1 mmol of base per liter of solution passed through a PBCR. For this reason, the buffer capacity of the sample must be much greater than would be predicted on the basis of nitrate reduction, if constant pH is to be maintained throughout the reduction process. Note also that oxygen reduction simultaneously increases the concentration of Cd^{2+} to a value of

approximately 0.5 m*M*. Nydahl estimated that at this concentration, cadmium hydroxide would begin to precipitate at a pH of about 8.5, and was likely to adhere to the surface of the cadmium particles. As a result, the reducing power of the reactor would decrease. This can be prevented if compounds such as ammonium chloride or EDTA that form soluble complexes with Cd^{2+} are added to the sample prior to reduction. Nydahl [61] suggested the use of imidazole (pk_b=7.09) which can be used to buffer samples and complex Cd^{2+} ($\beta_4 \simeq 7.5$) simultaneously.

3. Effect of Chloride

Nydahl [61] found that chloride ions greatly retard the rate at which nitrate is reduced to nitrite. Thus the reduction of nitrate in seawater ($[Cl^-] \simeq 0.3$ *M*) proceeds more slowly than in fresh water. This is generally of little consequence when PBCRs are used because of their relatively large reducing power. In fact, because chloride ions also decrease the rate at which nitrite is reduced to hydroxylamine, yields of nitrite may actually be increased in the presence of chloride, especially when highly reactive copperized cadmium is used as the reducing agent.

D. Experimental

1. Reagents

Sulfanilamide (SAN) and N-(1-Naphthyl)ethyenediamine (NED) reagents were prepared exactly as described in Chapter 3.

The ammonium chloride reagent was prepared by dissolving 10 g (0.19 mol) of ammonium chloride in 1 L of DDW.

Buffer solutions (0.1 *M*) with nominal pH values of 5.0, 6.0, 7.0, and 8.0 were prepared from acetic acid and sodium acetate,

2-(N-morpholino)ethanesulfonic acid (MES) and sodium hydroxide, imidazole and hydrochloric acid, and tris [hydroxymethyl] aminomethane (TRIS) and hydrochloric acid, respectively. These buffers were chosen because in each case, their pK_as or pK_bs are within 0.25 units of the desired pH. Brij-35 surfactant (1 mL L^{-1}) was added to each buffer.

Copper sulfate (0.01 M) was prepared by dissolving 2.5 g of $CuSO_4 \cdot 5H_2O$ in 1 L of DDW.

2. Standards

Primary (5 mM) and working nitrite standards were prepared exactly as described in Chapter 3.

Primary nitrate standards (5.0 mM) were prepared by dissolving 0.5056 g of dried, reagent grade KNO_3 in 1 L of DDW. Working standards were prepared by dilution of the primary standard by means of digital microliter pipets and volumetric flasks.

Seawater standards (spikes) were prepared as follows. Volumetric flasks (100 mL) were filled to the mark with low-nutrient filtered seawater. Then 1.00 mL of the seawater was withdrawn from each flask with a digital pipet and discarded. Next the required volume of primary nitrate or nitrite standard was added to the flasks by means of digital microliter pipets. The flasks were then diluted to the mark with DDW and mixed. This procedure ensured that the dilution of the seawater was small (1%) and that the dilution was uniform regardless of the concentration of the standard prepared.

The filtered, low nutrient seawater, collected in midsummer from Long Island Sound, was a gift of the Oceanographic Sciences Division of Brookhaven National Laboratory.

3. Cadmium Reactors

Packed bed cadmium reactors were prepared as follows. Cadmium filings (40-60 mesh) were stirred with a magnet to remove ferrous metal and then washed with methylene chloride to remove grease. The filings (~30 g) were air dried on filter paper in a hood, and then transferred to a 100 mL beaker. The filings were etched with 25 mL of 8 M nitric acid for about 1 minute and then rinsed thoroughly with DDW, 1.2 M hydrochloric acid, and again with DDW. Next the filings were treated with several portions of the copper sulfate solution until the blue color no longer faded from the solution. The copperized filings were then rinsed with ammonium chloride solution to remove colloidal copper and cadmium hydroxide. Copperized cadmium filings prepared in this way can be stored indefinitely under a solution of ammonium chloride.

PBCRs were prepared in small glass tubes (7 cm x 0.2 cm ID) with a constriction at one end. A small plug of glass wool was pushed to the constricted end of the tube with a stiff wire, and a small funnel was attached to the unconstricted end of the tube by means of a plastic sleeve. The funnel and tube were filled with ammonium chloride solution and copperized cadmium filings were added to the funnel, one spatula tipful at a time. Between additions, the walls of the tube were tapped with the spatula to ensure uniform packing. When the filings were within 0.2 cm of the top of the tube, a second plug of glass wool was added to secure the filings. The funnel was then removed and the PBCR was ready to install in the manifold.

Open tubular cadmium reactors were prepared from 0.127 cm ID x .229 cm OD cadmium tubing (Reactor Experiments, San Carlos, CA). Tubing was cut into desired lengths and wrapped around a 1 cm diameter

glass rod to form a closely spaced helix. Next the ends of the coiled tube were connected by a short length of plastic tubing, and the exposed surfaces of the cadmium coil were sprayed with several coats of acrylic lacquer. This allowed the reactors to be handled freely without fear of cadmium poisoning.

A syringe was used to wash the inner walls of the OTCRs with methylene chloride, which was subsequently removed by flushing the OTCR with nitrogen for several minutes. The OTCRs were copperized as follows. A 50 mL beaker was filled with equal volumes of imidazole buffer (pH=7.0) and copper sulfate solution (0.1 M). A syringe was attached to one end of the OTCR with a plastic sleeve and a short piece of plastic tubing was attached to the other end of the OTCR. The syringe was then used to draw the buffered copper solution into the OTCR. The solution was forced back and forth through the reactor for several minutes, after which the reactor was ready to be installed in the manifold. When the OTCR was not in use, it was removed from the manifold, filled with imidazole buffer, and sealed by joining the ends with a short length of plastic tubing.

Cadmium foil reactors were prepared from a 0.0025 cm cadmium foil (Alfa Ventron, Danvers, MA). The foil was polished with steel wool, rinsed with methylene chloride, and dried between tissues. The foil was then mounted between standard 6 or 12 inch dialysis blocks (#178-2538-07 or 178-2540-01, Gamma Enterprises, Mt. Vernon, NY), designed for use with the Technicon SMAC clincial CFA system. The foil was then copperized within the dialysis blocks by the same procedure used for OTCRs.

4. Manifolds

Manifolds used for nitrate and nitrite determinations with OTCRs and PBCRs during these experiments are shown schematically in Figures 4-1A and 4-1B, respectively. Note that the flow rates of the air delivery pump tubes are twice the normal values in the manifold used with OTCRs. Recall from Chapter 2 that the minimum air segment volume necessary to sufficiently occlude a tube of diameter d_t is equal to $0.92\ d_t^3$. The only cadmium tubing commercially available had an inside diameter of 0.13 cm, so an air segment volume of about 2 μL was required. This is about twice the volume required when d_t = 0.1 cm, as is the case for other components that make up the manifold.

5. pH Measurements

All pH measurements were made with an Orion 611 digital pH meter and a Ross combination pH/reference electrode (Orion Research, Inc., Cambridge, MA.)

E. Some Definitions

As discussed in the previous section, both nitrate and nitrite are reduced to lower oxidation state species in cadmium reactors, and the extent of reduction depends primarily on the size of the reactor, the flow rate of solution through the reactor, and the pH and chloride concentration of the solution in contact with the reactor. Since only nitrite reacts with the Griess reagents, ideal experimental conditions would be those where reduction of nitrate to nitrite is quantitative, while reduction of nitrite to lower oxidation state species is negligible. In this case determination of nitrite in the cadmium reactor effluent would yield the sum of nitrite and nitrate originally present

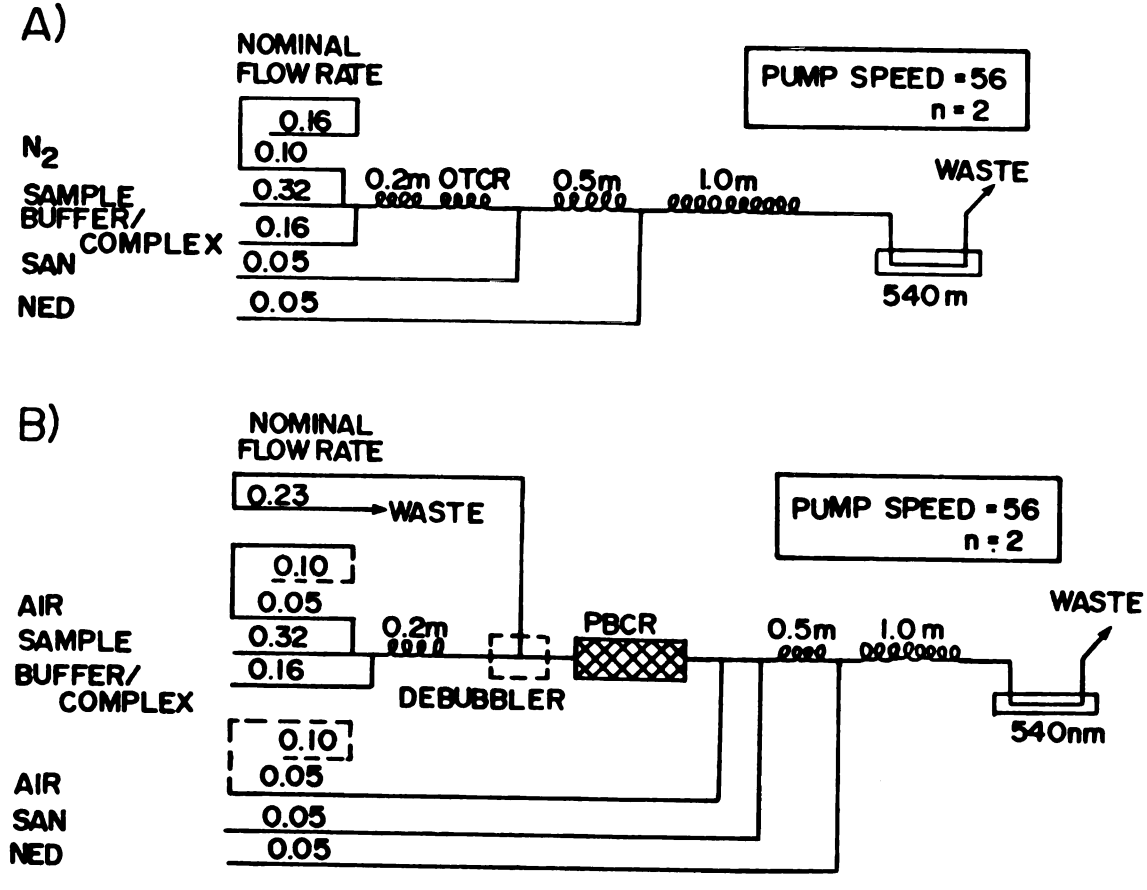

Figure 4-1. Diagrams of manifolds used to determine nitrate and nitrite with the mCFA instrument. A) System for open tubular and foil cadmium reactors. B) System for packed bed cadmium reactors.

in the sample. An independent determination of nitrite would then allow the nitrate concentration to be calculated by difference. For automated nitrate determination procedures that use small PBCRs for reduction, these conditions are generally closely approximated. The surface-to-volume ratio of such reactors is large, which favors rapid reduction of nitrate to nitrite, while the mean residence time is short, which minimizes reduction of nitrite to lower oxidation state species. The surface-to-volume ratio is much less favorable for OTCRs, and a large number of experiments had to be performed before results for nitrate determinations in water and seawater obtained with OTCRs were comparable to those obtained with PBCRs. Details of these experiments are summarized in the next section.

In future discussions a quantity called <u>percent recovery</u> is used to provide a quantitative measure of the reduction that occurs in a cadmium reactor. Percent recovery is defined as follows. First consider solutions that contain only nitrite. In this case percent recovery is the ratio (x 100) of absorbances measured for the end product of the Griess reaction when the same nitrite standard is determined with and without a cadmium reactor installed in the manifold. For example if absorbances of 0.587 and 0.603 were measured for the same nitrite standard with and without a cadmium reactor on line, the percent recovery would be 97.3 [(0.587/0.603) x 100)]. This implies that with the cadmium reactor on line 2.7% of the nitrite originally present in the standard was reduced to lower oxidation state species that do not form colored products with the Griess reagents. For solutions that contain nitrate, percent recovery was calculated by dividing the absorbance measured for a nitrate standard with a cadmium reactor

on line, by the absorbance measured for a nitrite standard with the same nominal concentration after the cadmium reactor had been removed from the manifold. In this case, however, some of the nitrite produced from nitrate reduction may be further reduced to lower oxidation states, and so percent recovery will reflect the net yield of nitrite resulting from these two competitive reduction reactions.

F. Preliminary Experiments

1. Open Tubular Cadmium Reactors

Results obtained in preliminary experiments with OTCRs conformed to trends reported by Nydahl [61] for nitrate reduction with PBCRs. Recoveries of nitrate were in the range of only 5 to 10% for untreated OTCRs. These low nitrate recoveries could not be attributed to nitrite reduction because recoveries calculated for nitrite standards were in the range of 98 to 99%. When OTCRs were activated by perfusion with a solution of 0.01 M copper sulfate, however, nitrate recoveries increased dramatically. Percent recoveries calculated for 25 μM nitrite and nitrate standards as a function of copperized OTCR length are given in Table 4-1. As expected percent recovery calculated for the nitrate standard increases as the length of the OTCR increases, but there is no clear trend in percent recovery calculated for the nitrite soltution. In these experiments, the buffer/complex reagent (see Figure 4-1) was an unbuffered solution of ammonium chloride containing copper sulfate (100 μL of 0.01 M $CuSO_4$ per 100 mL of 0.19 M NH_4Cl). The pH of this solution after mixing with the sample in the first coil was 4.58. After passage through a 15 cm copperized OTCR, the pH measured was 8.08, an increase of 3.5 pH units. Variation of the

Table 4-1. Percent recovery of nitrite and nitrate standards for copperized open tubular reactors of various lengths.

OTCR Length (cm)	Percent Recovery[a]	
	NO_2^-	NO_3^-
3	93.0	42.2
6	96.6	61.8
9	96.9	82.1
12	98.3	87.8
15	98.2	91.8
18	98.3	92.4
21	95.3	91.3
30	96.1	93.7

[a]Based on absorbance values recorded for 25 μM nitrite and nitrate standards as described in text.

nitrate concentration in the sample (0 to 35 μM) had no measurable effect on these results, which indicated that the pH change was due to oxygen reduction as reported by Nydahl. Thus the somewhat erratic percent recoveries listed in Table 4-1 are attributable to changes in pH that occurred during the course of reduction.

When this experiment was repeated sequentially with a 0.1 M acetate buffer (pH=4.75), a 0.1 M MES buffer (pH=6.0), a 0.1 M imidazole buffer (pH=7.0), and a 0.1 M Tris buffer (pH=8.2) in place of the ammonium chloride/copper sulfate reagent, the pH of solutions entering and exiting the OTCR remained constant to within 0.1 pH unit. Slopes, intercepts, and correlation coefficients for calibration curves calculated from the absorbance of 5, 15, and 25 μM nitrite and nitrate standards with and without the OTCR installed in the manifold at each pH can be found in Table 4-2. Also listed in this table are percent recoveries calculated for nitrite and nitrate standards on the basis of the ratio of the slopes of the calibration curves for nitrite and nitrite at each pH. Since the slopes of the calibration curves for nitrite at each pH were linear and constant to within about 4% without an OTCR on-line, the low percent recoveries calculated for nitrite and nitrate at the two lower pH levels cannot be attributed to changes in the sensitivity of the Griess reaction when different buffers were used. Instead low recoveries with these buffers are due to reduction of nitrite to lower oxidation state species (notice the large, negative y-intercept values) as observed by Nydahyl in his studies of PBCRs in this pH range. Percent recovery of nitrite is maximum at pH=8.2, while percent recovery for nitrate is maximum at pH=7.0.

Table 4-2. Linear regression parameters and percent recoveries calculated for nitrate and nitrite standards as a function of pH.

pH:	4.75		6.00		7.00		8.20	
	NO_2^-	NO_3^-	NO_2^-	NO_3^-	NO_2^-	NO_3^-	NO_2^-	NO_3^-
slope	.0099(.0246)[a]	.0074	.0139(.0238)	.0126	.0237(.0248)	.0203	.0240(.0248)	.0195
y-intercept	-.014(-.003)	-.011	-.023(.004)	-.014	-.006(-.002)	-.005	-.007(-.002)	-.006
r_{xy}	.9998(.9997)	.9997	.9995(.9996)	.9997	1.0000(.9997)	.9999	1.0000(.9999)	.9997
% Recovery	40.2	30.1	58.4	52.9	95.6	81.8	96.8	78.6

[a]Values in parentheses were calculated from absorbances measured for nitrite standards with the OTCR removed from the manifold.

Percent recoveries of nitrite and nitrate were further investigated over the pH range of 6.5 to 8.5 using imidazole (pH=6.5, 7.0, 7.5) and Tris (pH=8.0, 8.25, and 8.5) buffers. A short (10 cm) OTCR was used in these experiments so that changes in percent recoveries of nitrate would be more apparent. This experiment was also performed with a copperized PBCR using the manifold shown in Figure 4-1B. Percent recoveries calculated from experimental results obtained with the OTCR and the PBCR are plotted as a function of pH in Figure 4-2A and 4-2B, respectively. As before, percent recoveries were calculated on the basis of the ratio of the slopes of nitrite and nitrate calibration curves (5, 15, and 25 μM concentrations) with and without a cadmium reactor on line. Nitrite recoveries increase slightly as the pH increases in experiments with both reactor types, as expected. Nitrate recoveries calculated from data obtained with the PBCR also increases as the pH increases in agreement with Nydahl's study. Nitrate recoveries calculated from data collected with the OTCR, however, first increases slightly as the pH increases, and then decreases sharply with further increases in pH. Although this trend can be rationalized in terms of the decrease in the rate of nitrate (and nitrite) reduction that occurs as pH increases, it seems likely that the ability of imidazole to complex Cd^{2+} is also involved. There was no complexing agent in the Tris buffers and so formation of $Cd(OH)_2$ on the surface of the OTCR was a distinct possibility. This seems even more probable in light of some later experiments that are discussed shortly. Throughout these experiments nitrate recoveries were always highest when imidazole buffers were used.

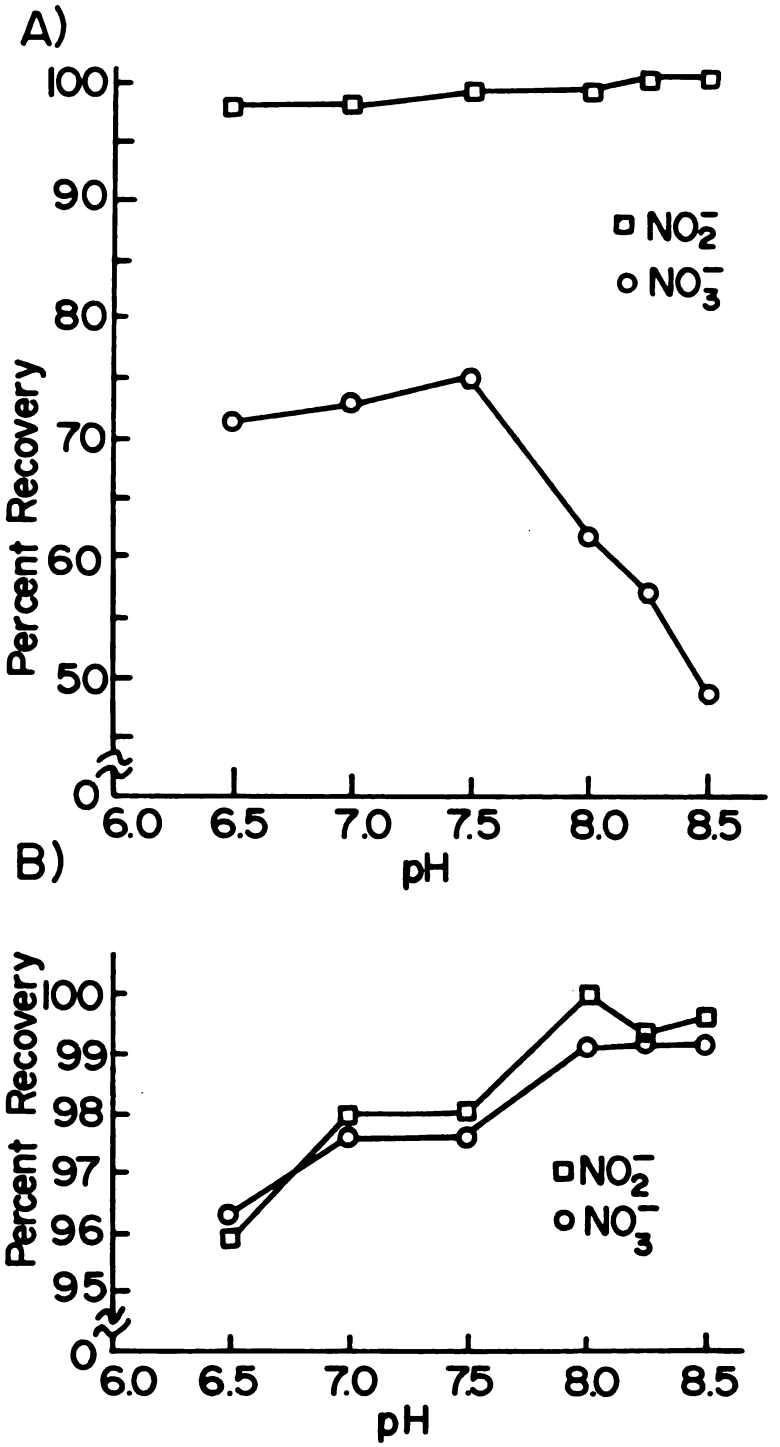

Figure 4-2. Percent recoveries of nitrate and nitrite. A) Open tubular cadmium reactor. B) Packed bed cadmium reactor.

In the next set of experiments percent recoveries were determined for nitrite and nitrate standards in the concentration range of 5 to 25 μM using the three imidazole buffers from the previous experiment and a 30 cm copperized OTCR. Slopes, Y-intercepts, correlation coefficients, and percent recoveries calculated for data from these experiments can be found in Table 4-3. These results were encouraging. Recoveries for both nitrite and nitrate were in the range of 95 to 97%. When low nutrient seawater that had been spiked with nitrate was determined with this OTCR, however, nitrate recoveries were less than 80%, although the calibration curves remained linear. This observation was not unexpected because Nydahl [61] reported a sharp decrease in the rate of nitrate reduction when the chloride concentration of the solution in contact with PBCRs increased. A plot of nitrite and nitrate recoveries as a function of chloride concentration is shown in Figure 4-3. Here calculations of percent recoveries are based on the absorbance measured for 25 μM nitrite and nitrate standards to which sodium chloride was added. Imidazole buffer (pH=7.5) and a 15 cm copperized OTCR were used for this experiment. At this point it became apparent that longer OTCRs would be necessary to approach quantitative reduction of nitrate in a seawater ($[Cl^-] \simeq 0.3M$) matrix. When a 60 cm copperized OTCR was installed in the manifold, however, the segmentation pattern of the analytical stream emerging from the reactor was irregular, recorded baseline signals were noisy, and peak shapes were severely distorted.

These problems were initially attributed to irregularities or partial blockages within the reactor. When several shorter OTCRs that individually supported stable segmentation patterns were connected

Table 4-3. Linear regression parameters and percent recoveries calculated for nitrate and nitrite standards with imidazole buffers and a 30 cm copperized OTCR.

pH:	6.5		7.0		7.5	
	NO_2^-	NO_3^-	NO_2^-	NO_3^-	NO_2^-	NO_3^-
slope	.0227(.0239)[a]	.0227	.0229(.0238)	.0230	.0231(.0238)	.0230
y-intercept	-.008(-.008)	-.005	-.003(-.007)	-.004	-.002(-.006)	-.001
r_{xy}	1.0000(1.0000)	1.0000	.9999(1.0000)	1.0000	1.0000(1.0000)	1.0000
% Recovery	95.0	95.0	96.2	96.6	97.1	96.6

[a]Values in parentheses were calculated from absorbances measured for nitrite standards with the OTCR removed from the manifold.

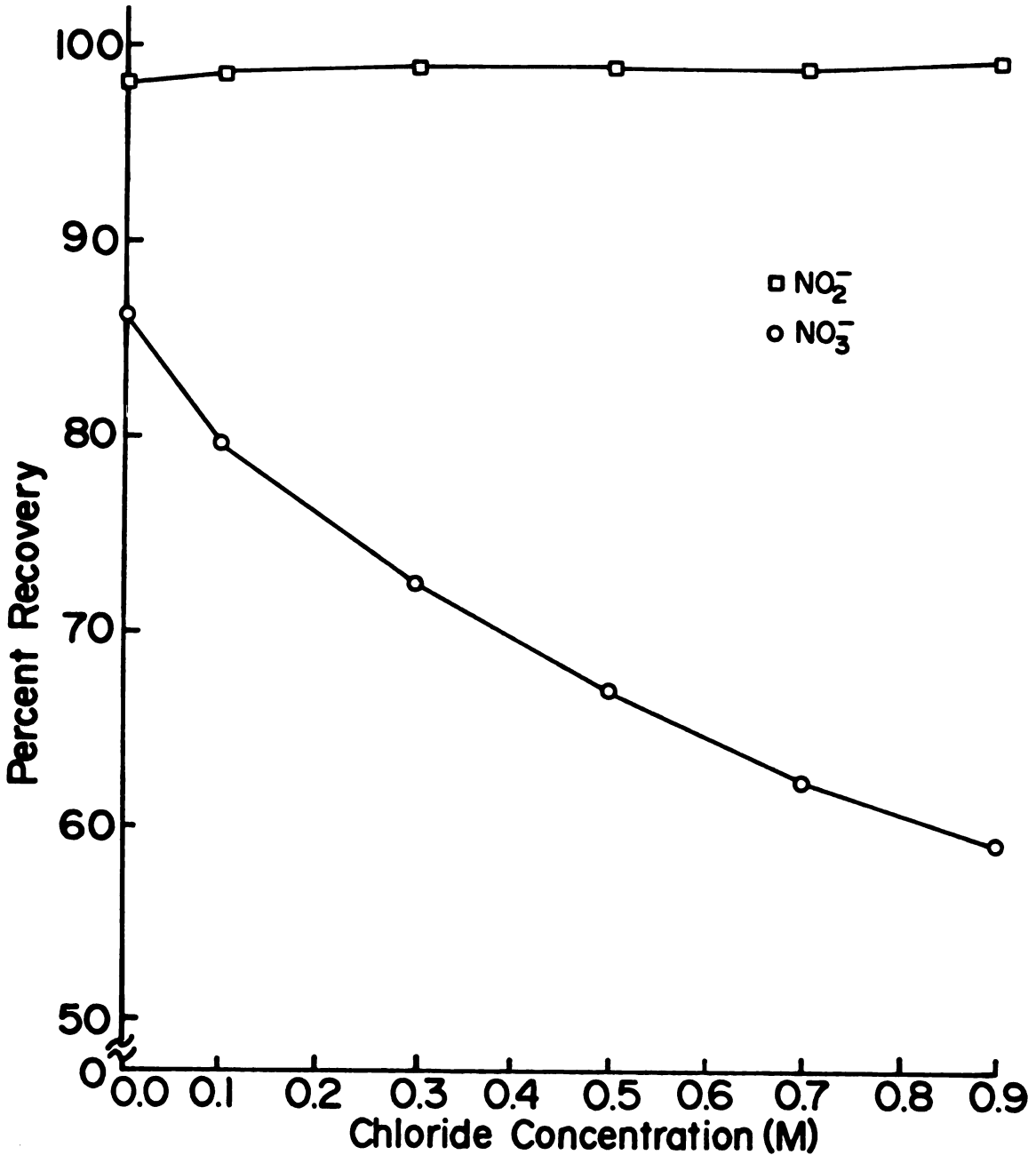

Figure 4-3. Effect of chloride concentration on percent recoveries of nitrate and nitrite with open tubular cadmium reactors.

together, however, the same symptoms were observed. This was puzzling at first, but it finally became apparent that oxygen in the air segments was being reduced at the reactor walls, which caused the air segments' volume to decrease. In longer OTCRs, the air segment volume became too small to occlude the tube and so the integrity of the analytical stream was lost. When nitrogen rather than air was used as the segmentation gas, stable segmentation patterns were achieved for OTCRs as long as 150 cm. At this point, the pH of the buffered analytical stream was measured before and after it had passed through the 60 cm OTCR, first with air, then with nitrogen as the segmentation gas. Results are shown in Table 4-4. The buffer capacity was clearly exceeded when air was used as the segmentation gas and a 60-cm OTCR was on-line, which confirmed the hypothesis that oxygen in the air segments was being reduced at the OTCR walls (see Equation 4-5) and also explained the distorted peak shapes and noisy base lines observed when the seawater spikes were passed through the 60 cm OTCR with air as the segmentation gas. As is demonstrated in the final section of this chapter, nitrate recoveries comparable to those measured with PBCRs can be achieved with a 60 cm OTCR when nitrogen is used to segment the analytical stream.

2. Cadmium Foil Reactors

As mentioned earlier, the ID of commercially available cadmium tubing is somewhat larger than the ID of other manifold components in the mCF system. Recall that, other factors being equal, dispersion in gas segmented reactors increases as the inside diameter of the reactor increases. It occurred to me that a cadmium reactor with improved wash characteristics could be fabricated by inserting a piece of cadmium

Table 4-4. Effect of segmentation gas on the pH measured for the effluent from a 60 cm OTCR.

Nominal pH	Segmentation Gas:	Measured pH			
		Air		Nitrogen	
		Distilled Water	Seawater	Distilled Water	Seawater
6.5		6.80(6.54)[a]	6.96(6.63)	6.52	6.64
7.0		7.35(7.01)	6.38(7.11)	7.01	7.12
7.5		8.59(7.49)	8.38(7.64)	7.50	7.64

[a] pH values in parentheses were measured before the buffered analytical stream entered the OTCR.

foil between the blocks of a dialyzer designed for use with the SMAC CF system. This approach was tried, but unfortunately it proved very difficult to produce a good seal between the dialysis blocks and the cadmium foil. Even when a seal was achieved temporarily, leaks began to develop within a few hours of operation time. This was not considered acceptable for routine use. In the few successful experiments with 12 inch dialyzer blocks, recoveries calculated for nitrite and nitrate standards were on the order of 97% and 75%, respectively. It did appear that sample interaction was lower in this reactor than in OTCRs, although insufficient data were collected to make a definitive comparison. In these experiments the analytical stream was buffered with imidazole (pH=7.0) and segmented with nitrogen. These results were encouraging, and if a solution to the problem of forming a good seal between the dialysis blocks and the cadmium foil could be solved, this system would warrant further study.

G. Final Experiments

The results of the final experiment in which the performance of a 60 cm copperized OTCR and a 7 cm x .2 cm ID copperized PBCR were compared for both distilled water standards and seawater spikes are summarized in Tables 4-5 and 4-6. The concentration range of standards and spikes for both nitrate (0 to 25 μM) and nitrite (0 to 2.5 μM) was chosen to be representative of concentrations normally encountered in unpolluted seawater. Data listed in Table 4-5 resulted from five replicate determinations of each standard and spike. Three sets of standards and spikes were prepared for this experiment. One set contained only nitrate, another set contained only nitrite, and a third

Table 4-5. Data from determinations of nitrate and nitrite in distilled water and seawater with OTCRs and PBCRs.

Nominal Concentration (μM)	Baseline Corrected Absorbance[a]			
	OTCR		PBCR	
$NO_2^- + NO_3^-$	Seawater[b]	Distilled Water	Seawater[b]	Distilled Water
0.5 + 5.0	.149 ± .001	.140 ± .001	.135 ± .001	.136 ± .002
1.5 + 15.0	.412 ± .001	.409 ± .001	.407 ± .001	.407 ± .001
2.5 + 25.0	.660 ± .001	.669 ± .001	.668 ± .001	.668 ± .003
NO_3^-				
5.0	.127 ± .002	.127 ± .001	.124 ± .001	.121 ± .001
15.0	.373 ± .001	.374 ± .003	.366 ± .001	.368 ± .002
25.0	.611 ± .001	.607 ± .001	.611 ± .001	.601 ± .002
NO_2^-				
0.5	.011 ± .001	.009 ± .001	.011 ± .001	.012 ± .001
1.5	.035 ± .001	.032 ± .001	.035 ± .002	.037 ± .002
2.5	.065 ± .001	.059 ± .001	.062 ± .001	.064 ± .001
	(Cadmium Reactors Off-Line)			
0.5 + 5.0	.013 ± .001	.011 ± .001	.010 ± .001	.012 ± .001
1.5 + 15.0	.037 ± .001	.038 ± .001	.037 ± .001	.040 ± .001
2.5 + 25.0	.062 ± .001	.063 ± .001	.060 ± .001	.065 ± .001
NO_2^-				
0.5	.013 ± .001	.011 ± .001	.011 ± .001	.012 ± .001
1.5	.036 ± .001	.038 ± .001	.037 ± .001	.039 ± .001
2.5	.067 ± .001	.063 ± .001	.064 ± .001	.067 ± .001

[a] Average of five replicate determinations.

[b] Refractive index correction = .004 ± .002.

Table 4-6. Linear Regression parameters for data listed in Table 4-5.

Regressions	OTCR		PBCR	
$NO_2^- + NO_3^-$	Seawater	Distilled Water	Seawater	Distilled Water
slope ± S.D.	.02323 ± .00006	.02405 ± .00006	.02423 ± .00006	.0243 ± .0002
Y-intercept ± S.D.	.024 ± .001	.009 ± .001	.004 ± .001	.005 ± .003
Std. error of est.	.006	.004	.004	.004
r_{xy}	.9999	1.0000	.9999	.9999
NO_3^-				
slope	.0241 ± .0001	.02400 ± .00007	.02435 ± .00007	.0241 ± .0001
Y-intercept	.010 ± .002	.007 ± .001	.002 ± .001	.001 ± .001
Std. error of est.	.003	.003	.001	.004
r_{xy}	.9999	1.0000	1.0000	.9999
NO_2^-				
slope ± S.D.	.0270 ± .0007	.0250 ± .0007	.0255 ± .0007	.0260 ± .0007
Y-intercept ± S.D.	-.004 ± .001	-.004 ± .001	-.002 ± .001	-.001 ± .002
Std. error of est.	.002	.002	.001	.001
r_{xy}	.9980	.9989	.9998	.9999
Combined				
slope ± S.D.	.02416 ± .00003	.02440 ± .00003	.02437 ± .00004	.02435 ± .00006
Y-intercept ± S.D.	.006 ± .000	.000 ± .000	.001 ± .001	.001 ± .001
Std. error of est.	.008	.005	.002	.003
r_{xy}	.9996	.9998	1.0000	.9999

Table 4-6 Continues.

Table 4-6 Continued.

Regressions	CADMIUM REACTORS OFF-LINE			
$NO_2^- + NO_3^-$	Seawater	Distilled Water	Seawater	Distilled Water
slope ± S.D.	.0245 ± .0007	.0260 ± .0007	.0250 ± .0007	.0265 ± .0007
Y-intercept ± S.D.	.001 ± .001	-.002 ± .001	-.002 ± .001	-.001 ± .001
Standard error of est.	.000	.001	.002	.001
r_{xy}	.9999	.9998	.9991	.9995
NO_2^-				
slope	.0270 ± .0007	.0260 ± .0007	.0265 ± .0007	.0275 ± .0007
Y-intercept	-.002 ± .001	-.002 ± .001	-.002 ± .001	-.002 ± .001
Std. error of est.	.003	.001	.000	.000
r_{xy}	.9964	.9998	.9999	.9999
Combined				
slope	.0258 ± .0005	.0260 ± .0005	.0258 ± .0005	.0270 ± .0005
Y-intercept	-.001 ± .001	-.002 ± .001	-.002 ± .001	-.001 ± .001
Std. error of est.	.002	.001	.002	.001
r_{xy}	.9963	.9998	.9982	.9995

set contained both nitrate and nitrite in the concentrations indicated in Table 4-5. The latter two standard and spike sets were also determined with the OTCR and PBCR removed from the manifolds shown in Figures 4-1A and 4-1B, respectively. Imidazole buffer (pH=7.0) containing 100 µL of 0.01 M $CuSO_4$ solution per 100 mL was used for both systems. Nitrogen was used to segment the analytical stream for determinations with the OTCR. Sample and wash times were 23 s and 7 s for experiments with the OTCR, and 40 s and 20 s for experiments with the PBCR. These values resulted in percent interaction of 1.0% or less for both systems.

Strip chart recordings of peaks obtained for nitrate and nitrite determinations in seawater with the OTCR and PBCR are reproduced in Figure 4-4 and Figure 4-5, respectively. Part A of both these figures shows peaks recorded for seawater spikes that contained only nitrite. The noise on these peaks resulted from refractive index differences between the distilled water used as the wash solution and the low nutrient seawater in which the spikes were prepared as discussed in Chapter 2. Peaks shown in part B of Figure 4-4 (OTCR system) are for seawater spikes that contained both nitrate and nitrite, while those shown in part B of Figure 4-5 (PBCR system) pertain to seawater spikes that contained only nitrate.

Figure 4-6 shows the correlation between absorbances measured with the OTCR system and absorbances measured with the PBCR system. In this figure the baseline (and blank, in the case of seawater spikes) corrected absorbance values determined for all standards and spikes with the OTCR system are plotted against those obtained with the PBCR system (see Table 4-5). The slope (0.999 ± 0.005), standard error of the

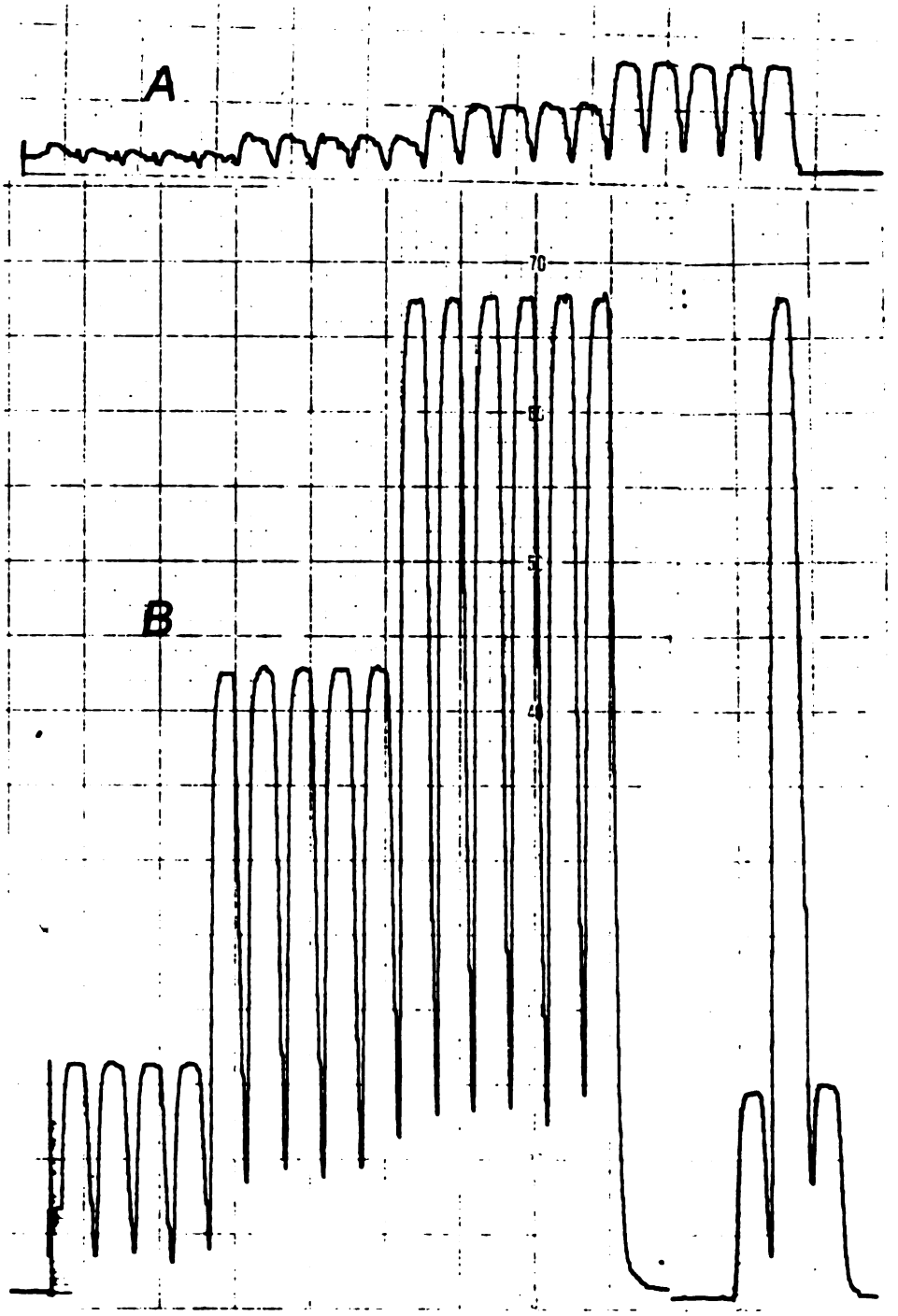

Figure 4-4. Peaks recorded for seawater spikes with a 60 cm open tubular cadmium reactor. A) Nitrite spikes. Nominal concentrations from left to right: blank, 0.5, 1.5, and 2.5 μM. B) Nitrate plus nitrite spikes. Nominal concentrations of $NO_2^- + NO_3^-$ from left to right: 0.5 + 5.0, 1.5 + 15.0, 2.5 + 25 μM. Sample and wash times were 23 s and 7 s, respectively.

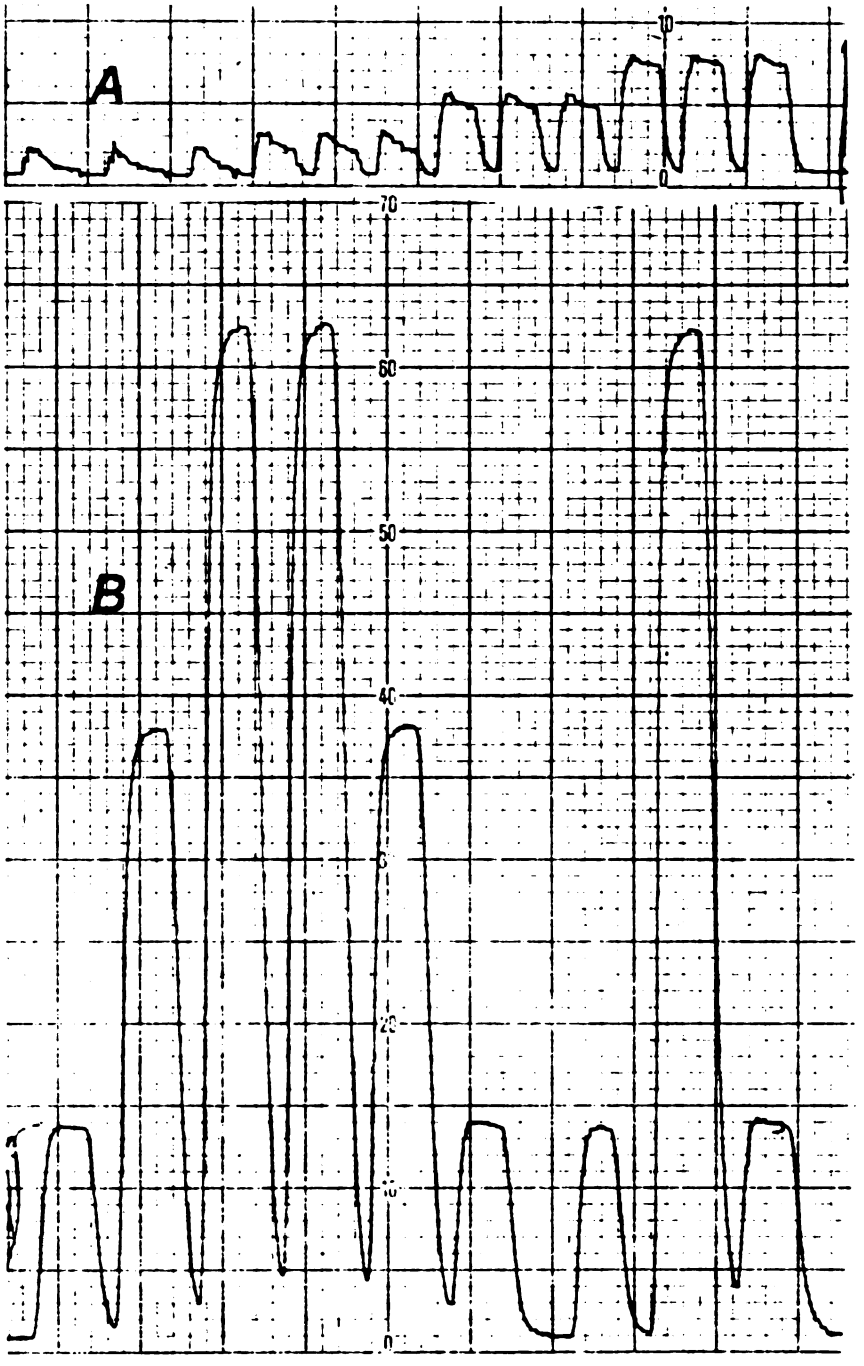

Figure 4-5. Peaks recorded for seawater spikes with a packed bed cadmium reactor. A) Nitrite spikes. Nominal concentrations from left to right as in Figure 4-4. B) Nitrate spikes. Nominal concentrations from left to right: 5.0, 15, and 25 μM. Sample and wash times were 40 s and 20 s, respectively.

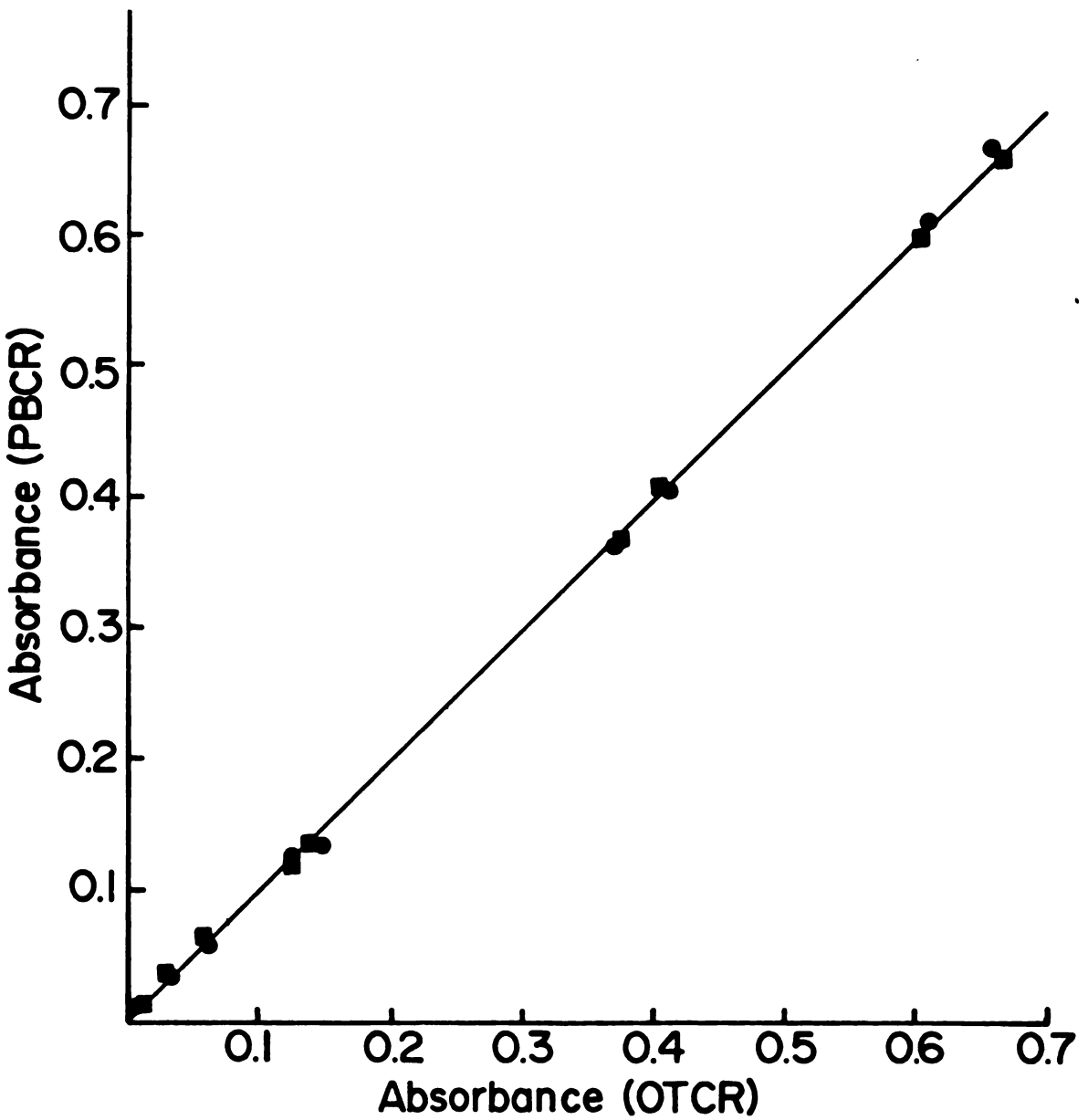

Figure 4-6. Correlation of data obtained with open tubular and packed bed cadmium reactors. ● = seawater spikes; ■ = distilled water standards.

estimate (0.005), Y-intercept (0.002 ± 0.002), and correlation coefficient (0.9998) of this plot indicate that results obtained with both systems are equivalent within the limits of experimental error.

H. Discussion

The goal of this research was to develop a new type of cadmium reactor that would be more compatible with air segmented, continuous flow analyzers than the PBCRs that are most frequently used for routine nitrate determinations in seawater samples. The OTCRs described here fulfill this objective. Inspection of Tables 4-5 and 4-6, and Figure 4-6 reveals that equivalent analytical results can be obtained with either reactor type, both for standards prepared in distilled water and for seawater spikes. Furthermore, dispersion that occurred in OTCRs where the analytical stream remained segmented during reduction was much less than that which occurred in PBCRs where the analytical stream was not segmented during reduction. This is shown clearly in Figures 4-4 and 4-5. Peaks with flats and less than 1% interaction were achieved in conjunction with the OTCR at a sampling rate of 120 hr^{-1}. Comparable performance in conjunction with the PBCR could only be achieved at half this sampling rate (60 hr^{-1}).

OTCRs are much more convenient to use than PBCRs that require elaborate procedures both for preparing cadmium filings and for packing prepared filings into small glass columns. OTCRs are also much less prone to clogging and channelling than PBCRs, and their use eliminates the need to debubble and rebubble the analytical stream before and after reduction. Thus when an OTCR is used in place of a PBCR for nitrate determinations, fewer pump channels and manifold components are

required and therefore less can go wrong. The fact that the analytical stream must be segmented with nitrogen rather than air when OTCRs are used is somewhat inconvenient, and might be particularly cumbersome for shipboard work where compressed gas cylinders must be secured to the outside bulkheads for reasons of safety.

Some work still remains to characterize OTCRs completely. No experiments were performed to determine the long-term stability of OTCRs. The optimum concentration of Cu^{2+} in the imidazole buffer should also be investigated more thoroughly. Addition of small amounts of copper to this reagent kept the activity of the OTCR high and uniform, but in larger amounts, reduction of nitrite to lower oxidation state species increased. Nonetheless, results presented here suggest that OTCRs are a practical alternative to PBCRs for routine nitrate determinations. Some field studies are now needed to determine how well OTCRs will perform in extended, routine operation.

CHAPTER 5

AN EXPERIMENTAL COMPARISON OF CFA AND FIA

A. Introduction

From the time of its inception, FIA has been promoted as a simpler, less costly, and more efficient alternative to CFA, although this assertion has been hotly contested in the recent literature [68-73]. Snyder [5] recently compared CFA and FIA and demonstrated that from a theoretical standpoint, dispersion is generally much lower in air segmented flow reactors than in nonsegmented flow reactors. This study predated the first report of single bead string reactors for FIA. Very recently Rocks and Riley [11] compared FIA and CFA from the standpoint of clinical applications and concluded that FIA would eventually replace CFA in the clinical laboratory. This review appears to have compared second, rather than third, generation CFA systems with FIA and therefore the conclusions drawn seem overly optimistic. To date, however, there has been no direct experimental comparison of CFA and FIA, perhaps because ground rules to prevent bias are difficult to establish, and also because a single channel, third generation CFA instrument is not commercially available. The miniature continuous flow analysis system that I developed during the course of my research can be configured for either CFA or FIA operation, and is therefore ideally suited to an experimental comparison of these two continuous flow analysis techniques.

The experimental comparison of CFA and FIA presented in this chapter is unique in several respects. Most importantly, instrumentation bias is minimal because the same pump, flow cell, and detector were used for both FIA and CFA experiments. Furthermore, for the first time, dispersion in open tubular reactors (OTR), single bead string reactors (SBSR), and air segmented reactors (ASR) is compared under identical experimental conditions. In the first set of experiments, dye dispersion in the three reactor types was monitored as a function of the volume of dye injected into the reactors and the liquid flow rate through the reactors. Here chemical reaction was not required for detection, and therefore recorded peak profiles provided an unambiguous indication of the extent of dispersion that occurred in each reactor at each flow rate. The situation is more complex when chemical reaction is required for detection, as is often the case for continuous flow determinations. Here recorded peak profiles will depend not only on the dispersion characteristics of the reactor, but also on the kinetics of the chemical reactions involved. Analytical rections with relatively slow kinetics were expected to bias the comparison of CFA and FIA in favor of CFA. To avoid this type of bias in the second set of experiments, I chose the colorimetric determination of chloride by reaction with mercuric thiocyanate and ferric nitrate [74] as a reference assay by which the performance of CFA and FIA could be compared. This reaction reaches equilibrium in a few seconds of reaction time.

B. Experimental

1. Dye Dispersion Experiments

The simple flow system used for dye dispersion experiments is shown schematically in Figure 5-1A. Here a single four-way slider valve was used to direct either the dye solution [phenol red (1.0 μmole) in 100 mL of pH 9.5 borate buffer] or the carrier solution (pH 9.5 borate buffer) into the reactors. Valve switching was controlled by a microprocessor as described in Chapter 2. The volume of dye injected as a function of pump speed and valve actuation time can be found in Table 5-1. Pump tubes with nominal flow rates of 1.0 mL min^{-1} were used for all experiments with OTRs and SBSRs. For experiments with ASRs at the two lower flow rates, however, pump tubes with nominal flow rates of 0.42 mL min^{-1} were used. This was necessary to achieve segmentation frequencies of at least 1.5 s^{-1} at all flow rates (see Table 5-1). Plastic OTRs, SBRs, and ASRs were fabricated in the lengths listed in Table 5-2. Fabrication details can be found in Chapter 2. Letters in parentheses in Table 5-2 are used to identify each reactor in the remainder of this discussion. Reactor lengths were chosen such that the dwell time of the dye slug in each reactor type would be about the same in each set of experiments.

Signals that resulted when 25, 50, 100, 200, 400, and 800 μL of dye were injected sequentially into each of the twelve reactors at four different flow rates were recorded with a strip chart recorder. In addition, five replicate determinations for one sample volume (usually 50 μL) were obtained at each flow rate for each reactor. The average and the standard deviation for each set of replicate determinations can be found in Table 5-3. Relative standard deviations of 1% or less were

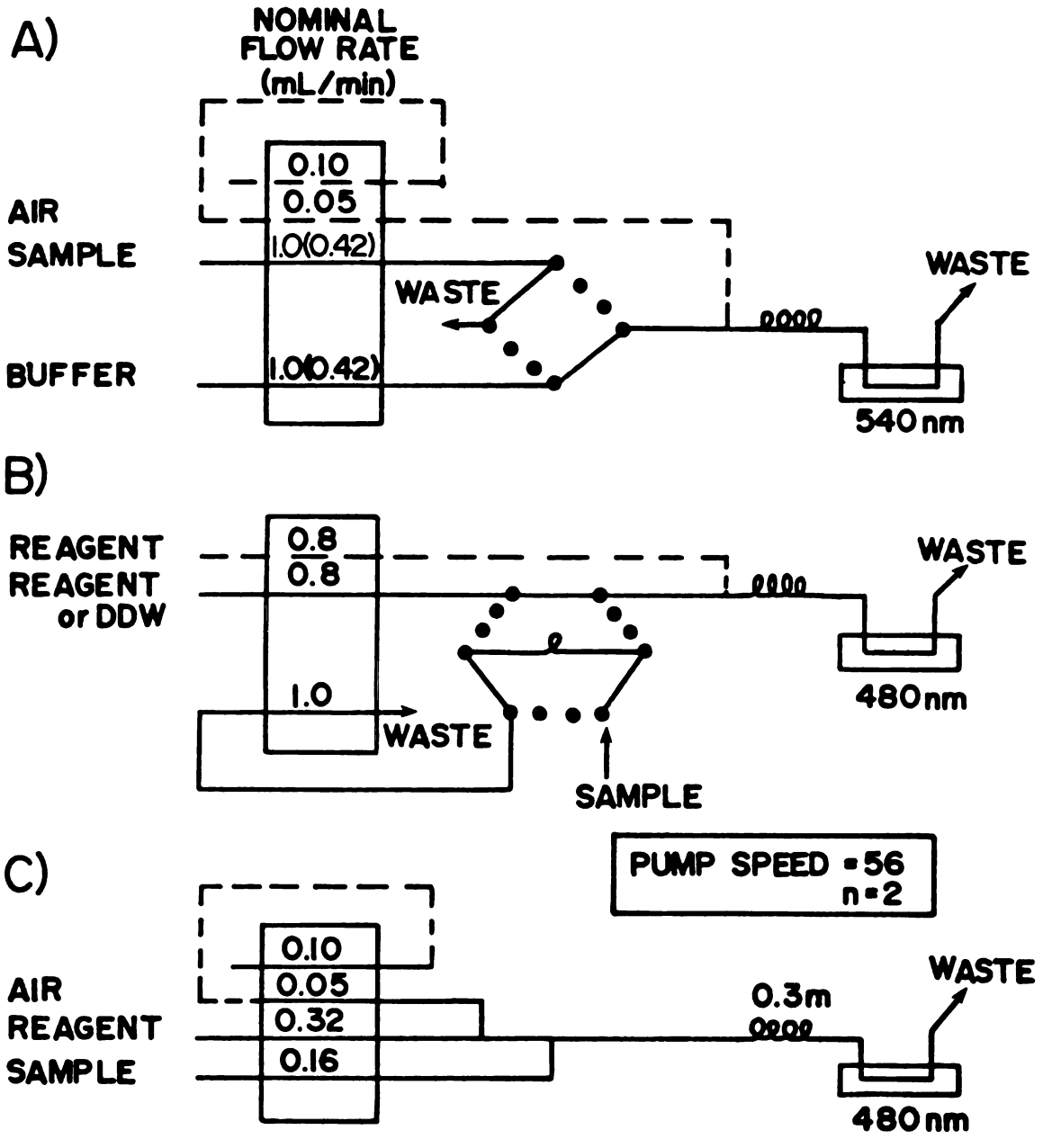

Figure 5-1. Composite diagrams of manifolds used to compare FIA and CFA. A = air, S = sample, C = carrier, R = reagent. A) Manifold used for dye dispersion experients. B) FIA manifold for chloride determinations. C) mCFA manifold for chloride determinations.

Table 5-1. Sample volume as a function of sample time for dye dispersion experiments.

Pump Speed	Flow Rate (mL min^{-1})	Sample Volume (μL) 25	50	100	200	400	800
		Sampling Time					
21[a], 45[b]	0.5	3.0	6.0	12.0	24.0	48.0	96.0
42[a], 90[b]	1.0	1.5	3.0	6.0	12.0	24.0	48.0
63[a]	1.5	1.0	2.0	4.0	8.0	16.0	32.0
84[a]	2.0	.75	1.5	3.0	6.0	12.0	24.0

[a]Pump tubes with nominal flow rate of 1.0 mL/min at standard speed.

[b]Pump tubes with nominal flow rate of 0.42 mL/min at standard speed used with ASRs only.

Table 5-2. Reactor lengths used for dye dispersion experiments.

Reactor Type	Length (cm)			
OTR	10 (A)	50 (B)	100 (C)	200 (D)
SBSR	10 (E)	25 (F)	50 (G)	100 (H)
ASR	10 (I)	30 (J)	50 (K)	75 (L)

Table 5-3. Precision of dye dispersion experiments.[a]

Reactor	Flow Rate (mL min^{-1}) 0.5	1.0	1.5	2.0
A — OTR	0.217 ± .003	.241 ± .002	.258 ± .007	.274 ± .004
B — OTR	0.232[b] ± .001	.280[b] ± .000	.170 ± .002	.164 ± .002
C — OTR	0.153[b] ± .001	.150[b] ± .001	.160[b] ± .001	.204[b] ± .001
D — OTR	0.124[b] ± .001	.227[c] ± .002	.257[c] ± .001	.305[c] ± .000
E — SBSR	0.323 ± .002	.334 ± .002	.350 ± .003	.364 ± .003
F — SBSR	0.247 ± .002	.254 ± .002	.273 ± .003	.285 ± .003
G — SBSR	0.173 ± .002	.183 ± .002	.194 ± .002	.203 ± .001
H — SBSR	0.128 ± .001	.138 ± .001	.148 ± .002	.146 ± .002
I — ASR	0.436 ± .004	.430 ± .000	.408 ± .004	.392 ± .015
J — ASR	0.424 ± .002	.422 ± .003	.371 ± .007	.364 ± .009
K — ASR	0.440 ± .002	.435 ± .001	.368 ± .008	.352 ± .014
L — ASR	0.433 ± .002	.431 ± .002	.354 ± .009	.309 ± .017

[a] Sample volume = 50 µL unless otherwise indicated.

[b] 100 µL sample volume.

[c] 200 µL sample volume.

calculated for all data sets except those obtained with ASRs at the two higher flow rates. The higher relative standard deviations calculated for these data (3-5%) resulted from unfavorable experimental conditions that could not be avoided. At the two lower flow rates the dye slug was divided into about 10 segments (e.g., 6 s/slug x 1.6 segments/s = 9.6 segments/slug; 3 s/slug x 3.2 segments/s = 9.6 segments/slug), while at the two higher flow rates, the dye slug was divided into only about 5 segments (e.g., 2 s/slug x 2.25 segments/s = 4.5 segments/slug; 1.5 s/slug x 3.00 segments/s = 4.5 segments/slug). For this reason proportioning errors were much more pronounced at the higher flow rates. Under normal operating conditions used for CFA, this situation would not arise. In any case, the precision of these two data sets is sufficient for qualitative comparisons.

Tracings of peaks recorded when 50 µL of dye were injected into each reactor are shown in Figure 5-2. This figure provides a great deal of qualitative insight into the dispersion characteristics of the three reactor types. Examination of the peak profiles obtained with the four OTRs (A,B,C,D), reveals that peak heights decrease and peak widths broaden as the reactor length increases. Of course, reactor length and dwell time of the sample slug in the reactor are two sides of the same coin. It is generally accepted [75] that dispersion in OTRs increases with the square root of either the reactor length or the mean dwell time of the sample slug in the reactor. This relationship was found to hold to a fair approximation under all experimental conditions. Notice also that as reactor lengths were increased, the peaks became more symmetrical as predicted by the 'tanks-in-series' model of

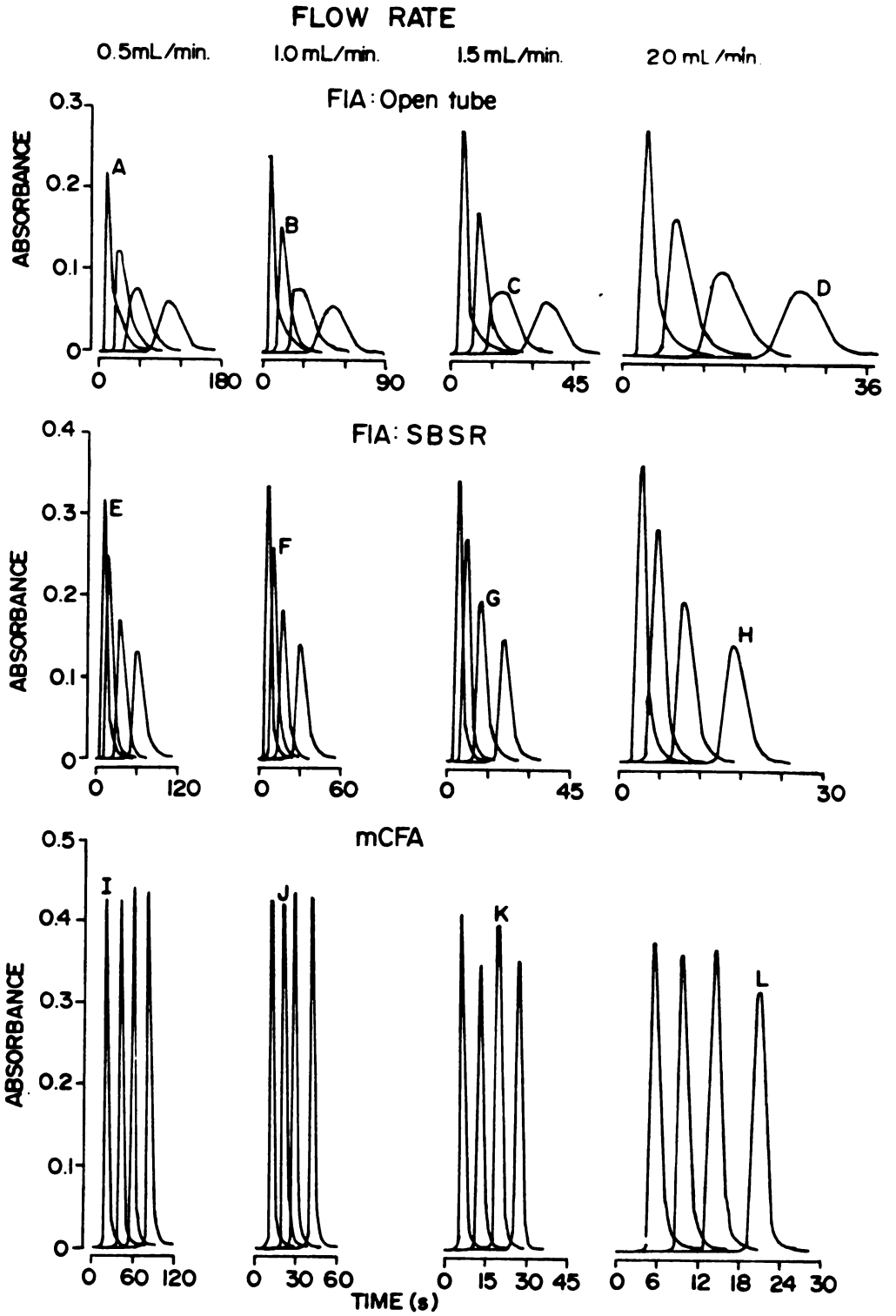

Figure 5-2. Curve tracings of peaks from dye dispersion experiments with open tubular reactors, single bead string reactors, and air segmented reactors.

dispersion in OTRs [76]. Another clearly visible trend is the increase in peak heights and decrease in peak widths that occurred as the flow rate increased. This trend is due primarily to the decreased residence time of the dye slug in the reactor, and to a lesser extent, an increase in secondary flow effects. These same trends hold for peaks recorded for the four SBSRs (E,F,G,H). Note, however, that at comparable residence times, peak widths for SBSRs were about half those recorded for OTRs. Also tailing, which was particularly noticeable in peaks recorded for the shortest OTR (A), was much less pronounced in the SBSR (E) of comparable length, especially at lower flow rates. In general, peaks recorded for SBSRs were more symmetrical than those recorded for OTRS. This suggests that the mixing efficiency of SBSRs is better than in OTRs as reported by Reijn, et al. [37] who stressed that dispersion is not synonymous with adequate mixing, especially in OTRs. The peaks recorded for the four ASRs (I,J,K,L) exhibited very different characteristics. Notice first that reactor length had very little effect on either peak heights or peak widths. Note that subtle differences in peak heights and widths that might be expected were masked by mixing effects that occurred in the sampling valve before the dye slug was segmented with air. Under normal operating conditions for CFA where pecked sampling is employed, sharper peaks would have been recorded. Nonetheless the ability of air segments to minimize dispersion is readily apparent. This study shows very clearly that under comparable experimental conditions the extent of dispersion in the three reactor types can be ranked as follows: ASR<SBSR<OTR.

2. Chloride Determinations

In the second set of experiments, the three reactor types were evaluated in terms of their performance in the simple colorimetric determination of chloride. The reaction sequence is shown below.

$$Hg(SCN)_2 + 2Cl^- \rightarrow HgCl_2 + 2SCN^- \qquad (5\text{-}1)$$

$$SCN^- + Fe^{3+} \rightarrow Fe(SCN)^{2+} \qquad (5\text{-}2)$$

$$\lambda_{max} \simeq 480 \text{ nm}$$

Although it has been suggested [77] that the major product of Reaction 5-2 is $Fe(SCN)_2^+$, and that even higher order complexes might also be formed, the 1:1 complex indicated is the mostly likely product [74]. The reagent solution was prepared by dissolving 0.626 g of mercury (II) thiocyanate, 30.3 g of iron (III) nitrate, 3.3 mL of concentrated nitric acid, and 150 mL of methanol in about 500 mL of dionized distilled water (DDW) contained in a 1 L volumetric flask. The solution was diluted to the mark with DDW, mixed, and transferred to an amber colored bottle. Then 1 mL Brij-35 surfactant was added. This reagent formulation is identical to the one recommended by Hansen and Ruzicka [77]. The primary chloride standard (1000 ppm) was prepared by dissolving 1.648 g of sodium chloride in 1 L of DDW. Working standards in the range of 5 to 45 ppm were prepared by dilution of the primary standard with digital microliter pipets and volumetric flasks. The FIA and CFA manifolds used for these experiments are shown schematically in Figures 5-1B and 5-1C, respectively. Samples were introduced into the FIA system by means of a six-port rotary valve equipped with a 60 µL

sample loop. Pecked sampling was used to introduce samples into the CFA manifold.

When chloride standards in the concentration range of 5 to 35 ppm were injected into the single line FIA manifold (Figure 5-1B) at 30 s intervals, the peaks shown in Figure 5-3 were recorded. Note that there is a large blank signal (i.e., injection of DDW resulted in a peak) and also that each positive peak was followed by a negative peak before the signal returned to base line. These effects are frequently observed when a colorless sample is injected into a colored reagent stream [78] or when there are large differences between the viscosities of the sample and the reagent stream [79]. The effects are due to temporal changes in refractive index and concentration along the dispersed sample slug. It is interesting that this behavior was not observed in an almost identical experiment described by Ruzicka and Hansen [77], probably because the internal volume (18 μL) of the flow cell they used was nine times greater than that (2 μL) of the flow cell used in these experiments.

The above problem was eliminated by adding a second pump tube to the FIA system (dashed line in Figure 5-1B). Here samples were injected into a distilled water carrier stream that merged with the reagent stream in a tee mixer. Thus the extent to which the reagent stream was diluted remained relatively constant when samples were injected. Peaks obtained with the two line FIA system (50 cm OTR) are shown in Fig. 5-4A. As expected, no response was observed when distilled water was injected into the system, but peaks and the base line signal were excessively noisy. This was due to poor mixing between the reagent and sample carrier streams. When the 50 cm OTR was

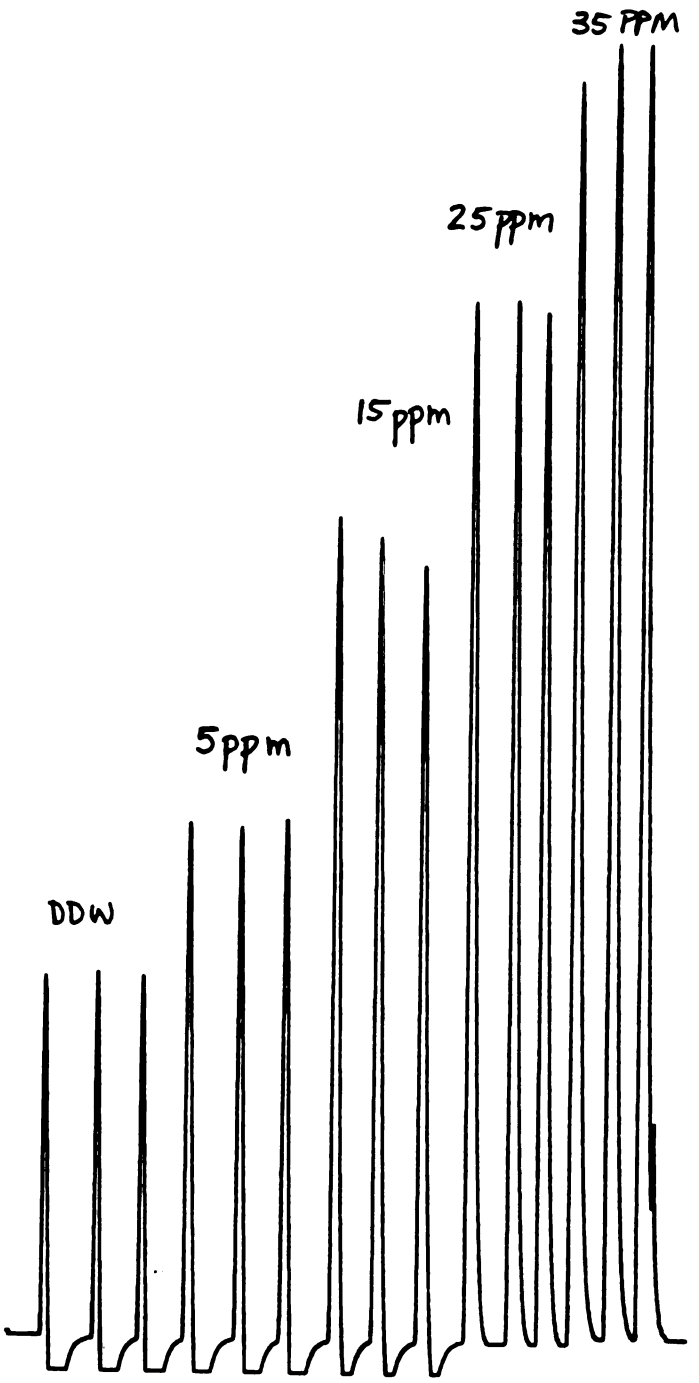

Figure 5-3. Peaks recorded for chloride determinations with the single line FIA manifold.

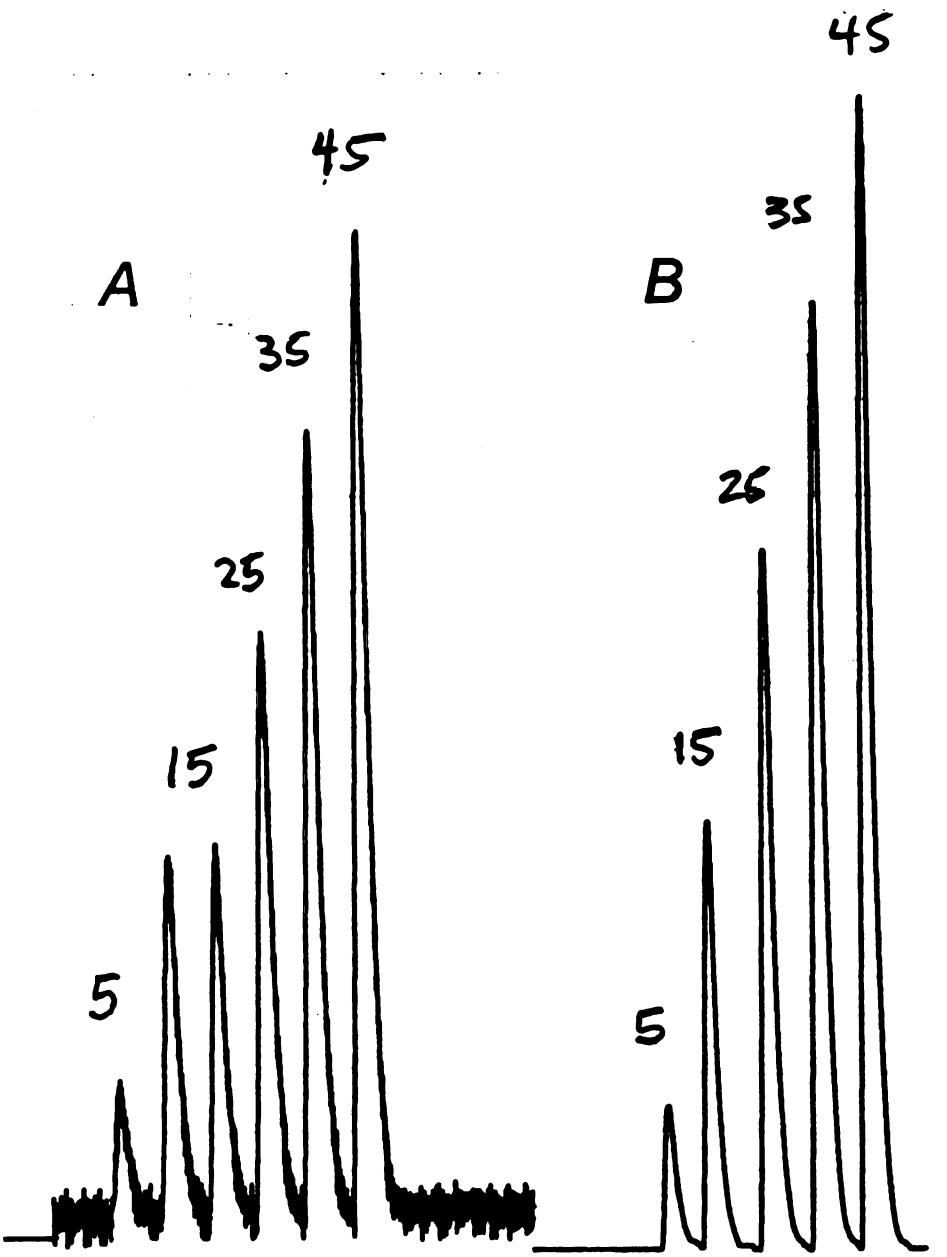

Figure 5-4. Peaks recorded for chloride determinations with a merging zones FIA manifold. A) 50 cm open tubular reactor. B) 50 cm single bead string reactor.

replaced with a 50 cm SBSR, the peaks shown in Figures 5-4B were recorded. Note that base line noise was reduced to negligible levels and that peak heights increased and returned to baseline more rapidly. Here we see clearly the advantages of using SBSRs for routine FIA determinations. Dispersion is decreased so the sampling frequency can be increased, and the mixing efficiency is much improved relative to a comparable OTR. Further experiments showed that good results were still obtained when the length of the SBSR was reduced to 25 cm. At a flow rate of 1.6 mL min^{-1} (carrier, 0.8 mL min^{-1}; reagent, 0.8 mL min^{-1}), sampling rates of 180 hr^{-1} were achieved using the 25 cm SBSR without significant interaction. When the pump speed was doubled, it was possible to increase the sampling rate to 360 hr^{-1}. Peaks recorded at this sampling rate shown in Figure 5-5A.

Next the same chloride standards were determined with the CFA manifold shown schematically in Figure 5-1C. The pump speed and segmentation frequency were 56 and 2 s^{-1}, respectively. Peaks recorded with the CFA system at a sampling rate of 360 hr^{-1} (t_s = 5 s, t_w = 5 s) are shown in Figure 5-5B. Data from chloride determination experiments for both FIA and CFA systems are compiled in Table 5-4. Note that in all cases, less reagent and sample were required for CFA determinations. Furthermore the linearity of the standard curves and the precision of analytical results is somewhat better for the CFA system than the FIA system.

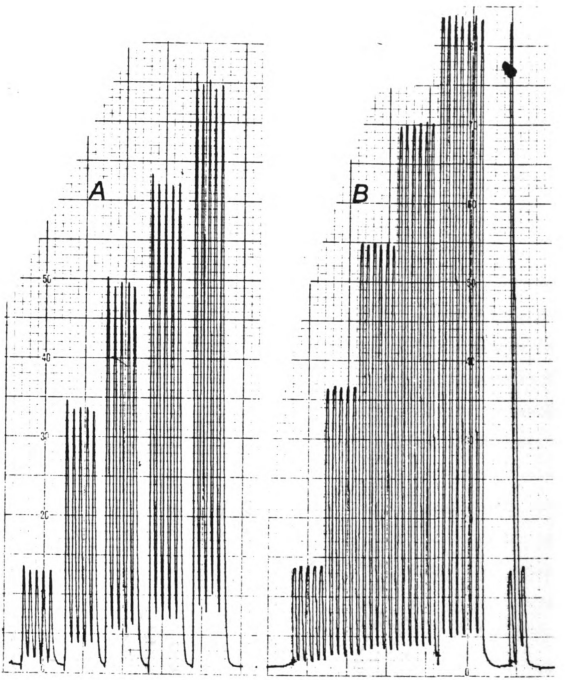

Figure 5-5. Peaks recorded for chloride determinations at a sampling rate of 360 hr^{-1}. A) FIA with merging zones and a 25 cm single bead string reactor. B) mCFA.

Table 5-4. Comparison of mCFA and FIA: Colorimetric chloride determinations.

	mCFA[a]			FIA[b]		
Analysis rate (h^{-1})	360	240	180	360	240	180
Sample time (s)	5	10	15	—	—	—
Wash time (s)	5	5	5	—	—	—
Sample volume (μL)	18	36	54	60	60	60
Reagent volume (μL)[c]	71	107	142	267	400	533
Precision (% RSD)[d]	0.43	0.25	0.34	1.72	0.44	0.67
% Interaction	0.6	0.6	0.5	≃1-2	> 1	> 1
Slope	0.020	.021	.021	.018	.019	.019
Y intercept	0.032	.034	.033	.036	.040	.037
r_{xy} (correl. coeff.)	0.998	.998	.998	.997	.997	.997

[a] Pump speed = 56, n=2, t = 30 s, d_t = 0.1 cm.

[b] Pump speed = 84, 25 cm SBSR.

[c] CFA: The volume of reagent delivered during one sample and wash interval. FIA: The volume of reagent delivered during the time interval between sample injections.

[d] Calculated from 5 replicate determinations of the 15 ppm chloride standard.

C. Discussion

The foregoing experiments underscore the fundamental differences between FIA and CFA. In FIA the sample enters the reactor as a slug and begins to disperse into the carrier stream at the moment of injection. Note that the sample loop is itself a mixing stage, as is the flow cell. Except in cases where samples are not required to undergo chemical reaction prior to detection, such as when FIA is used to transport samples to an ion selective electrode, some dispersion of the sample slug is necessary. In single line FIA systems, in fact, dispersion is the only mechanism by which the sample and reagent can interact. In dual line FIA systems where the sample and reagent are merged in a tee connector, mixing is improved somewhat but is still far from complete. For colorimetric determinations, this is a major weakness in the FIA approach to continuous flow analysis, because it is generally necessary to compromise between adequate mixing of the sample and reagent on the one hand, and excessive broadening of the sample slug on the other. There are a number of 'little tricks', however, that can be used to enhance mixing and minimize dispersion in FIA that help to make this compromise more favorable. As shown in the experimental section, these include inducing secondary flow by using tightly coiled rather than straight OTRs, and using SBSRs rather than OTRs. Both these approaches are successful because they disrupt the parabolic velocity profile associated with laminar flow. Another effective way to increase residence time without excessive dispersion is simply to inject the sample into the carrier stream and then stop the pump [80]. To a close approximation when the flow stops, dispersion stops. After sufficient reaction time has elapsed, the pump is restarted and the

reacted sample is propelled into the detector. Of course this approach is somewhat cumbersome and has some rather obvious limitations.

The situation is quite different for CFA because the process of mixing the sample with reagent is not dependent on sample dispersion. Recall that in CFA the sample slug is divided into a number of nominally identical segments before it enters the reactor. Then each segment is proportioned with reagent, and mixing within each segment is enhanced by the microcirculation pattern (bolus flow) that develops naturally in a segmented, flowing stream. Furthermore, dispersion in CFA is minimized by one 'big trick', the bubble. Air segments provide barriers to the establishment of parabolic velocity profiles in all zones of a CFA system: pecked sampling greatly reduces dispersion that would otherwise arise during the sampling process; segmented flow greatly reduces dispersion in the reactor; and bubble-through flow cells reduce dispersion associated with detection. In addition, other factors being equal, dispersion decreases as the flow rate decreases which leads to conservation of samples and reagents.

From the foregoing experiments, it is clear that for equilibrium based to colorimetric determinations, CFA retains a slight edge over FIA even for relatively simple chemistries with fast reaction rates. It cannot be denied, however, that in the limit FIA is more simple, operationally, than CFA. Consider the case where a sample is reacted with a single reagent and detected. The minimum requirements for an FIA system are a single channel pump, an injection valve, and a recording detector. The same determination with CFA would require three pump channels (one each for sample, air, and reagent), and the detector signal would have to be gated to eliminate the air bubble

artifact. Otherwise a fourth pump channel would be required to debubble the analytical stream prior to detection. Also, when an automatic sampler is not available, as was the case for my work, introduction of samples with a valve in FIA is much less taxing than manual, pecked sampling used for CFA, because no timing is required. Thus for single reagent colorimetric determinations where the differences in performance between CFA and FIA are small, FIA may be preferred due to the relative ease and simplicity with which determinations can be performed. On the other hand, for colorimetric determinations requiring multiple reagent additions, dialysis, or reaction times exceeding about 30 s, the increased complexity of CFA is more than offset by its higher performance. The point at which this trade-off is reached, however, is not clear-cut, and the choice between these two continuous flow techniques will be strongly influenced by the analyst's ingenuity and predisposition to CFA and FIA.

CHAPTER 6

FUTURE APPLICATIONS

A. Overview

The miniature continuous flow analysis system described and characterized in the prceeding chapters has proved to be a versatile instrument. In conjunction with the electronic bubble gate, state-of-the-art performance for air-segmented continuous flow analysis can be achieved with relative ease at low cost. Flow injection analysis can be performed with the same basic system except that a multiport valve is used for sample introduction, and the bubble gate is removed from the detection circuitry. The modular design of this system, and the ease with which it can be configured for either CFA or FIA are unique features that offer a number of intriguing possibilities for future analytical applications. A few of these are outlined in the paragraphs that follow.

B. Automated Sample Pretreatment and Pre- and Post-Column Reactors for Liquid Chromatography

A survey of the recent literature concerning detection schemes for liquid chromatography (LC) reveals a progressive shift in interest from universal to selective detectors. This trend reflects the growing awareness that because of the complex matrices associated with samples of biological or environmental origin, a truly universal LC detector

would create more problems than it would solve. Of the many conceivable selective LC detectors, those based on UV-VIS absorption, fluorescence, or electroactivity are most widely used. Often both the selectivity and the sensitivity achieved with these detectors can be increased by several orders of magnitude if sample constituents of interest are derivatized with appropriate reagents prior to detection, either before or after chromatographic separation. Generally sample pretreatment and derivatization steps are labor intensive, and it is therefore not surprising that continuous flow analyzers, which allow these procedures to be automated, are beginning to gain acceptance as efficient and reliable adjuncts to LC systems. To date continuous flow post-column reactors have received the most attention. This subject has been extensively reviewed by Frei and co-workers [81-85].

There has been a great deal of discussion about the optimum design for LC post-column reactors. Obviously, the extra-column band broadening that occurs in post-column reactors must be held to a minimum to prevent loss of chromatographic resolution. There are three basic types of post-column reactors. In two of these, coiled open tubular reactors and packed bed reactors, the column effluent is not segmented. In the third type, segmented open tubular reactors, the column effluent is segmented either with gas or an immiscible liquid. Very recently Scholten, et al. [86] presented results of experiments with all three post-column reactor types and concluded that segmented reactors were to be preferred even when the kinetics of the post-column reaction were relatively fast. This is not surprising in light of the experimental comparison of FIA and CFA presented in Chapter 5. Scholten used second generation CFA equipment for this study and found,

predictably, that most of the extra-column band broadening that occurred could be attributed to mixing in debubblers and phase separators. As Snyder [31] pointed out, extra-column band broadening can be reduced still further with third generation CF systems that are equipped with gated detectors which eliminate the need for phase separation. At present, single channel third generation CF systems are not available commercially. The single channel mCF system is ideally suited for post column reactor applications and is sufficiently simple to be fabricated in-house at low cost. In addition the mCF system should be well suited for sample preparation (dialysis, solvent extraction, derivatization) prior to the chromatographic step. In this case of course, the effluent from the mCF system would be interfaced to the sample injection valve of the liquid chromatograph rather than a detector. For either application, the mCF system should produce better results than any presently available commercial systems.

C. Continuous Flow Kinetics Determinations

There are presently two approaches to kinetics determinations with continuous flow analyzers. In the case of third generation CFA systems [4], the analytical stream flows sequentially through several gated detectors which are interconnected by means of thermostated delay coils. Because the integrity of the analytical stream is maintained during detection, dispersion between detectors is minimal. Thus the steady state signal recorded at each detector provides a measure of the extent of the chemical reaction at fixed time intervals. This approach is somewhat cumbersome unless a computer is available for data acquisition and processing. In the case of FIA systems the so-called

'stopped-flow' [87] technique (not to be confused with conventional rapid-mixing stopped-flow analyzers) is generally used. Here some portion of the dispersed sample zone is stopped within the flow cell, after sufficient time has elapsed for mixing, by turning off the pump. After the flow stops the progress of a chemical reaction can be monitored continuously over any desired time interval.

The FIA approach is attractive because of its simplicity. Only one detector is required and data can be acquired with a strip chart recorder. For determinations that require preliminary reactions prior to the final analytical reaction, or that require sample pretreatment such as dialysis, CFA may still be preferred despite its complexity. Neither technique is applicable for kinetics determinations where the reaction half-life is on the order of the mixing time (~5-10 s) of the continuous flow analyzer. This constraint is not prohibitive for a number of kinetics based determinations of clinical interest, however, and it would be worthwhile to compare the performance of continuous flow analyzers with that of conventional stopped-flow analyzers for these applications.

D. Active Open Tubular Reactors

Robert Thompson, a recent graduate of the Crouch research group, used the mCF system to do some nice work with open tubular immobilized enzyme reactors [44,88]. There are several opportunities for continued research in this area. These include characterization of reactors to which more than one enzyme has been bonded, the use of several immobilized enzymes reactors for a single determination, and characterization of immobilized enzyme single bead string reactors. Readers with an

interest in this line of research are directed to Thompson's Ph.D. dissertation [44]. Nonenzymatic active tubular reactors also warrant further investigation. As demonstrated in Chapter 4, open tubular cadmium reactors can be used for nitrate determinations and they are more compatible with CFA then packed bed cadmium reactors. Other metals such as iron, copper, and zinc in the form of narrow open tubes may also have useful applications for routine determinations with CFA and FIA.

E. Extended Data Acquisition and Processing Systems

A dedicated microcomputer based data acquisition and processing system would greatly extend the usefulness of the mCF system. This, along with the automatic sampler recently acquired by the Crouch group, should go a long way toward eliminating the drudgery and tedium that characterized the manual sampling and data processing required for many of the experiments performed during the course of my research. The general purpose FORTH based data acquisition routines developed by Eugene Ratzlaff [41] are already available to members of the Crouch research group. These routines could be stored in read only memory and should be extended to allow for curve regeneration, peak finding, baseline drift corrections and sample interaction corrections. Software routines could also be written to control the pump and sampler. These routines would be particularly useful for FIA experiments. Although a software bubble gating routine could also be written, my own feeling is that analog bubble gating is just as effective and it has the advantage of freeing the microcomputer to perform higher level tasks.

LIST OF REFERENCES

LIST OF REFERENCES

1. L.T. Skeggs, Amer. J. Clin. Path. 28, 311-322 (1957).

2. K.K. Stewart, G.R. Beecher and P.E. Hare, Fed. Proc. 33, 1439-(1974).

3. J. Ruzicka and E.H. Hansen, Anal. Chim. Acta 78, 145-157 (1975).

4. L.R. Snyder, J. Levine, R. Stoy and A. Conetta, Anal. Chem. 48, 942A-956A (1976).

5. L.R. Snyder, Anal. Chim. Acta 114, 3-18 (1980).

6. W.B. Furman, Continuous Flow Analysis: Theory and Practice, Marcel Dekker, New York (1976).

7. D. Betteridge, Anal. Chem. 50, 832A-846A (1978).

8. J. Ruzicka and E.H. Hansen, Anal. Chim Acta 114, 19-44 (1980).

9. C. Ranger, Anal. Chem. 53, 20A-32A (1981).

10. J. Ruzicka and E. Hansen, Flow Injection Analysis, John Wiley and Sons, New York (1981).

11. B. Rocks and C. Riley, Clin. Chem. (Winston-Salem, NC) 28, 409-421 (1982).

12. K.K. Stewart, Talanta 28, 789-797 (1981).

13. H. Mottola, Anal. Chem. 53, 1312A-1316A (1981).

14. A.T. James and A.J. Martin, Analyst 77, 915-932 (1952).

15. W.J. Blaedel and G.P. Hicks, Anal. Chem. 34, 388-394 (1962).

16. D.H. Spackman, W.H. Stein and S. More, Anal. Chem. 30, 1190-1206 (1958).

17. W.H.C. Walker, in Continuous Flow Analysis: Theory and Practice (W.B. Furman, ed.) Marcel Dekker, New York (1976) pp. 207-255.

18. W.H.C. Walker, C.A. Pennock and G.K. McGowan, Clin. Chim. Acta 27, 421-435 (1970).

19. R.E. Thiers, R.R. Cole and W.J. Kirsch, Clin. Chim. (Winston-Salem, NC) 13, 451-467 (1967).

20. L.R. Snyder and H.J. Adler, Anal. Chem. 48, 1022-1027 (1976).

21. J. Hrdina, 6th Colloq. Amino Acid Analysis, Technicon Corp., Monograph No. 3, 1967.

22. R.D. Begg, Anal. Chem. 44, 631-632 (1972).

23. R.E. Thiers, A.H. Reed and K. Delander, Clin. Chem. (Winston-Salem, NC) 17, 42-48 (1971).

24. W.H.C. Walker and K.R. Andrew, Clin. Chim. Acta 57, 181-185 (1974).

25. L.R. Snyder and H.J. Adler, Anal. Chem. 48, 1017-1022 (1976).

26. H. Diebler, M. Pelavin, in Advances in Automated Analysis, Technicon Symposia 1972, , Mediad Inc., Tarrytown, NY, Vol. I (1972) pp. 7-13.

27. R.L. Habig, B.W. Schlein, L. Walters and R.E. Thiers, Clin. Chem. 15, 1045-1055 (1969).

28. W.E. Neeley, S. Wardlaw and M.E.T. Swinnen, Clin. Chem. (Winston-Salem, NC) 20, 78-80 (1974).

29. C.J. Patton, M. Rabb and S.R. Crouch, Anal. Chem. 54, 1113-1118 (1982).

30. W.H.C. Walker, Clin. Chim. Acta 32, 305-306 (1971).

31. L.R. Snyder, J. Chromatogr. 125, 287-306 (1976).

32. L.R. Snyder, in Advances in Automated Analysis: Technicon International Congress 1976, Mediad Inc., Tarrytown, NY, Vol. I, (1977) pp. 76-81.

33. J. Ruzicka and E.H. Hansen, Flow Injection Analysis, John Wiley and Sons, New York, (1981) p. 16.

34. J.T. Vanderslice, K.K. Stewart, A.G. Rosenfeld and D.J. Higgs, Talanta 28, 11-18 (1981).

35. R. Tijssen, Anal. Chim. Acta 114, 71-89 (1980).

36. K. Hofman and I. Halasz, J. Chromatogr. 173, 211-228 (1979).

37. J.M. Reijn, W.E. Van Der Linden and H. Poppe, Anal. Chim. Acta 123, 229-237 (1981).

38. J.M. Reijn, W.E. Van Der Linden and H. Poppe, Anal. Chim. Acta 126, 1-13 (1981).

39. O. Levenspiel, Chemical Reaction Engineering, 2nd ed., John Wiley and Sons, New York (1972).

40. K. Hofman and I. Halasz, J. Chromatogr. 199, 3-22 (1980).

41. E. Ratzlaff, Ph.D. Dissertation, Michigan State University, 1982.

42. A. Savitzky and M.J.E. Golay, Anal. Chem. 36, 1627-1639 (1964).

43. E. Amador, Clin. Chem. (Winston-Salem, NC) 18, 164 (1972).

44. R.Q. Thompson, PH.D. Dissertation, Michigan State University, 1982, pp. 154-155.

45. W.H.C. Walker, J. Townsend and P.M. Keane, Clin. Chim. Acta 36, 119-125 (1972).

46. E.B.M. DeJong and A.H. Weyden, Anal. Chim. Acta 114, 311-317 (1980).

47. M.A. Macaulay, J.M. Mathers, C.L. Jacklyn and C.A. Munro, Clin. Biochem. 9, 111-116 (1976).

48. W.E. Neeley, S.C. Wardlaw, T. Yates, W.G. Hollingsworth and W.G. Swinnen, Clin. Chem. 22, 227-231 (1976).

49. T.E. Whitledge, S.C. Malloy, C.J. Patton and C.D. Wirick, Automated Nutrient Analyses in Seawater, Technical Report, Brookhaven National Laboratory, Upton, NY (1981) pp. 50-53.

50. R.E. Thiers, J. Meyn and R.F. Wilderman, Clin. Chem. 16, 832-839 (1970).

51. E.A.G. Zagatto, A.O. Jacintho, J. Mortatti and F. Bergamin, Anal. Chim. Acta 120, 399-403 (1980).

52. V.W. Truedale and C.J. Smith, Analyst 1976 101, 19-31 (1976).

53. F.J.A. Armstrong, C.R. Stearns and J.D.H. Strickland, Deep-Sea Res. 14, 381-389 (1967).

54. T.J. Chow, and M.S. Johnstone, Anal. Chim. Acta 27, 441-446 (1962).

55. J.B. Mullin and J.P. Riley, Anal. Chim. Acta 12, 464-480 (1955).

56. D.R. Senn and P.W. Carr, Anal. Chem. 48, 954-958 (1976).

57. M.P. Stainton, Anal. Chem. 46, 1616 (1974).

58. R.B. Willis, Anal. Chem. 52, 1377-1379 (1980).

59. W. Davison and C. Woof, Analyst 103, 403-406 (1978).

60. J.D.H. Strickland and T.R. Parsons, A Manual of Seawater Analysis, 2nd ed., Queens Printer, Ottawa (1965), p. 203.

61. F. Nydahl, Talanta 23, 349-357 (1976).

62. E.D. Wood, F.A.J. Armstrong and F.A. Richards, J. Mar. Biol. Ass. U.K. 47, 23-31 (1967).

63. A. Otsuki, Anal. Chim. Acta 99, 375-377 (1978).

64. G.A. Sherwood and D.C. Johnson, Anal. Chim. Acta 129, 87-100 (1981).

65. P.G. Brewer and J.P. Riley, Deep-Sea Research 12, 765-772 (1965).

66. F. Nydahl, Talanta 21, 1259-1267 (1974).

67. J.P. Riley and G. Skirrow, Chemical Oceanography, Academic Press, New York, (1965) pp. 204-205.

68. M. Margoshes, Anal. Chem. 49, 17-19 (1977).

69. J. Ruzicka, E.H. Hansen, H. Masbaek and F.J. Krug, Anal. Chem. 49, 1858-1861 (1977).

70. M. Margoshes, Anal. Chem. 49, 1861-1862 (1977).

71. M. Margoshes, Anal. Chem. 54, 678A-679A (1982).

72. C.B. Granger, Anal. Chem. 54, 1106A (1982).

73. M. Margoshes, Anal. Chem. 54, 1106A (1982).

74. D.M. Zall, D. Fisher and M.Q. Garner, Anal. Chem. 28, 1665-1668 (1956).

75. J. Ruzicka and E. Hansen, Flow Injection Analysis, John Wiley and Sons, New York, (1981) p. 20.

76. J. Ruzicka, and E. Hansen, Flow Injection Analysis, John Wiley and Sons, New York, (1981) p. 41.

77. E.H. Hansen and J. Ruzicka, J. Chem. Ed. 56, 677-680 (1979).

78. J. Ruzicka and E. Hansen, Flow Injection Analysis, John Wiley and Sons, New York, (1981) p. 144.

79. D. Betteridge, Talanta 23, 409-410 (1976).

80. J. Ruzicka and E. Hansen, Flow Injection Analysis, John Wiley and Sons, New York, (1981) p. 21.

81. R.W. Frei and W. Santi, Z. Anal. Chem. 277, 303-310 (1975).

82. R.W. Frei, L. Michel, and W. Santi, J. Chromatogr. 142, 261-270 (1977).

83. R.W. Frei and A.H.M.T. Scholten, J. Chromatogr. Sci. 17, 152-160 (1979).

84. R.W. Frei, J. Chromatogr. 165, 75-86 (1979).

85. R.W. Frei, Chromatographia 15, 161-166 (1982).

86. A.H.M.T. Scholten, U.A.Th. Brinkman, and R.W. Frei, Anal. Chem. 54, 1932-1938 (1982).

87. J. Ruzicka and E.H. Hansen, Flow Injection Analysis, John Wiley and Sons, New York, (1981) pp. 61-65.

88. R.Q. Thompson, C.J. Patton and S.R. Crouch, Clin. Chem. (Winston-Salem, NC) 28, 556-557 (1982).